A virtual element method for transversely isotropic elasticity

Daniel van Huyssteen

M.Sc. Eng Dissertation
in the Department of Mechanical Engineering
Faculty of Engineering and the Built Environment
University of Cape Town

October 2018

Declaration

I, Daniel van Huyssteen, hereby:

(a) grant the University of Cape Town free license to reproduce the above thesis in whole or in part, for the purpose of research;

(b) declare that:

(i) the above thesis is my own unaided work, both in concept and execution, and that apart from the normal guidance from my supervisor, I have received no assistance apart from that explicity stated in the Acknowledgements.

(ii) neither the substance nor any part of the above thesis has been submitted in the past, or is being, or is to be submitted for a degree at this university or at any other university.

I know the meaning of plagiarism and declare that all the work in the document, save for that which is properly acknowledged, is my own. This dissertation has been submitted to the Turnitin module and I confirm that my supervisor has seen my report and any concerns revealed by such have been resolved with my supervisor.

I am now presenting the dissertation for examination for the degree of M.Sc. Eng (Mechanical).

Signed by candidate

D. van Huyssteen
29 October 2018

Prof B.D. Reddy
29 October 2018

APPLICATION FORM

Please Note:
Any person planning to undertake research in the Faculty of Engineering and the Built Environment (EBE) at the University of Cape Town is required to complete this form **before** collecting or analysing data.The objective of submitting this application *prior* to embarking on research is to ensure that the highest ethical standards in research, conducted under the auspices of the EBE Faculty, are met. Please ensure that you have read, and understood the **EBE Ethics in Research Handbook**(available from the UCT EBE, Research Ethics website) prior to completing this application form: http://www.ebe.uct.ac.za/usr/ebe/research/ethics.pdf

APPLICANT'S DETAILS		
Name of principal researcher, student or external applicant		Daniel van Huyssteen
Department		Mechanical Engineering - CERECAM
Preferred email address of applicant:		Vhydan001@myuct.ac.za
If a Student	Your Degree e.g., MSc, PhD, etc.,	MSc (Eng)
	Name of Supervisor (if supervised)	Professor Batmanathan Dayanand (Daya) Reddy
If this is a research contract, indicate the source of funding/sponsorship		-
Project Title		Analysis and Applications of the Virtual Element Method

I hereby undertake to carry out my research in such a way that:

- there is no apparent legal objection to the nature or the method of research; and
- the research will not compromise staff or students or the other responsibilities of the University;
- the stated objective will be achieved, and the findings will have a high degree of validity;
- limitations and alternative interpretations will be considered;
- the findings could be subject to peer review and publicly available; and
- I will comply with the conventions of copyright and avoid any practice that would constitute plagiarism.

SIGNED BY	Full name	Signature	Date
Principal Researcher/ Student/External applicant	Daniel van Huyssteen	Signed by candidate	**03 Feb 2017**

APPLICATION APPROVED BY	Full name	Signature	Date
Supervisor (where applicable)	BD Reddy	BDReddy	**03 Feb 2017**
HOD (or delegated nominee) Final authority for all applicants who have answered NO to all questions in Section1, and for all Undergraduateresearch (Including Honours)	T. Bello-Ochende Click here to enter text.		11/10/2018 Click here to enter a date.
Chair : Faculty EIR Committee For applicants other than undergraduate students who have answered YES to any of the above questions	Click here to enter text.		Click here to enter a date.

Abstract

This work studies the approximation of plane problems concerning transversely isotropic elasticity, using a low-order virtual element method (VEM). The VEM is an alternative finite element method characterised by complete freedom in determining element geometries that are otherwise polygonal in two dimensions, or polyhedral in three. Transversely isotropic materials are characterised by an axis of symmetry perpendicular to a plane of isotropy, and have applications ranging from fibre reinforcement to biological materials. The governing equations of the transversely isotropic elasticity problem are derived and a virtual element formulation of the problem is presented along with a sample implementation of the method. This work focuses on the treatment of near-incompressibility and near-inextensibility. These are explored both for homogeneous problems, in which the plane of isotropy is fixed; and non-homogeneous problems, in which the fibre directions defining the plane of isotropy vary with position. In the latter case various options are explored for approximating the non-homogeneous terms at an element level. The VEM approximations are shown through a range of numerical examples to be robust and locking-free, for a selection of element geometries, and fibre directions corresponding to mild and strong inhomogeneity.

Acknowledgements

My sincere gratitude goes to:

Professor B.D. (Daya) Reddy for his consistently calm and considered supervision. Without his guidance this work would not have been possible.

The National Research Foundation of South Africa, through the South African Research Chair in Computational Mechanics, for their support.

My parents, Richard and Karen, for their extensive support and belief in me over the past six years.

Aaron Graham, Heidi Burger and Emma Griffiths for their friendship and willing advice over the past two years.

Natalie Bent for her efficient administration that allows the students at CERECAM to focus on their research.

Contents

List of Figures

List of Tables

Direction and Naming Convention

Generic notation

Ω	Domain
Γ	Boundary
Γ_d	Dirichlet boundary
Γ_n	Neumann boundary
$\boldsymbol{n}$, n_i	Outward facing normal vector
$\boldsymbol{b}$, b_i	Body force
$\bar{\boldsymbol{t}}$, $\bar{t}_i$	Prescribed traction
$\bar{\boldsymbol{u}}$, $\bar{u}_i$	Prescribed displacement
$\boldsymbol{u}$, u_i	Displacement field
$\boldsymbol{\varepsilon}$, ε_{ij}	Strain field
$\boldsymbol{\sigma}$, σ_{ij}	Stress field
$\mathbb{C}$	Elasticity tensor
$\mathcal{L}^2$	Space of square-integrable functions
$\mathcal{H}^1$	Sobolev space
ψ	Strain energy density
$\boldsymbol{Q}$, Q_{ij}	Symmetry transformation
$\boldsymbol{\varepsilon}^V$, $\varepsilon_i^{\mathrm{V}}$	Strain field expressed in Voigt Notation
$\boldsymbol{\sigma}^V$, σ_i^{V}	Stress field expressed in Voigt Notation

Virtual element method notation

$\mathcal{T}_h$	Collection of polygons
E_i	i-th element
V_i	i-th vertex of an element
e_i	i-th edge of an element
n_V	Number of vertices of an element
n_e	Number of edges of an element
n_{dof}	Number of degrees of freedom of an element
$\boldsymbol{V}_h$	Global virtual element space
$\boldsymbol{V}_{h\|E}$	Local virtual element space
Π_E^{∇}	Projection operator
$\boldsymbol{\phi}$, ϕ_{ij}	Matrix of basis functions
$\boldsymbol{N}$, N_{ij}	Matrix of standard Lagrangian approximation functions
$\boldsymbol{B}$, B_{ij}	Gradient of standard Lagrangian approximation functions
$\boldsymbol{K}_c^E$	Consistency stiffness matrix for element E
$\boldsymbol{\mathcal{D}}$	Matrix of scaled linear basis functions
$\boldsymbol{K}_{stab}^E$	Stabilization stiffness matrix for element E
$\boldsymbol{K}^E$	Stiffness matrix for element E
$\boldsymbol{F}_{\bar{\boldsymbol{t}}}$	Component of loading due to tractions
$\boldsymbol{F}_{\boldsymbol{b}}$	Component of loading due to body forces
$\boldsymbol{F}$	Loading/force vector

Fibre description notation

$a(\boldsymbol{x})$	Family of functions describing fibre position
$\boldsymbol{a}$	Axis of symmetry of transversely isotropic materials
$\hat{a}$	Angle between axis of symmetry $\boldsymbol{a}$ and the horizontal x-axis

Chapter 1

Introduction

In this chapter we describe the subject and motivation of this dissertation before providing some background information to set the scene for this work. We then detail the objectives of this work and highlight its scope and limitations. Finally, the structure of the rest of the dissertation is described.

1.1 Subject and motivation

Partial differential equations (PDEs) and systems of partial differential equations are used to describe the physics of a broad range of natural phenomena and engineering applications including thermal energy transfer, diffusion, electrostatics, electromagnetism, fluid dynamics, and elasticity [1]. It is generally not possible to solve systems of PDEs analytically, and approximation techniques need to be employed. These include finite difference methods and finite volume methods [2, 3], the latter being used extensively to solve fluid dynamics problems [4].

In the context of solid mechanics the finite element method [5] has become the standard approach and is widely used in commercial software for this purpose. It has been very successful in solving problems involving complexities from non-linearities to complex geometries [6, 7]. Near-incompressibility and small length scales can lead to pathologies such as volumetric and shear locking respectively. There exist a variety of approaches including mixed methods, non-conforming approaches and discontinuous Galerkin approaches [8, 9, 10] to address these problems.

A recent development in the context of finite element methods is the virtual element method (VEM). In contrast to the geometric restrictions on finite elements, which are most generally triangular or quadrilateral in 2D, and tetrahedral or hexahedral in 3D, the VEM permits elements to be arbitrary polyhedra in three dimensions or polygons in two. Applications of the VEM to the elasticity problem have dealt mostly with linear and non-linear isotropic elasticity and plasticity. There has been little investigation into the behaviour of anisotropic and non-homogeneous elasticity, which create additional challenges for VEM approaches.

1.2 Background information

1.2.1 Finite element methods

The finite element method has become the standard approach used for generating approximate solutions to problems in solid mechanics. The method is characterised by the partitioning of a domain into a collection of elements, assuming a simple (polynomial) form for the solution on each element, and from these elements assembling a global system of simultaneous equations to be solved. An explicit approximation of the solution is made at an element level by using shape functions to relate the nodal degrees of freedom to the approximation.

In the finite element method global function spaces of admissible solutions (trial functions) and arbitrary (test) functions are defined and built up element-wise by local function spaces. These spaces contain functions that are globally continuous on the domain and are square-integrable. Globally continuous polynomial approximations of the local function spaces are then made such that the approximations of the test and trial functions are of the same order. Low-order finite element methods are susceptible to numerical pathologies such as locking when modelling nearly incompressible materials. This has been remedied in various ways, for example, through the use of mixed and under-integrated methods, and discontinuous Galerkin methods.

1.2.1.1 Mixed finite element methods

An alternative approach to solving the problem of locking in low-order finite element methods is to use a mixed formulation. Mixed methods [9, 11] introduce an additional variable in the form of a Lagrange multiplier to the relevant constraint. This additional degree of freedom prevents the artificial stiffening that arises when modelling near-incompressible materials with standard finite element methods and circumvents locking. When using mixed formulations it is important to choose appropriate elements to approximate the primary and secondary variables to ensure convergence. It has been shown that in particular cases there is an equivalence between selective under-integration of standard finite element methods and mixed methods [12, 13].

1.2.1.2 Discontinuous methods

Discontinuous methods [14] are similar to standard finite element methods, the distinction being that the global function spaces are now discontinuous across element boundaries. This discontinuity makes for a more inclusive function space than with conforming finite element methods. Discontinuous methods allow greater flexibility with regard to meshing, and when designed appropriately, are stable and uniformly convergent even in situations of near-incompressibility for low-order approximations [15, 16, 17].

1.2.2 Virtual element methods

A recent, and rapidly developing, approach to approximating the solution to PDEs is the virtual element method. The VEM permits elements to be arbitrary polyhedra in three dimensions and arbitrary polygons in two. Elements need not be convex, may contain co-planar or collinear edges, and may have arbitrarily small edges. The VEM formulation is very robust and the flexibility of meshing allows meshes to be easily constructed on complex domains. There has been much work on the mathematical formulation of the method and its application and implementation to 2D and 3D problems. Notable early contributions [18, 19] considered the application of the method to the Poisson equation in two dimensions. The method was then extended to two and three dimensional linear elasticity in [20, 21]. In [22] a second order mixed virtual element formulation was developed for two dimensional linear elasticity problems involving near-incompressibility. The successes of the VEM in modelling linear elasticity problems spurred the development of a virtual element for non-linear elasticity problems involving finite deformations of isotropic materials [23, 24], elastoplasticity [25, 20, 26] and contact [27].

In the context of elasticity problems the VEM has been applied largely to isotropic materials. There has, however, been some investigation into the treatment of isotropic materials with inextensible fibres [28]. The VEM can be easily extended from the case of linear isotropic elasticity problems to include the behaviour of homogeneous anisotropic materials. Challenges arise, however, for problems involving non-homogeneous anisotropic materials, in which material properties vary spatially.

1.2.3 Transversely isotropic materials

Transversely isotropic materials [29, 30, 31] are a class of anisotropic materials characterised by an axis of symmetry perpendicular to a plane of isotropy. The transversely isotropic material model has applications ranging from fibre-reinforced composites [32] to biological tissues, such as collagen [33] and ligaments [34, 35], wood [36], and even rock mechanics [37]. To illustrate the nature of transversely isotropic materials we present in Figure 1.1 examples of these materials. Figure 1.1(a) shows a homogeneous fibre-reinforced material, Figure 1.1(b) shows a ligament, Figure 1.1(c) shows wood as an non-homogeneous transversely isotropic material with a spatially varying fibre orientation, and Figure 1.1(d) shows rock strata as a non-homogeneous transversely isotropic laminar material with properties varying through the thickness of the material.

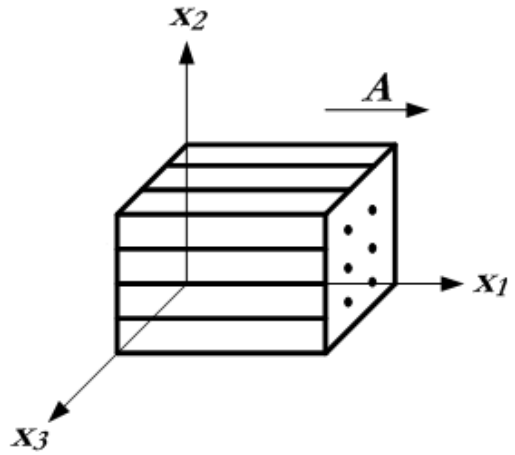

(a) Fibre-reinforced material [38]

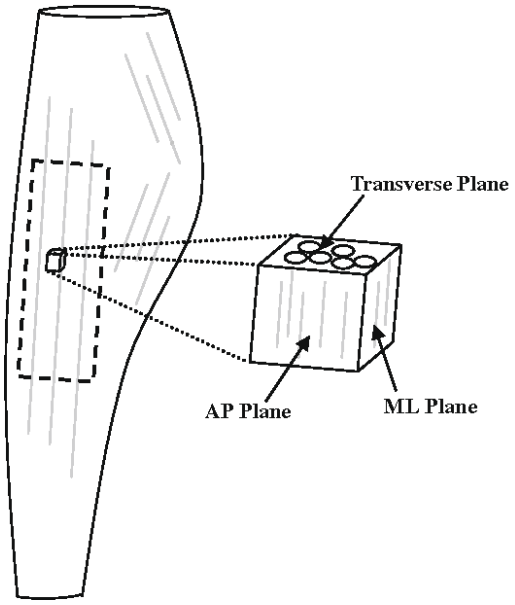

(b) Transversely isotropic ligament [35]

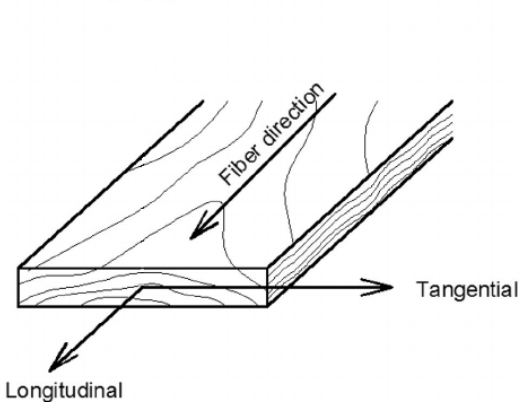

(c) Transversely isotropic wood [39]

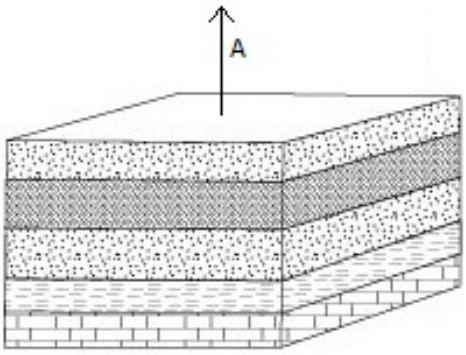

(d) Transversely isotropic rock [40]

Figure 1.1 Transversely isotropic materials exemplified by (a) fibre-reinforced material, (b) ligament, (c) wood, and (d) rock strata

The wide range of applications warrants a thorough analysis of and development of computational models for the material. In [41] a detailed treatment of the boundary value problem for homogeneous transversely isotropic linear elastic materials is presented and conditions for well-posedness are established. The work extends the treatment in [42] in which limiting extensibilty is investigated in an otherwise isotropic material. There has been little investigation of the effects of and numerical pathologies arising from inextensible or nearly inextensible fibres with varying fibre orientation. Further, there has been little investigation into the effects of the degree of inhomogeneity beyond simple functionally graded materials [43, 44].

1.3 Objectives

In this work we aim to apply the virtual element method to elasticity problems involving both homogeneous and non-homogeneous materials and compare the ability of the VEM to model these materials with respect to that of the finite element method. We aim to investigate the ability of the VEM to model near-incompressible materials and near-inextensible fibres. Additionally, we aim to investigate the effects of fibre orientation for homogeneous transversely isotropic materials and that of the degree of inhomogeneity of fibres for non-homogeneous transversely isotropic materials. These effects are to be investigated for varying degrees of anisotropy.

The objectives of this work are therefore to:

1. Formulate and implement a virtual element method for plane homogeneous linear elasticity problems
2. Investigate the ability of the VEM to model nearly incompressible isotropic materials
3. Investigate the effect of the degree of anisotropy for homogeneous transversely isotropic materials
4. Extend the VEM to accommodate non-homogeneous transversely isotropic materials
5. Investigate the convergence behaviour of the VEM in modelling non-homogeneous materials
6. Investigate the effects of the degree of anisotropy on compressible and nearly incompressible non-homogeneous transversely isotropic materials

Limitations and scope This work is limited to plane problems under the assumption of plane strain. Further, the displacements are considered to be small and as such, materials are modelled as linear elastic. Finally, the formulation of the virtual element method is limited to low order elements for which displacements are piecewise linear along the edges of elements.

1.4 Plan of development

The plan of the rest of this work is as follows. In Chapter 2 we present the governing equations of linear elasticity problems and derive a weak formulation of the problem. We then derive general constitutive relations for linear elasticity and apply symmetry transformations to form the reduced relations for orthotropic, transversely isotropic, and isotropic materials. We then present the material parameters and conditions for well-posedness of isotropic and transversely isotropic materials. In Chapter 3 we present a detailed formulation of the virtual element method followed by a sample implementation of the method for a homogeneous transversely isotropic material in Chapter 4. In Chapter 5 we present the results of numerical tests for homogeneous materials. We present the results for compressible and nearly incompressible materials, followed by those of nearly incompressible homogeneous transversely isotropic materials for a range of fibre parameters. In Chapter 6 we present results of numerical tests for non-homogeneous transversely isotropic materials. We present results for varying degrees of inhomogeneity and anisotropy for both compressible and nearly incompressible materials. We conclude the work in Chapter 7 with a discussion of the results and some concluding remarks.

Chapter 2

Governing equations

In this chapter we present the governing equations of the boundary value problem for linear elasticity followed by a derivation of a weak formulation of the problem. We then derive the most general constitutive relations for linear elasticity before reducing these relations to orthotropic, transversely isotropic and isotropic material models. Thereafter we provide more detail on the components of the transversely isotropic constitutive tensor and present requirements for positive definiteness and pointwise stability of isotropic and transversely isotropic constitutive relations.

In this chapter and throughout we use a combination of coordinate free and index notations. We choose a fixed Cartesian coordinate system x_i with orthonormal basis e_i. In coordinate free notation we denote scalar quantities by lower case Roman or Greek letters, vector quantities by bold Roman letters, second-order tensors by bold upper case Roman letters or bold lower case Greek letters and fourth-order tensors by calligraphic letters. This general notation is exemplified in Table 2.1.

Quantity	Coordinate Free Notation	Index Notation
Scaler	a, b, α, β	a, b, α, β
Vector	$\boldsymbol{a}, \boldsymbol{u}$	a_i, u_i
Second-Order Tensor	$\boldsymbol{Q}, \boldsymbol{\sigma}, \boldsymbol{\varepsilon}$	$Q_{ij}, \sigma_{ij}, \varepsilon_{ij}$
Fourth-Order Tensor	$\mathbb{C}$	$\mathbb{C}_{ijkl}$

Table 2.1 *Generalised notation*

Further, we denote prescribed quantities by an over-bar, e.g. $\bar{\boldsymbol{t}}$, $\bar{\boldsymbol{u}}$, and nodal values with a hat, e.g. $\hat{\boldsymbol{u}}$ and $\hat{\boldsymbol{v}}$.

2.1 Governing equations of continuous media

Consider an arbitrary elastic body occupying a bounded domain $\Omega \in \mathbb{R}^d$, $d = \{2, 3\}$, shown in Figure 2.1 for $d = 2$. The body has boundary $\Gamma = \Gamma_d \cup \Gamma_n$ with outward facing normal $\boldsymbol{n}$ and with Γ_d and Γ_n denoting the Dirichlet and Neumann boundaries respectively, with $\Gamma_d \cap \Gamma_n = 0$. The body is subjected to a body force $\boldsymbol{b}$, a prescribed traction $\bar{\boldsymbol{t}}$ and a prescribed displacement $\bar{\boldsymbol{u}}$ on Γ_d.

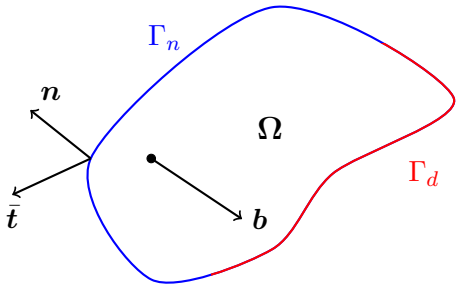

Figure 2.1 Arbitrary elastic body

Hereinafter we will denote by $\boldsymbol{u}$ the displacement field, by $\boldsymbol{\varepsilon}$ the strain field obtained from the symmetric gradient operator $\boldsymbol{\varepsilon} = \boldsymbol{\varepsilon}(\boldsymbol{u})$, and the stress field by $\boldsymbol{\sigma}$. Assuming infinitesimal deformations the governing equations are:

$$\text{equilibrium equation:} \qquad \text{div}\boldsymbol{\sigma} + \boldsymbol{b} = \boldsymbol{0} \tag{2.1}$$

$$\text{Hooke's law:} \qquad \boldsymbol{\sigma} = \mathbb{C}\boldsymbol{\varepsilon} \tag{2.2}$$

$$\text{strain-displacement relation:} \qquad \boldsymbol{\varepsilon}(\boldsymbol{u}) = \frac{1}{2}(\nabla \boldsymbol{u} + [\nabla \boldsymbol{u}]^T) \quad \text{or} \quad \varepsilon_{ij}(\boldsymbol{u}) = \frac{1}{2}(u_{i,j} + u_{j,i}) \tag{2.3}$$

where $\mathbb{C}$ denotes the elasticity tensor, with boundary conditions

$$\boldsymbol{\sigma} \cdot \boldsymbol{n} = \bar{\boldsymbol{t}} \qquad \text{on } \Gamma_n, \tag{2.4}$$

$$\boldsymbol{u} = \bar{\boldsymbol{u}} \qquad \text{on } \Gamma_d. \tag{2.5}$$

Equations (2.1)-(2.5) constitute the boundary value problem for linear elastic bodies.

2.2 Weak formulation

As required for finite element methods, we construct a weak formulation of the boundary value problem. The weak formulation serves to reduce the order of approximation and continuity requirements of the solution. A further benefit of the weak formulation is the naturally arising Neumann boundary conditions that are then easily applied.

We denote by $\mathcal{L}^2(\Omega)$ the space of square-integrable functions on Ω, and by $\mathcal{H}^1(\Omega)$ the Sobolev space of functions that, together with their first derivatives, are square-integrable, and set

$$\mathcal{V} = \left\{ \boldsymbol{v} \in \left[\mathcal{H}^1(\Omega)\right]^d : \boldsymbol{v}|_{\Gamma_d} = \boldsymbol{0} \right\}. \tag{2.6}$$

To account for the non-homogeneous boundary condition (equation (2.5)) we define the function $\boldsymbol{u}_d \in \left[\mathcal{H}^1(\Omega)\right]^d$ such that

$$\boldsymbol{u}_d|_{\Gamma_d} = \bar{\boldsymbol{u}}. \tag{2.7}$$

Multiplying equation (2.1) by an arbitrary function $\boldsymbol{v} \in \mathcal{V}$ and integrating over the domain we have

$$\int_\Omega \boldsymbol{v} \cdot \mathrm{div}\boldsymbol{\sigma} \; d\Omega + \int_\Omega \boldsymbol{v} \cdot \boldsymbol{b} \; d\Omega = 0 \qquad \forall \boldsymbol{v} \in \mathcal{V}. \tag{2.8}$$

Applying Green's theorem equation (2.8) becomes

$$\int_\Omega \boldsymbol{\varepsilon}(\boldsymbol{v}) : \boldsymbol{\sigma} \; d\Omega = \oint_\Gamma \boldsymbol{v} \cdot \boldsymbol{\sigma}\boldsymbol{n} \; d\Gamma + \int_\Omega \boldsymbol{v} \cdot \boldsymbol{b} \; d\Omega \qquad \forall \boldsymbol{v} \in \mathcal{V}. \tag{2.9}$$

We then incorporate the Neumann boundary condition and use (2.6); these yield

$$\int_\Omega \boldsymbol{\varepsilon}(\boldsymbol{v}) : \boldsymbol{\sigma} \; d\Omega = \int_{\Gamma_n} \boldsymbol{v} \cdot \bar{\boldsymbol{t}} \; d\Gamma + \int_\Omega \boldsymbol{v} \cdot \boldsymbol{b} \; d\Omega \qquad \forall \boldsymbol{v} \in \mathcal{V}. \tag{2.10}$$

The bilinear form $a(\cdot,\cdot)$ and the linear functional $\ell(\cdot)$ are defined by

$$a : [\mathcal{H}^1(\Omega)]^d \times [\mathcal{H}^1(\Omega)]^d \to \mathbb{R}, \qquad a(\boldsymbol{u},\boldsymbol{v}) = \int_\Omega \boldsymbol{\sigma}(\boldsymbol{u}) : \boldsymbol{\varepsilon}(\boldsymbol{v}) \; d\Omega, \tag{2.11a}$$

$$\ell : [\mathcal{H}^1(\Omega)]^d \to \mathbb{R}, \qquad \ell(\boldsymbol{v}) = \int_\Omega \boldsymbol{b} \cdot \boldsymbol{v} + \int_{\Gamma_n} \bar{\boldsymbol{t}} \cdot \boldsymbol{v} \; d\Gamma - a(\boldsymbol{u}_d, \boldsymbol{v}). \tag{2.11b}$$

The weak form of the problem is then as follows: given $\boldsymbol{b} \in [\mathcal{L}^2(\Omega)]^d$ and $\bar{\boldsymbol{t}} \in [\mathcal{L}^2(\Gamma_n)]^d$, find $\boldsymbol{U} \in [\mathcal{H}^1(\Omega)]^d$ such that $\boldsymbol{U} = \boldsymbol{u} + \boldsymbol{u}_d, \boldsymbol{u} \in \mathcal{V}$, and

$$a(\boldsymbol{u},\boldsymbol{v}) = \ell(\boldsymbol{v}) \qquad \forall \boldsymbol{v} \in \mathcal{V}. \tag{2.12}$$

2.3 Linear elasticity

We begin by defining a strain energy density function that relates the stored energy in a material per unit volume to the deformation. We will denote the strain energy density by ψ:

$$\psi = \hat{\psi}(\boldsymbol{\varepsilon}). \tag{2.13}$$

The stress is then obtained from

$$\boldsymbol{\sigma} = \frac{\partial \psi}{\partial \boldsymbol{\varepsilon}} \quad \text{or} \quad \sigma_{ij} = \frac{\partial \psi}{\partial \varepsilon_{ij}}. \tag{2.14}$$

For a linear elastic material the energy density function is given by

$$\psi = \frac{1}{2}\boldsymbol{\varepsilon} : \mathbb{C}\boldsymbol{\varepsilon} = \frac{1}{2}\mathbb{C}_{ijkl}\varepsilon_{ij}\varepsilon_{kl}, \tag{2.15}$$

from which we obtain the Hookean relation [45]

$$\boldsymbol{\sigma} = \mathbb{C}\boldsymbol{\varepsilon} \quad \text{or} \quad \sigma_{ij} = \mathbb{C}_{ijkl}\varepsilon_{kl}. \tag{2.16}$$

Here $\mathbb{C}$ is a fourth order constitutive tensor with 81 components generally. Since $\boldsymbol{\sigma}$ and $\boldsymbol{\varepsilon}$ are symmetric it follows that we have the symmetries

$$\mathbb{C}_{ijkl} = \mathbb{C}_{jikl} \quad \text{and} \quad \mathbb{C}_{ijkl} = \mathbb{C}_{ijlk}. \tag{2.17}$$

This reduces the number of components from 81 to 36. Finally, since

$$\mathbb{C}_{ijkl} = \frac{\partial^2\hat{\psi}}{\partial\varepsilon_{kl}\partial\varepsilon_{ij}} = \frac{\partial^2\hat{\psi}}{\partial\varepsilon_{ij}\partial\varepsilon_{kl}} = \mathbb{C}_{klij} \tag{2.18}$$

it follows that the number of independent components of $\mathbb{C}$ is reduced to 21.

2.3.1 Material classes

In this section we present the formulation of a few common material classes by using material symmetries. Each symmetry results in invariance of the constitutive tensor to specific symmetry transformations. We represent these symmetry transformations by orthogonal second order tensors $\boldsymbol{Q}$ such that $\boldsymbol{Q}^{-1} = \boldsymbol{Q}^T$ and [45]:

$$det(Q_{ij}) = \begin{cases} +1 & \text{rotation,} \\ -1 & \text{reflection.} \end{cases}$$

The constitutive tensor under these transformations is then expressed as

$$\mathbb{C}_{ijkl} = Q_{ip}Q_{jq}Q_{kr}Q_{ls}\mathbb{C}_{pqrs}. \tag{2.19}$$

For the purposes of illustrating the effects of the symmetry transformations we introduce Voigt notation which allows us to express the fourth-order constitutive tensor as a second order tensor. Consider first the general second-order stress and strain tensors:

$$\boldsymbol{\sigma} = \begin{bmatrix} \sigma_{11} & \sigma_{12} & \sigma_{13} \\ \sigma_{21} & \sigma_{22} & \sigma_{23} \\ \sigma_{31} & \sigma_{32} & \sigma_{33} \end{bmatrix}, \qquad \boldsymbol{\varepsilon} = \begin{bmatrix} \varepsilon_{11} & \varepsilon_{12} & \varepsilon_{13} \\ \varepsilon_{21} & \varepsilon_{22} & \varepsilon_{23} \\ \varepsilon_{31} & \varepsilon_{32} & \varepsilon_{33} \end{bmatrix}.$$

These symmetric tensors have 6 unique components and can be expressed as vector quantities by

$$\boldsymbol{\sigma}^{\mathrm{V}} = \begin{bmatrix} \sigma_{11} \\ \sigma_{22} \\ \sigma_{33} \\ \sigma_{23} \\ \sigma_{13} \\ \sigma_{12} \end{bmatrix}, \qquad \boldsymbol{\varepsilon}^{\mathrm{V}} = \begin{bmatrix} \varepsilon_{11} \\ \varepsilon_{22} \\ \varepsilon_{33} \\ 2\varepsilon_{23} \\ 2\varepsilon_{13} \\ 2\varepsilon_{12} \end{bmatrix},$$

where to preserve the symmetry of the shear stress-strain relations we multiply the shear strains by 2. We are then able to express the constitutive relation as [45]

$$\begin{bmatrix} \sigma_{11} \\ \sigma_{22} \\ \sigma_{33} \\ \sigma_{23} \\ \sigma_{13} \\ \sigma_{12} \end{bmatrix} = \begin{bmatrix} \mathbb{C}_{1111} & \mathbb{C}_{1122} & \mathbb{C}_{1133} & \mathbb{C}_{1123} & \mathbb{C}_{1113} & \mathbb{C}_{1112} \\ & \mathbb{C}_{2222} & \mathbb{C}_{2233} & \mathbb{C}_{2223} & \mathbb{C}_{2213} & \mathbb{C}_{2212} \\ & & \mathbb{C}_{3333} & \mathbb{C}_{3323} & \mathbb{C}_{3313} & \mathbb{C}_{3312} \\ & & & \mathbb{C}_{2323} & \mathbb{C}_{2313} & \mathbb{C}_{2312} \\ & \text{sym} & & & \mathbb{C}_{1313} & \mathbb{C}_{1312} \\ & & & & & \mathbb{C}_{1212} \end{bmatrix} \begin{bmatrix} \varepsilon_{11} \\ \varepsilon_{22} \\ \varepsilon_{33} \\ 2\varepsilon_{23} \\ 2\varepsilon_{13} \\ 2\varepsilon_{12} \end{bmatrix}. \tag{2.20}$$

2.3.1.1 Orthotropic materials

Orthotropic materials have three mutually orthogonal planes of reflection symmetry. These symmetry transformations are given by

$$\boldsymbol{Q}^a = \begin{bmatrix} -1 & 0 & 0 \\ 0 & 1 & 0 \\ 0 & 0 & 1 \end{bmatrix}, \quad \boldsymbol{Q}^b = \begin{bmatrix} 1 & 0 & 0 \\ 0 & -1 & 0 \\ 0 & 0 & 1 \end{bmatrix} \text{ and } \quad \boldsymbol{Q}^c = \begin{bmatrix} 1 & 0 & 0 \\ 0 & 1 & 0 \\ 0 & 0 & -1 \end{bmatrix}.$$

Applying these symmetry relations by using equation (2.19) reduces the number of independent components of $\mathbb{C}$. For example, consider the relation $\boldsymbol{Q}^c$, for $\mathbb{C}_{1111}$ we have

$$\begin{aligned} \mathbb{C}_{1111} &= Q^c_{1p} Q^c_{1q} Q^c_{1r} Q^c_{1s} \mathbb{C}_{pqrs} \\ &= \delta_{1p}\delta_{1q}\delta_{1r}\delta_{1s}\mathbb{C}_{pqrs} \\ &= \mathbb{C}_{1111}. \end{aligned}$$

The component $\mathbb{C}_{1111}$ is therefore unaffected by this transformation. Consider now the component $\mathbb{C}_{1123}$; we have

$$\begin{aligned}\mathbb{C}_{1123} &= Q^c_{1p}Q^c_{1q}Q^c_{2r}Q^c_{3s}\mathbb{C}_{pqrs}\\ &= \delta_{1p}\delta_{1q}\delta_{2r}(-\delta_{3s})\mathbb{C}_{pqrs}\\ &= -\mathbb{C}_{1123},\end{aligned}$$

which is only satisfied if $\mathbb{C}_{1123} = 0$, thus eliminating a component of $\mathbb{C}$. After applying all three symmetry relations we find that orthotropic materials have 9 independent components [46]; that is,

$$\begin{bmatrix}\sigma_{11}\\ \sigma_{22}\\ \sigma_{33}\\ \sigma_{23}\\ \sigma_{13}\\ \sigma_{12}\end{bmatrix} = \begin{bmatrix}\mathbb{C}_{1111} & \mathbb{C}_{1122} & \mathbb{C}_{1133} & 0 & 0 & 0\\ & \mathbb{C}_{2222} & \mathbb{C}_{2233} & 0 & 0 & 0\\ & & \mathbb{C}_{3333} & 0 & 0 & 0\\ & & & \mathbb{C}_{2323} & 0 & 0\\ & \text{sym} & & & \mathbb{C}_{1313} & 0\\ & & & & & \mathbb{C}_{1212}\end{bmatrix}\begin{bmatrix}\varepsilon_{11}\\ \varepsilon_{22}\\ \varepsilon_{33}\\ 2\varepsilon_{23}\\ 2\varepsilon_{13}\\ 2\varepsilon_{12}\end{bmatrix}. \tag{2.21}$$

2.3.1.2 Transversely isotropic materials

Transversely isotropic materials are characterised by a single plane of isotropy. These materials have three mutually orthogonal planes of reflection symmetry, as with orthotropic materials, plus an axial symmetry. Assuming symmetry about the z-axis we have the following transformations:

$$\boldsymbol{Q}^a = \begin{bmatrix}-1 & 0 & 0\\ 0 & 1 & 0\\ 0 & 0 & 1\end{bmatrix}, \qquad \boldsymbol{Q}^b = \begin{bmatrix}1 & 0 & 0\\ 0 & -1 & 0\\ 0 & 0 & 1\end{bmatrix},$$

$$\boldsymbol{Q}^c = \begin{bmatrix}1 & 0 & 0\\ 0 & 1 & 0\\ 0 & 0 & -1\end{bmatrix}, \qquad \boldsymbol{Q}^d = \begin{bmatrix}\cos\theta & \sin\theta & 0\\ -\sin\theta & \cos\theta & 0\\ 0 & 0 & 1\end{bmatrix} \text{ with } 0 \leq \theta \leq 2\pi,$$

which reduce the number of independent components of $\mathbb{C}$ to 5:

$$\begin{bmatrix} \sigma_{11} \\ \sigma_{22} \\ \sigma_{33} \\ \sigma_{23} \\ \sigma_{13} \\ \sigma_{12} \end{bmatrix} = \begin{bmatrix} \mathbb{C}_{1111} & \mathbb{C}_{1122} & \mathbb{C}_{1133} & 0 & 0 & 0 \\ & \mathbb{C}_{1111} & \mathbb{C}_{1133} & 0 & 0 & 0 \\ & & \mathbb{C}_{3333} & 0 & 0 & 0 \\ & & & \mathbb{C}_{2323} & 0 & 0 \\ & \text{sym} & & & \mathbb{C}_{2323} & 0 \\ & & & & & \frac{1}{2}\left(\mathbb{C}_{1111} - \mathbb{C}_{1122}\right) \end{bmatrix} \begin{bmatrix} \varepsilon_{11} \\ \varepsilon_{22} \\ \varepsilon_{33} \\ 2\varepsilon_{23} \\ 2\varepsilon_{13} \\ 2\varepsilon_{12} \end{bmatrix}. \tag{2.22}$$

2.3.1.3 Isotropic materials

The simplest class of materials is isotropic materials; these are materials that exhibit identical properties in all directions. Isotropic materials are defined by 2 independent material parameters. The general isotropic stress-strain relation is given by

$$\begin{bmatrix} \sigma_{11} \\ \sigma_{22} \\ \sigma_{33} \\ \sigma_{23} \\ \sigma_{13} \\ \sigma_{12} \end{bmatrix} = \begin{bmatrix} \mathbb{C}_{1111} & \mathbb{C}_{1122} & \mathbb{C}_{1122} & 0 & 0 & 0 \\ & \mathbb{C}_{1111} & \mathbb{C}_{1122} & 0 & 0 & 0 \\ & & \mathbb{C}_{1111} & 0 & 0 & 0 \\ & & & \mathbb{C}_{2323} & 0 & 0 \\ & \text{sym} & & & \mathbb{C}_{2323} & 0 \\ & & & & & \mathbb{C}_{2323} \end{bmatrix} \begin{bmatrix} \varepsilon_{11} \\ \varepsilon_{22} \\ \varepsilon_{33} \\ 2\varepsilon_{23} \\ 2\varepsilon_{13} \\ 2\varepsilon_{12} \end{bmatrix}. \tag{2.23}$$

In terms of the Lamé parameters λ and μ this becomes

$$\boldsymbol{\sigma} = \lambda \mathrm{tr}\boldsymbol{\varepsilon}\boldsymbol{I} + 2\mu\boldsymbol{\varepsilon} \tag{2.24}$$

or, in matrix form,

$$\begin{bmatrix} \sigma_{11} \\ \sigma_{22} \\ \sigma_{33} \\ \sigma_{23} \\ \sigma_{13} \\ \sigma_{12} \end{bmatrix} = \begin{bmatrix} \lambda+2\mu & \lambda & \lambda & 0 & 0 & 0 \\ & \lambda+2\mu & \lambda & 0 & 0 & 0 \\ & & \lambda+2\mu & 0 & 0 & 0 \\ & & & \mu & 0 & 0 \\ & \text{sym} & & & \mu & 0 \\ & & & & & \mu \end{bmatrix} \begin{bmatrix} \varepsilon_{11} \\ \varepsilon_{22} \\ \varepsilon_{33} \\ 2\varepsilon_{23} \\ 2\varepsilon_{13} \\ 2\varepsilon_{12} \end{bmatrix}. \tag{2.25}$$

The Lamé parameters may be expressed in terms of Young's modulus E_y and Poisson's ratio ν; that is,

$$\lambda = \frac{E_y \nu}{(1+\nu)(1-2\nu)}, \tag{2.26}$$

$$\mu = \frac{E_y}{2(1+\nu)}. \tag{2.27}$$

For positive definiteness of the strain energy we require [47]

$$\boldsymbol{\varepsilon} : \mathbb{C}\boldsymbol{\varepsilon} > 0 \qquad \forall \boldsymbol{\varepsilon}, \tag{2.28}$$

for which the conditions

$$\lambda + \frac{2}{3}\mu > 0 \quad \text{and} \tag{2.29}$$

$$\mu > 0 \tag{2.30}$$

are sufficient and assumed to hold. We denote by k the bulk modulus which relates hydrostatic pressure to volumetric strain by

$$\mathrm{tr}\boldsymbol{\sigma} = k\mathrm{tr}\boldsymbol{\varepsilon}, \tag{2.31}$$

where k is given by

$$k = \lambda + \frac{2}{3}\mu = \frac{E}{3(1-2\nu)}. \tag{2.32}$$

The implication of equation (2.31) is that as $k \to \infty$, $tr(\boldsymbol{\varepsilon}) \to 0$ which corresponds to zero volume change, called incompressibility. From equation (2.32) it is clear that we approach incompressibility as $\nu \to 0.5$ and $\lambda \to \infty$.

2.4 Transversely isotropic materials

For a transversely isotropic linearly elastic material with fibre direction given by the unit vector $\boldsymbol{a}$, the constitutive tensor is given by (see [41])

$$\begin{aligned}
&\mathbb{C} = \lambda \boldsymbol{I} \otimes \boldsymbol{I} + 2\mu_T \mathbb{I} + \beta \boldsymbol{M} \otimes \boldsymbol{M} + \alpha \left(\boldsymbol{I} \otimes \boldsymbol{M} + \boldsymbol{M} \otimes \boldsymbol{I} \right) + \gamma \mathbb{M} \\
&\text{or} \\
&\mathbb{C}_{ABCD} = \lambda \delta_{AB} \delta_{CD} + 2\mu_T \delta_{AC} \delta_{BD} + \beta M_{AB} M_{CD} + \alpha \left(\delta_{AB} M_{CD} + M_{AB} \delta_{CD} \right) \\
&\qquad + 2 \left(\mu_L - \mu_T \right) \left(\delta_{AC} M_{BD} + M_{AC} \delta_{BD} \right),
\end{aligned} \tag{2.33}$$

with $\boldsymbol{I}$ the second order identity tensor, $\mathbb{I}$ the fourth order identity tensor, $\boldsymbol{M} = \boldsymbol{a} \otimes \boldsymbol{a}$ and $\mathbb{M}$ the fourth order tensor defined by

$$\mathbb{M}\boldsymbol{R} = \boldsymbol{M}\boldsymbol{R} + \boldsymbol{R}\boldsymbol{M} \quad \text{for any second-order tensor } \boldsymbol{R}. \tag{2.34}$$

As with isotropic materials, λ denotes the first Lamé parameter, with μ_L the shear modulus in the longitudinal direction, and μ_T the shear modulus in the plane of isotropy. Additionally γ is defined as

$$\gamma = 2(\mu_L - \mu_T). \tag{2.35}$$

The linear stress-strain relation is then given by

$$\begin{aligned}
&\boldsymbol{\sigma} = \lambda (tr\boldsymbol{\varepsilon}) \boldsymbol{I} + 2\mu_T \boldsymbol{\varepsilon} + \beta (\boldsymbol{M} : \boldsymbol{\varepsilon}) \boldsymbol{M} + \alpha ((\boldsymbol{M} : \boldsymbol{\varepsilon}) \boldsymbol{I} + (tr\boldsymbol{\varepsilon}) \boldsymbol{M}) + 2(\mu_L - \mu_T)(\boldsymbol{\varepsilon}\boldsymbol{M} + \boldsymbol{M}\boldsymbol{\varepsilon}) \\
&\text{or} \\
&\sigma_{ij} = \lambda \varepsilon_{kk} \delta_{ij} + 2\mu_T \varepsilon_{ij} + \beta M_{kl} \varepsilon_{kl} M_{ij} + \alpha \left(M_{kl} \varepsilon_{kl} \delta_{ij} + \varepsilon_{kk} M_{ij} \right) + 2(\mu_L - \mu_T)(\varepsilon_{ik} M_{kj} + M_{ik} \varepsilon_{kj}).
\end{aligned} \tag{2.36}$$

We can write the transversely isotropic material parameters in terms of more familiar engineering properties. We denote by E_L and ν_L the Young's modulus and Poisson's ratio in the longitudinal direction, and by E_T and ν_T the Young's modulus and Poisson's ratio in the plane of isotropy. We then have the relations (see [41])

$$\begin{aligned}
\lambda &= \frac{E_T(\nu_L^2 E_T + \nu_T E_L)}{(1+\nu_T)(E_L(1-\nu_T) - 2\nu_L^2 E_T)}, \\
\alpha &= \frac{E_T[E_L \nu_L (1+\nu_T) - \nu_L^2 E_T - \nu_T E_L]}{(1+\nu_T)(E_L(1-\nu_T) - 2\nu_L^2 E_T)}, \text{ and} \\
\beta &= \frac{E_L^2(1-\nu_T^2) - E_T^2 \nu_L^2 + E_T E_L (1 - 2\nu_T \nu_L - 2\nu_L)}{(1+\nu_T)(E_L(1-\nu_T) - 2\nu_L^2 E_T)} - 4\mu_L.
\end{aligned} \tag{2.37}$$

Henceforth, to focus on behaviour in the incompressible and inextensible limits we will assume that

$$\begin{aligned} &\nu_L = \nu_T = \nu, \text{ and} \\ &\mu_T = \mu_L. \end{aligned} \tag{2.38}$$

Furthermore, we set

$$p = \frac{E_L}{E_T}. \tag{2.39}$$

Thus p will be used as a measure of the degree of anisotropy of a material. We can now write the transversely isotropic material properties in terms of p and the engineering properties as before with

$$\begin{aligned} \frac{\lambda}{E_T} &= \frac{\nu(\nu+p)}{(1+\nu)(p(1-\nu)-2\nu^2)}, \\ \frac{\alpha}{E_T} &= \frac{\nu^2(p-1)}{(1+\nu)(p(1-\nu)-2\nu^2)}, \text{ and} \\ \frac{\beta}{E_T} &= \frac{p^2(1-\nu^2)+p(1-2\nu-2\nu^2)-\nu^2}{(1+\nu)(p(1-\nu)-2\nu^2)} - \frac{1}{2(1+\nu)}. \end{aligned} \tag{2.40}$$

From equation (2.40) we note that

$$\begin{cases} \lambda \text{ is bounded as } \nu \to \frac{1}{2}, \text{ if } p > 1, \text{ and as } p \to \infty \text{ (inextensibility)} \\ \lambda \to \infty \text{ as } \nu \to \frac{1}{2}, \text{ for } p = 1 \text{ (isotropy)} \end{cases}$$

$$\begin{cases} \alpha \text{ is bounded as } \nu \to \frac{1}{2}, \text{ if } p > 1 \\ \alpha \to 0 \text{ as } p \to 1 \text{ (isotropy)} \end{cases}$$

$$\begin{cases} \beta \text{ is bounded as } \nu \to \frac{1}{2}, \text{ if } p > 1 \\ \beta \to \infty \text{ as } p \to \infty \text{ (inextensibility)} \end{cases}$$

We find that as $\nu \to \frac{1}{2}$, if $p = 1$ then $\lambda \to \infty$, corresponding to the normal case of isotropic near-incompressibility. Additionally, as $p \to \infty$ we find $\beta \to \infty$, corresponding to near-inextensibility. Sufficient conditions to ensure pointwise stability of transversely isotropic materials are (see [41])

$$\lambda + \frac{2}{3}\mu > 0, \tag{2.41}$$

$$\mu > 0, \text{ and} \tag{2.42}$$

$$p \geq 1. \tag{2.43}$$

We therefore assume these conditions to hold.

Hereinafter we will adopt the following notation to describe the orientation of fibres in transversely isotropic materials. We will denote by $a(\boldsymbol{x})$ the family of curves describing fibre position. The fibre orientation, or axis of symmetry, is then given by the unit tangent vector to $a(\boldsymbol{x})$, which we denote by $\boldsymbol{a}$ as before. In cases of constant fibre orientation we will denote by $\hat{a}$ the angle between the axis of symmetry $\boldsymbol{a}$ and the horizontal x-axis.

Chapter 3

Formulation of the virtual element method

In this chapter we develop the method of approximating the solution to problems posed by systems of partial differential equations using a virtual element method. The VEM is an adaptation of the finite element method that allows complete freedom in the selection of element geometries. We will develop a virtual element method formulation of the problem posed in Chapter 2 for two-dimensional problems.

We partition a two-dimensional polygonal domain Ω into a collection of non-overlapping polygons $\mathcal{T}_h$. These polygons need not be convex, may contain collinear edges and may have arbitrarily small edges. We however make the restrictions that each polygon must contain its own centroid, and must have finite area.

Consider an arbitrary element E depicted in Figure 3.1.

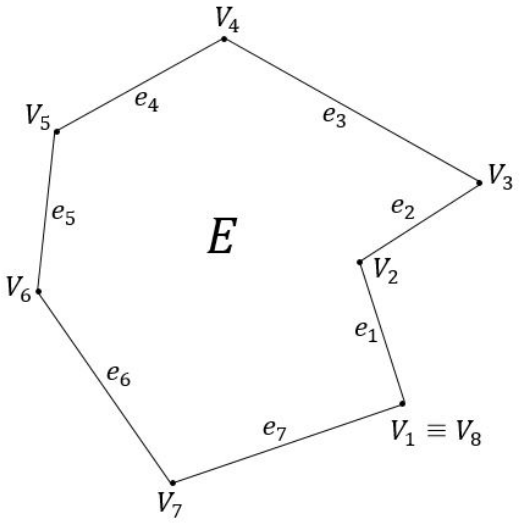

Figure 3.1 Arbitrary virtual element

We number the element vertices V_i counter-clockwise with indices in the range of 1 to n_V. We denote by e_i the edge connecting V_i and V_{i+1}; again the indices are in the range of 1 to n_V as $n_e = n_V$. The degrees of freedom, i.e. displacement, of some arbitrary function on an element are the values of the function evaluated at the element vertices. Therefore, $n_{dof} = 2n_V$ for two-dimensional problems.

3.1 Virtual element space

The virtual element space V_h is defined element-wise by defining local spaces $V_{h|E}$.
We construct a conforming approximation in a space $V_h \subset V$. The space V_h comprises functions that are continuous on Ω, piecewise linear on the boundary ∂E of each element, and with $\mathrm{div}\boldsymbol{\varepsilon}(\boldsymbol{v}_h)$ vanishing on E [18, 19]:

$$V_{h|E} = \left\{ \boldsymbol{v}_h \in V \;\middle|\; \boldsymbol{v}_h \in [C(\Omega)]^2 ,\ \mathrm{div}\boldsymbol{\varepsilon}(\boldsymbol{v}_h) = \mathbf{0} \text{ on } E,\ \boldsymbol{v}_h|_e \in \mathcal{P}_1(e) \right\}. \tag{3.1}$$

Here and henceforth $\mathcal{P}_1(X)$ denotes the space of polynomials of degree ≤ 1 on the set $X \subset \mathbb{R}^d$ $(d = 1, 2)$. The element-wise virtual displacement space is then given by

$$\boldsymbol{V}_{h|E} = \left[V_{h|E}\right]^2 . \tag{3.2}$$

Any function $\boldsymbol{v}_h$ in $V_{h|E}$ is therefore characterised by three important properties:

- $\boldsymbol{v}_h$ is a polynomial of degree ≤ 1 on ∂E,
- $\boldsymbol{v}_h$ is globally continuous on ∂E, and
- $\mathrm{div}\boldsymbol{\varepsilon}(\boldsymbol{v}_h) = \mathbf{0}$ on E.

3.2 L^2 projection

We introduce a projection operator Π_E^∇ that takes a function in the local virtual element space and projects it onto the subspace of constants, where the projection is defined by its gradient such that

$$\Pi^\nabla : \boldsymbol{V}_{h|E} \to [\mathcal{P}_0(E)]^2 , \text{ with} \tag{3.3}$$

$$\int_E \Pi_E^\nabla(\boldsymbol{v}_h)\, d\Omega = \int_E \boldsymbol{\varepsilon}(\boldsymbol{v}_h)\, d\Omega. \tag{3.4}$$

The operator represents the best approximation of the strain, using an $L^2(E)$ orthogonal projection, in the space of constants. Note: since $\Pi_E^\nabla(\boldsymbol{v}_h)$ is constant we can write

$$\Pi_E^\nabla(\boldsymbol{v}_h) = \frac{1}{|E|} \int_E \boldsymbol{\varepsilon}(\boldsymbol{v}_h)\, d\Omega, \tag{3.5}$$

which is equivalent to the mean value of the strain on an element.

3.2.1 VEM approximations

As with the finite element method we introduce approximations of the displacement and strain fields in terms of nodal degrees of freedom. We approximate the displacement field on an element by

$$\boldsymbol{u}_h = \boldsymbol{\phi}\hat{\boldsymbol{u}}_h|_E \tag{3.6}$$

where $\boldsymbol{\phi}$ is a $2 \times n_{dof}$ matrix; that is,

$$\boldsymbol{\phi} = \begin{bmatrix} \phi_1 & 0 & \phi_2 & 0 & \dots & 0 \\ 0 & \phi_1 & 0 & \phi_2 & \dots & \phi_{n_{dof}} \end{bmatrix}, \tag{3.7}$$

and ϕ_i is the basis function corresponding to the i^{th} degree of freedom. All computations will be carried out on the edges of elements, on which the basis functions are piecewise linear. Thus, the basis functions ϕ_i are not explicitly known and not required; they however collapse to simple Lagrangian functions on the boundary of an element:

$$\boldsymbol{u}_h|_{\partial E} = \boldsymbol{N}\hat{\boldsymbol{u}}_h, \text{ and} \tag{3.8}$$

$$\boldsymbol{\varepsilon}(\boldsymbol{u}_h) = \boldsymbol{B}\hat{\boldsymbol{u}}_h, \tag{3.9}$$

where we denote by $\hat{\boldsymbol{u}}_h$ the nodal values of $\boldsymbol{u}_h$.

3.2.2 Computing the projection

The projection of a function is constant for low-order virtual elements which allows us to write (3.4) as

$$\Pi_E^{\nabla}(\boldsymbol{u}_h) = \frac{1}{|E|}\int_E \boldsymbol{\varepsilon}(\boldsymbol{u}_h)d\Omega = \frac{1}{2}\frac{1}{|E|}\int_E \left[(u_h)_{i,j} + (u_h)_{j,i}\right] d\Omega. \tag{3.10}$$

Applying Green's theorem to equation (3.10) we get

$$\Pi_E^{\nabla}(\boldsymbol{u}_h) = \frac{1}{2}\frac{1}{|E|}\oint_{\partial E} \left[(u_h)_i n_j + (u_h)_j n_i\right] d\Gamma, \tag{3.11}$$

into which we substitute the approximation (3.8) yielding

$$\Pi_E^{\nabla}(\boldsymbol{u}_h) = \frac{1}{2}\frac{1}{|E|}\int_{e\in\partial E} \left[N_{ik}\hat{u}_k n_j + N_{jk}\hat{u}_k n_i\right] d\Gamma. \tag{3.12}$$

The integrals in (3.12) are computable as the basis functions are known on an element boundary. Thus the projection is available as a function of the nodal degrees of freedom.

3.3 Discrete bilinear form

To construct the virtual element formulation we begin with the discrete bilinear form

$$a_h^E(\boldsymbol{u},\boldsymbol{v}) = \int_E \boldsymbol{\varepsilon}(\boldsymbol{v}_h) : \mathbb{C}\boldsymbol{\varepsilon}(\boldsymbol{u}_h) d\Omega, \tag{3.13}$$

such that $a_h^E(\cdot,\cdot)$ denotes the contribution of element E to the bilinear form $a(\cdot,\cdot)$. We set

$$\boldsymbol{\varepsilon}(\boldsymbol{v}_h) = \Pi_E^\nabla(\boldsymbol{v}_h) + (\boldsymbol{\varepsilon}(\boldsymbol{v}_h) - \Pi_E^\nabla(\boldsymbol{v}_h)). \tag{3.14}$$

Substituting equation (3.14) into equation (3.13) we get

$$a_h^E(\boldsymbol{u},\boldsymbol{v}) = \int_E \left[\Pi_E^\nabla(\boldsymbol{v}_h) + (\boldsymbol{\varepsilon}(\boldsymbol{v}_h) - \Pi_E^\nabla(\boldsymbol{v}_h))\right] : \mathbb{C}\left[\Pi_E^\nabla(\boldsymbol{u}_h) + (\boldsymbol{\varepsilon}(\boldsymbol{u}_h) - \Pi_E^\nabla(\boldsymbol{u}_h))\right] d\Omega, \tag{3.15}$$

which we expand, yielding

$$\begin{aligned} a_h^E(\boldsymbol{u},\boldsymbol{v}) = &\int_E \Pi_E^\nabla(\boldsymbol{v}_h) : \mathbb{C}\Pi_E^\nabla(\boldsymbol{u}_h) d\Omega + \int_E \Pi_E^\nabla(\boldsymbol{v}_h) : \mathbb{C}\left(\boldsymbol{\varepsilon}(\boldsymbol{u}_h) - \Pi_E^\nabla(\boldsymbol{u}_h)\right) d\Omega \\ &+ \int_E \left(\boldsymbol{\varepsilon}(\boldsymbol{v}_h) - \Pi_E^\nabla(\boldsymbol{v}_h)\right) : \mathbb{C}\Pi_E^\nabla(\boldsymbol{u}_h) d\Omega + \int_E \left(\boldsymbol{\varepsilon}(\boldsymbol{v}_h) - \Pi_E^\nabla(\boldsymbol{v}_h)\right) : \mathbb{C}\left(\boldsymbol{\varepsilon}(\boldsymbol{u}_h) - \Pi_E^\nabla(\boldsymbol{u}_h)\right) d\Omega. \end{aligned} \tag{3.16}$$

From the equation (3.4) the second and third terms on the right hand side of equation (3.16) are zero. The discrete bilinear form is then made up of two terms; a consistency term and a stabilization term:

$$a_h^E(\boldsymbol{u},\boldsymbol{v}) = \underbrace{\int_E \Pi_E^\nabla(\boldsymbol{v}_h) : \mathbb{C}\Pi_E^\nabla(\boldsymbol{u}_h) d\Omega}_{\text{Consistency term}} + \underbrace{\int_E \left(\boldsymbol{\varepsilon}(\boldsymbol{v}_h) - \Pi_E^\nabla(\boldsymbol{v}_h)\right) : \mathbb{C}\left(\boldsymbol{\varepsilon}(\boldsymbol{u}_h) - \Pi_E^\nabla(\boldsymbol{u}_h)\right) d\Omega}_{\text{Stabilization term}}. \tag{3.17}$$

3.3.1 Consistent term

To compute the consistency term we substitute (3.12) into the consistency term in (3.17) which yields the expression

$$\int_E \Pi_E^\nabla(\boldsymbol{v}_h) : \mathbb{C}\Pi_E^\nabla(\boldsymbol{u}_h) d\Omega = \hat{\boldsymbol{v}}^T \boldsymbol{K}_c^E \hat{\boldsymbol{u}}, \tag{3.18}$$

in which $\boldsymbol{K}_c^E$ is the consistency stiffness matrix for element E.

3.3.2 Stabilization term

The basic idea behind the virtual element method is to only perform integrals on element boundaries, and as the basis functions ϕ_i are unknown on the interior of an element it is impossible to exactly compute the stabilization term and it must be approximated. There are several methods that can be employed, see for example [20, 21]. We choose to use the stabilization method presented in [48] as it has proven very robust. We present a derivation of this term.

We begin by expanding the stabilization term in (3.17):

$$a^E_{stab_h}(\boldsymbol{u},\boldsymbol{v}) = \int_E \boldsymbol{\varepsilon}(\boldsymbol{v}_h) : \mathbb{C}\boldsymbol{\varepsilon}(\boldsymbol{\varepsilon}(\boldsymbol{u}_h) - \Pi^\nabla_E(\boldsymbol{u}_h))d\Omega - \int_E \Pi^\nabla_E(\boldsymbol{v}_h) : \mathbb{C}(\boldsymbol{\varepsilon}(\boldsymbol{u}_h) - \Pi^\nabla_E(\boldsymbol{u}_h))d\Omega. \tag{3.19}$$

From the definition of the projection (3.4) the second term in (3.19) is equal to zero. We expand the remaining term to obtain

$$\begin{aligned} a^E_{stab_h}(\boldsymbol{u},\boldsymbol{v}) &= \int_E \boldsymbol{\varepsilon}(\boldsymbol{v}_h) : \mathbb{C}\boldsymbol{\varepsilon}(\boldsymbol{u}_h)d\Omega - \int_E \boldsymbol{\varepsilon}(\boldsymbol{v}_h) : \mathbb{C}\Pi^\nabla_E(\boldsymbol{u}_h)d\Omega \\ &= \int_E \boldsymbol{\varepsilon}(\boldsymbol{v}_h) : \mathbb{C}\boldsymbol{\varepsilon}(\boldsymbol{u}_h)d\Omega - \int_E \Pi^\nabla_E(\boldsymbol{v}_h) : \mathbb{C}\Pi^\nabla_E(\boldsymbol{u}_h)d\Omega \\ &- \int_E (\boldsymbol{\varepsilon}(\boldsymbol{v}_h) - \Pi^\nabla_E(\boldsymbol{v}_h)) : \mathbb{C}\Pi^\nabla_E(\boldsymbol{u}_h)d\Omega. \end{aligned} \tag{3.20}$$

From the definition (3.4) the third term in (3.20) is equal to zero, we therefore have

$$a^E_{stab_h}(\boldsymbol{u},\boldsymbol{v}) = \int_E \boldsymbol{\varepsilon}(\boldsymbol{v}_h) : \mathbb{C}\boldsymbol{\varepsilon}(\boldsymbol{u}_h)d\Omega - \int_E \Pi^\nabla_E(\boldsymbol{v}_h) : \mathbb{C}\Pi^\nabla_E(\boldsymbol{u}_h)d\Omega. \tag{3.21}$$

We will denote by $\boldsymbol{\mathcal{D}}$ the $n_{dof} \times 6$ matrix relating the nodal degrees of freedom of a linear vector polynomial $\boldsymbol{a}$ to its degrees of freedom $\boldsymbol{s}$ relative to a scaled linear monomial basis $(1, \xi, \eta)$:

$$\boldsymbol{a} = \boldsymbol{\mathcal{D}}\boldsymbol{s}_a. \tag{3.22}$$

We can then write the degrees of freedom of $\boldsymbol{v}_h$ and $\boldsymbol{u}_h$ in terms of linear approximations by

$$\hat{\boldsymbol{u}}^\Pi_h = \boldsymbol{\mathcal{D}}\boldsymbol{s}_u \tag{3.23}$$

$$\hat{\boldsymbol{v}}^\Pi_h = \boldsymbol{\mathcal{D}}\boldsymbol{s}_v. \tag{3.24}$$

The scaled linear basis monomials are given by

$$\xi(\boldsymbol{x}) = \frac{x - x_c}{d_E} \quad \text{, and} \quad \eta(\boldsymbol{x}) = \frac{y - y_c}{d_E}, \tag{3.25}$$

where d_E denotes the diameter of the element, which is defined as the largest distance between any two vertices of element E.

The matrix $\boldsymbol{\mathcal{D}}$ is given by

$$\boldsymbol{\mathcal{D}} = \begin{bmatrix} 1 & 0 & \xi(V_1) & 0 & \eta(V_1) & 0 \\ 0 & 1 & 0 & \xi(V_1) & 0 & \eta(V_1) \\ 1 & 0 & \xi(V_2) & 0 & \eta(V_2) & 0 \\ 0 & 1 & 0 & \xi(V_2) & 0 & \eta(V_2) \\ \vdots & \vdots & \vdots & \vdots & \vdots & \vdots \\ 1 & 0 & \xi(V_{n_V}) & 0 & \eta(V_{n_V}) & 0 \\ 0 & 1 & 0 & \xi(V_{n_V}) & 0 & \eta(V_{n_V}) \end{bmatrix}. \tag{3.26}$$

Here $\hat{\boldsymbol{u}}_h$ and $\hat{\boldsymbol{v}}_h$ are the exact nodal degrees of freedom of the trial and test functions, and $\hat{\boldsymbol{u}}_h^{\Pi}$ and $\hat{\boldsymbol{v}}_h^{\Pi}$ are the nodal degrees of freedom of linear approximations of the trial and test functions.
We now replace the stabilization term by the approximation

$$a^E_{stab_h}(\boldsymbol{u}, \boldsymbol{v}) \approx C(\hat{\boldsymbol{v}}_h^T \hat{\boldsymbol{u}}_h - \hat{\boldsymbol{v}}_h^{\Pi^T} \hat{\boldsymbol{u}}_h^{\Pi}) \tag{3.27}$$

where C is a suitable scalar. We then have

$$\begin{aligned} a^E_{stab_h}(\boldsymbol{u}, \boldsymbol{v}) &= C\left[\hat{\boldsymbol{v}}_h^T \hat{\boldsymbol{u}}_h - \boldsymbol{s}_v^T \boldsymbol{\mathcal{D}}^T \boldsymbol{\mathcal{D}} \boldsymbol{s}_u\right] && (3.28)\\ &= C\left[\hat{\boldsymbol{v}}_h^T \hat{\boldsymbol{u}}_h - \boldsymbol{s}_v^T \boldsymbol{\mathcal{D}}^T \boldsymbol{\mathcal{D}} \left(\boldsymbol{\mathcal{D}}^T \boldsymbol{\mathcal{D}}\right)^{-1} \left(\boldsymbol{\mathcal{D}}^T \boldsymbol{\mathcal{D}}\right) \boldsymbol{s}_u\right] && (3.29)\\ &= C\left[\hat{\boldsymbol{v}}_h^T \hat{\boldsymbol{u}}_h - \hat{\boldsymbol{v}}_h^T \boldsymbol{\mathcal{D}}^{-T} \boldsymbol{\mathcal{D}}^T \boldsymbol{\mathcal{D}} \left(\boldsymbol{\mathcal{D}}^T \boldsymbol{\mathcal{D}}\right)^{-1} \boldsymbol{\mathcal{D}}^T \boldsymbol{\mathcal{D}} \boldsymbol{\mathcal{D}}^{-1} \hat{\boldsymbol{u}}_h\right] && (3.30)\\ &= C\hat{\boldsymbol{v}}_h^T \left[\boldsymbol{I} - \boldsymbol{\mathcal{D}} \left(\boldsymbol{\mathcal{D}}^T \boldsymbol{\mathcal{D}}\right)^{-1} \boldsymbol{\mathcal{D}}^T\right] \hat{\boldsymbol{u}}_h. && (3.31) \end{aligned}$$

We need to choose a suitable value for the scalar C, which needs to be some value representative of the constitutive tensor. We consider the transversely isotropic material properties λ, α, β and μ_T. As seen in Section 2.4 $\lambda, \beta \to \infty$ as $\nu \to 0.5$, to keep the VEM locking free we therefore reject these options. We choose $C = \mu_T$ as it is bounded and is representative of both isotropic and transversely isotropic materials. We then have

$$\boldsymbol{K}^E_{stab} = \mu_T \left[\boldsymbol{I} - \boldsymbol{\mathcal{D}} \left(\boldsymbol{\mathcal{D}}^T \boldsymbol{\mathcal{D}}\right)^{-1} \boldsymbol{\mathcal{D}}^T\right]. \tag{3.32}$$

As we have used scaled coordinates no area scaling of the stabilisation term is necessary. In the case of isotropic materials equation (3.32) is simply given by

$$\boldsymbol{K}^E_{stab} = \mu \left[\boldsymbol{I} - \boldsymbol{\mathcal{D}} \left(\boldsymbol{\mathcal{D}}^T \boldsymbol{\mathcal{D}}\right)^{-1} \boldsymbol{\mathcal{D}}^T\right].$$

The complete stiffness matrix is then given by

$$\boldsymbol{K}^E = \boldsymbol{K}_c^E + \boldsymbol{K}_{stab}^E. \tag{3.33}$$

3.4 Loading term

From equation (2.11b) the loading term (linear functional) has the form

$$\ell(\boldsymbol{v}) = \int_\Omega \boldsymbol{b} \cdot \boldsymbol{v}\, d\Omega + \int_{\Gamma_n} \bar{\boldsymbol{t}} \cdot \boldsymbol{v}\, d\Gamma. \tag{3.34}$$

We denote by $\bar{\boldsymbol{t}}$ the vector function describing the components of the traction forces:

$$\bar{\boldsymbol{t}} = \begin{bmatrix} \bar{t}_x(\boldsymbol{x}) \\ \\ \bar{t}_y(\boldsymbol{x}) \end{bmatrix}. \tag{3.35}$$

We then compute the component of the force vector arising from tractions at an element level by

$$\boldsymbol{F}_{\bar{\boldsymbol{t}}} = \int_{\partial E} \boldsymbol{\phi}^T \bar{\boldsymbol{t}}\, d\Gamma = \int_{\partial E} \boldsymbol{N}^T \bar{\boldsymbol{t}}\, d\Gamma. \tag{3.36}$$

We denote by $\boldsymbol{b}$ the vector function describing the components of the body forces:

$$\boldsymbol{b} = \begin{bmatrix} b_x(\boldsymbol{x}) \\ \\ b_y(\boldsymbol{x}) \end{bmatrix}. \tag{3.37}$$

We then compute the component of the force vector arising from body forces at an element level by

$$\boldsymbol{F}_{\boldsymbol{b}} = \int_E \boldsymbol{\phi}^T \boldsymbol{b}\, d\Omega. \tag{3.38}$$

In the absence of a quadrature rule on arbitrary polygons it is sufficient to approximate the loading contribution from body forces by

$$\boldsymbol{F}_{\boldsymbol{b}} \approx |E| \boldsymbol{b}(\boldsymbol{x}_c), \tag{3.39}$$

and distributing the body force equally over the nodes. The complete loading term is then given by

$$\boldsymbol{F} = \boldsymbol{F}_{\bar{\boldsymbol{t}}} + \boldsymbol{F}_{\boldsymbol{b}}. \tag{3.40}$$

Chapter 4

Implementation of the virtual element method

In this chapter we describe in detail, by means of an example, the implementation of the virtual element method. We choose the example of Cook's membrane problem. This sample problem is solved using a mesh of four Voronoi elements. We present all data in this chapter to three significant figures to allow for accurate comparison should the reader wish to implement the method him/herself. We choose to use a homogeneous transversely isotropic material in this example problem as the method can be easily extended from there to accommodate isotropic and non-homogeneous transversely isotropic materials. The MATLAB code used to solve this problem can be found in Appendix A.

Cook's membrane problem consists of an irregularly tapered panel fully fixed along its left edge with a uniformly distributed load along its right edge. The applied load is $P = 100N$ and the material has a transverse Young's modulus of $E_T = 250Pa$, an anisotropy ratio of $p = 5$, fibres oriented at $\hat{a} = \frac{\pi}{4}$ and is nearly incompressible with a Poisson's ratio of $\nu = 0.49995$. Figures 4.1(a) and (b) respectively show the geometry of the Cook membrane problem and the discretisation of the domain used in this example problem.

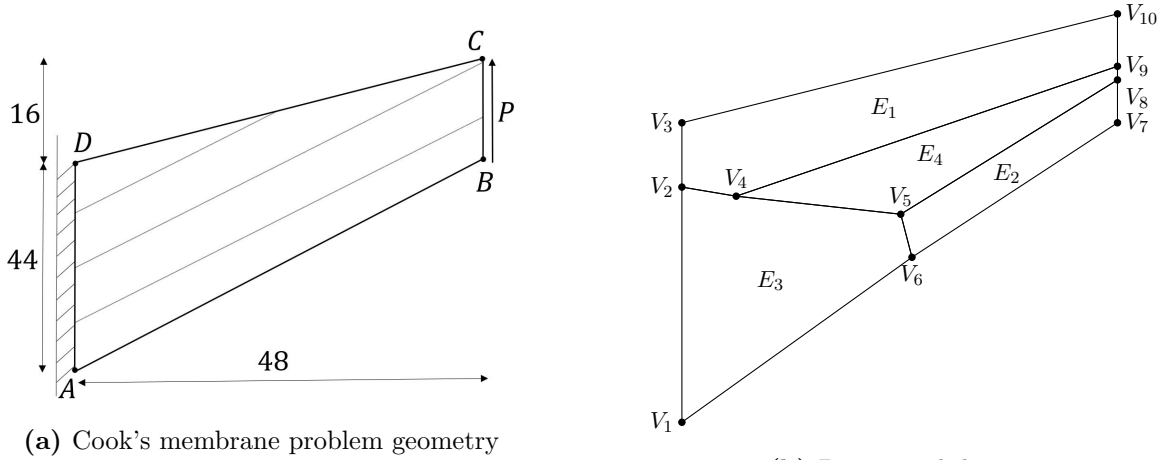

(a) Cook's membrane problem geometry

(b) Discretised domain

Figure 4.1 The Cook problem: showing (a) the problem geometry with fibres inclined at $\hat{a} = \frac{\pi}{4}$, and (b) the discretisation of the domain

4.1 Domain information

The domain is discretised into a collection of elements with nodes at the vertices, as shown in Figure 4.1(b).

Degrees of freedom We create a global position array containing the x- and y- coordinates of each node. We name this array $\mathbf{XY}_g$. The first row in the global position array contains the x-coordinates and the second row the y-coordinates, with column i corresponding to the i-th vertex. The global position array of the sample domain is given below:

$$\mathbf{XY}_g = \begin{bmatrix} 0 & 0 & 0 & 5.980 & 24.117 & 25.353 & 48 & 48 & 48 & 48 \\ 0 & 34.553 & 44 & 33.216 & 30.564 & 23.240 & 44 & 50.298 & 52.303 & 60 \end{bmatrix}.$$

Interconnectivity We now introduce the interconnectivity array (ICA). The ICA is a matrix that describes how the nodes are connected to form elements. The non-zero entries of each row of the ICA describe an element, with the columns containing the numbers of the nodes forming the element. We choose the convention of anticlockwise node numbering.

$$\mathbf{ICA} = \begin{bmatrix} 9 & 10 & 3 & 2 & 4 \\ 7 & 8 & 5 & 6 & 0 \\ 4 & 2 & 1 & 6 & 5 \\ 9 & 4 & 5 & 8 & 0 \end{bmatrix}$$

4.2 Element parameters

In this section we present the process of calculating the local stiffness matrix $\boldsymbol{K}_E$ of element E_1 only. In practice this process would be repeated for all elements in the domain. Figure 4.2 depicts our sample element, labelled in the convention defined in Chapter 3. For clarity in this section we will number nodes/vertices in the form $V_{LocalNumber(GlobalNumber)}$.

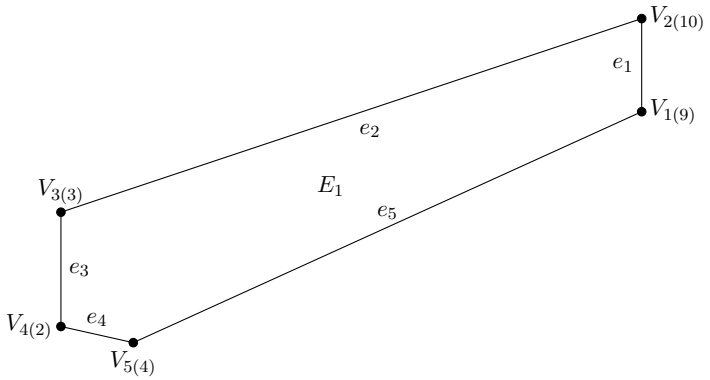

Figure 4.2 Element one (E_1)

Element vertices We begin by creating a vector containing the the node numbers of the nodes making up the element. This is simply a vector of all the non-zero entries of the row of the ICA corresponding to a specific element. This vector of vertices is given below for element E_1.

$$\textbf{vertices} = \begin{bmatrix} 9 & 10 & 3 & 2 & 4 \end{bmatrix}$$

We then determine the number of vertices of the element from the length of the **vertices** vector:

$$n_V = 5.$$

We now create a local position array containing the x- and y-coordinates of the vertices of the element. This is created by extracting the columns of $\mathbf{XY}_g$ indicated by the **vertices** vector.

$$\mathbf{XY}_E = \begin{bmatrix} 48 & 48 & 5.980 & 0 & 24.117 \\ 52.303 & 60 & 44 & 34.553 & 33.216 \end{bmatrix}$$

Area, centroid and diameter We now have the information required to calculate the area and coordinates of the centroid of the element. The area $|E|$ and centroid $\boldsymbol{x}_c$ of the element are calculated from

$$\begin{aligned}
|E| &= \frac{1}{2}\sum_{i=1}^{n_V}\left[X_e^i Y_e^{i+1} - X_e^{i+1}Y_e^i\right], \\
\boldsymbol{x_c} &= (x_c, y_c), \\
x_c &= \frac{1}{6|E|}\sum_{i=1}^{n_V}\left[\left(X_e^i + X_e^{i+1}\right)\left(X_e^i Y_e^{i+1} - X_e^{i+1}Y_e^i\right)\right], \\
y_c &= \frac{1}{6|E|}\sum_{i=1}^{n_V}\left[\left(Y_e^i + Y_e^{i+1}\right)\left(X_e^i Y_e^{i+1} - X_e^{i+1}Y_e^i\right)\right].
\end{aligned}$$

For our example element we have

$$\begin{aligned}
|E| &= 496.627, \\
x_c &= 22.294, \\
y_c &= 46.157.
\end{aligned}$$

The element diameter, d_E, is simply the largest distance between any two vertices of the element. The diameter of element E_1 is

$$d_E = 54.328.$$

4.3 The consistency term

Calculating the projection We recall from equation (3.12) that the projection operator is defined by

$$\Pi_E^{\nabla}(\boldsymbol{u}_h) = \frac{1}{2}\frac{1}{|E|}\int_{e\in\partial E}\left[N_{ik}\hat{u}_k n_j + N_{jk}\hat{u}_k n_i\right] d\Gamma. \tag{4.1}$$

As in [19, 48] we choose to write the projection in terms of a matrix operator and nodal degrees of freedom such that

$$\Pi_E^{\nabla}(\boldsymbol{u}_h) = \boldsymbol{\Pi}_E^{\nabla}\hat{\boldsymbol{u}}_h. \tag{4.2}$$

For ease of computational implementation we choose to write equation (4.1) in Voigt notation:

$$\boldsymbol{\Pi}_E^{\nabla}\hat{\boldsymbol{u}}_h = \frac{1}{|E|}\int_{e\in\partial E}\boldsymbol{\mathcal{N}}^V\boldsymbol{N}d\Gamma\hat{\boldsymbol{u}}_h, \tag{4.3}$$

where $\boldsymbol{\mathcal{N}}^V$ denotes the edge normal in Voigt notation:

$$\boldsymbol{\mathcal{N}}^V = \begin{bmatrix} n_x & 0 \\ 0 & n_y \\ n_y & n_x \end{bmatrix}. \tag{4.4}$$

We are then able to compute the projection matrix operator by

$$\boldsymbol{\Pi}_E^\nabla = \frac{1}{|E|} \int_{e \in \partial E} \boldsymbol{\mathcal{N}}^V \boldsymbol{N} d\Gamma. \tag{4.5}$$

The calculation of $\boldsymbol{\Pi}_E^\nabla$ requires the integration of $\boldsymbol{N}$ along the element boundary. However, N_i is only non-zero on edges e_i and e_{i-1}. This allows us to loop over the nodes and integrate the basis functions corresponding to each node individually. The function is linear from $N_i(V_i) = 1$ to $N_i(V_{i\pm1}) = 0$, which makes the integral easy to compute. The portion of the matrix corresponding to vertex i (V_i) is computed from

$$\Pi_i^\nabla = \frac{|e_i|}{2} \boldsymbol{\mathcal{N}}_i^V + \frac{|e_{i-1}|}{2} \boldsymbol{\mathcal{N}}_{i-1}^V.$$

The portion of the $\boldsymbol{\Pi}_E^\nabla$ matrix corresponding to node 1 in our example element (global node 9) is computed to be

$$\Pi_{1(9)}^\nabla = \begin{bmatrix} 0.027 & 0 \\ 0 & -0.042 \\ -0.042 & 0.027 \end{bmatrix}.$$

The resulting 3×2 Π_i^∇ matrices are then assembled to form the complete $3 \times 2n_V$ $\boldsymbol{\Pi}_E^\nabla$ projection matrix for the element:

$$\boldsymbol{\Pi}_E^\nabla = \begin{bmatrix} 0.027 & 0 & -0.008 & 0 & -0.026 & 0 & -0.011 & 0 & 0.018 & 0 \\ 0 & -0.042 & 0 & 0.048 & 0 & 0.048 & 0 & -0.006 & 0 & -0.048 \\ \underbrace{-0.042 \quad 0.027}_{\Pi_{1(9)}^\nabla} & & \underbrace{0.048 \quad -0.008}_{\Pi_{2(10)}^\nabla} & & \underbrace{0.048 \quad -0.026}_{\Pi_{3(3)}^\nabla} & & \underbrace{-0.006 \quad -0.011}_{\Pi_{4(2)}^\nabla} & & \underbrace{-0.048 \quad 0.018}_{\Pi_{5(4)}^\nabla} & \end{bmatrix}.$$

From equation (3.18) the consistency part of the stiffness matrix is given by

$$\begin{aligned} \boldsymbol{K}_c^E &= \int_E \boldsymbol{\Pi}_E^{\nabla^T} \underline{\mathbb{C}} \boldsymbol{\Pi}_E^\nabla d\Omega, \\ &= |E| \boldsymbol{\Pi}_E^{\nabla^T} \underline{\mathbb{C}}_E \boldsymbol{\Pi}_E^\nabla, \end{aligned} \tag{4.6}$$

where $\underline{\mathbb{C}}_E$ denotes the 3×3 constitutive matrix for the element. In the case of plane strain $\underline{\mathbb{C}}$ is given by

$$\underline{\mathbb{C}} = \begin{bmatrix} \lambda + 2\mu_T + 2(\gamma+\alpha)a_1^2 + \beta a_1^4 & \lambda + \alpha + \beta a_1^2 a_2^2 & (\alpha+\gamma)a_1 a_2 + \beta a_1^3 a_2 \\ & \lambda + 2\mu_T + 2(\gamma+\alpha)a_2^2 + \beta a_2^4 & (\alpha+\gamma)a_1 a_2 + \beta a_1 a_2^3 \\ \text{sym} & & \mu_T + \frac{\gamma}{2} + \beta a_1^2 a_2^2 \end{bmatrix}. \quad (4.7)$$

For our example element the consistency term of the local stiffness matrix is given by

$$\boldsymbol{K}_c^E = \begin{bmatrix} 229.099 & -142.944 & -180.079 & 93.771 & -242.850 & 147.231 & -20.837 & 25.171 & 214.668 & -123.229 \\ -142.944 & 437.958 & -14.276 & -537.633 & 122.274 & -508.914 & 95.912 & 86.781 & -60.966 & 521.808 \\ -180.079 & -14.276 & 294.884 & 168.689 & 226.306 & 51.505 & -84.015 & -101.801 & -257.096 & -104.118 \\ 93.771 & -537.633 & 168.689 & 740.204 & -43.410 & 643.266 & -167.232 & -159.048 & -51.818 & -686.789 \\ -242.850 & 122.274 & 226.306 & -43.410 & 265.608 & -117.441 & -1.102 & -45.626 & -247.963 & 84.203 \\ 147.231 & -508.914 & 51.505 & 643.266 & -117.441 & 595.647 & -122.883 & -112.972 & 41.588 & -617.027 \\ -20.837 & 95.912 & -84.015 & -167.232 & -1.102 & -122.883 & 67.625 & 51.408 & 38.328 & 142.795 \\ 25.171 & 86.781 & -101.801 & -159.048 & -45.626 & -112.972 & 51.408 & 51.580 & 70.847 & 133.659 \\ 214.668 & -60.966 & -257.096 & -51.818 & -247.963 & 41.588 & 38.328 & 70.847 & 252.063 & 0.349 \\ -123.229 & 521.808 & -104.118 & -686.789 & 84.203 & -617.027 & 142.795 & 133.659 & 0.349 & 648.348 \end{bmatrix}.$$

4.4 Stabilization matrix

Calculating $\boldsymbol{\mathcal{D}}$ Calculating the matrix $\boldsymbol{\mathcal{D}}$ is a straightforward process as all we need to do is compute the scaled coordinates at the vertices of an element. The scaled coordinates given by equation (3.25) are shown again below:

$$\xi(\boldsymbol{x}) = \frac{x - x_c}{d_E}, \qquad \eta(\boldsymbol{x}) = \frac{y - y_c}{d_E},$$

and the matrix $\boldsymbol{\mathcal{D}}$ given by equation (3.26), and again below:

$$\boldsymbol{\mathcal{D}} = \begin{bmatrix} 1 & 0 & \xi(V_1) & 0 & \eta(V_1) & 0 \\ 0 & 1 & 0 & \xi(V_1) & 0 & \eta(V_1) \\ 1 & 0 & \xi(V_2) & 0 & \eta(V_2) & 0 \\ 0 & 1 & 0 & \xi(V_2) & 0 & \eta(V_2) \\ \vdots & \vdots & \vdots & \vdots & \vdots & \vdots \\ 1 & 0 & \xi(V_{n_V}) & 0 & \eta(V_{n_V}) & 0 \\ 0 & 1 & 0 & \xi(V_{n_V}) & 0 & \eta(V_{n_V}) \end{bmatrix}.$$

For our example element E_1,

$$\boldsymbol{\mathcal{D}} = \begin{bmatrix} 1 & 0 & 0.473 & 0 & 0.113 & 0 \\ 0 & 1 & 0 & 0.473 & 0 & 0.113 \\ 1 & 0 & 0.473 & 0 & 0.255 & 0 \\ 0 & 1 & 0 & 0.473 & 0 & 0.255 \\ 1 & 0 & -0.410 & 0 & -0.040 & 0 \\ 0 & 1 & 0 & -0.410 & 0 & -0.040 \\ 1 & 0 & -0.410 & 0 & -0.214 & \\ 0 & 1 & 0 & -0.410 & 0 & -0.214 \\ 1 & 0 & -0.300 & 0 & -0.238 & 0 \\ 0 & 1 & 0 & -0.300 & 0 & -0.238 \end{bmatrix}.$$

Recalling equation (3.32) we are now able to compute the stabilization matrix from

$$\boldsymbol{K}_s^E = \mu_T \left[\boldsymbol{I} - \boldsymbol{\mathcal{D}} \left(\boldsymbol{\mathcal{D}}^T \boldsymbol{\mathcal{D}} \right)^{-1} \boldsymbol{\mathcal{D}} \right],$$

which for our element E_1 is given by

$$\boldsymbol{K}_s^E = \begin{bmatrix} 33.624 & 0 & -31.422 & 0 & 18.962 & 0 & -3.486 & 0 & -17.678 & 0 \\ 0 & 33.624 & 0 & -31.422 & 0 & 18.962 & 0 & -3.486 & 0 & -17.678 \\ -31.422 & 0 & 29.784 & 0 & -19.332 & 0 & 7.828 & 0 & 13.141 & 0 \\ 0 & -31.422 & 0 & 29.784 & 0 & -19.332 & 0 & 7.828 & 0 & 13.141 \\ 18.962 & 0 & -19.332 & 0 & 16.869 & 0 & -19.471 & 0 & 2.973 & 0 \\ 0 & 18.962 & 0 & -19.332 & 0 & 16.869 & 0 & -19.471 & 0 & 2.973 \\ -3.486 & 0 & 7.828 & 0 & -19.471 & 0 & 49.980 & 0 & -34.851 & 0 \\ 0 & -3.486 & 0 & 7.828 & 0 & -19.471 & 0 & 49.980 & 0 & -34.851 \\ -17.678 & 0 & 13.141 & 0 & 2.973 & 0 & -34.851 & 0 & 36.415 & 0 \\ 0 & -17.678 & 0 & 13.141 & 0 & 2.973 & 0 & -34.851 & 0 & 36.415 \end{bmatrix}.$$

Local stiffness matrix The local stiffness matrix is the calculated by summing the consistency and stabilization terms:

$$\boldsymbol{K}^E = \boldsymbol{K}_c^E + \boldsymbol{K}_s^E.$$

The local stiffness matrix for element E_1 is given by

$$\boldsymbol{K}^E = \begin{bmatrix} 262.723 & -142.944 & -211.501 & 93.771 & -223.889 & 147.231 & -24.323 & 25.171 & 196.989 & -123.229 \\ -142.944 & 471.582 & -14.276 & -569.054 & 122.274 & -489.953 & 95.912 & 83.295 & -60.966 & 504.130 \\ -211.501 & -14.276 & 324.668 & 168.689 & 206.974 & 51.505 & -76.187 & -101.801 & -243.955 & -104.118 \\ 93.771 & -569.054 & 168.689 & 769.988 & -43.410 & 623.934 & -167.232 & -151.220 & -51.818 & -673.648 \\ -223.889 & 122.274 & 206.974 & -43.410 & 282.477 & -117.441 & -20.573 & -45.626 & -244.990 & 84.203 \\ 147.231 & -489.953 & 51.505 & 623.934 & -117.441 & 612.515 & -122.883 & -132.442 & 41.588 & -614.054 \\ -24.323 & 95.912 & -76.187 & -167.232 & -20.573 & -122.883 & 117.605 & 51.408 & 3.477 & 142.795 \\ 25.171 & 83.295 & -101.801 & -151.220 & -45.626 & -132.442 & 51.408 & 101.559 & 70.847 & 98.808 \\ 196.989 & -60.966 & -243.955 & -51.818 & -244.990 & 41.588 & 3.477 & 70.847 & 288.479 & 0.349 \\ -123.229 & 504.130 & -104.118 & -673.648 & 84.203 & -614.054 & 142.795 & 98.808 & 0.349 & 684.764 \end{bmatrix}.$$

4.5 Global stiffness matrix

Once the local stiffness matrix has been computed it must be assembled into the global stiffness matrix as with traditional finite element methods. For a two-dimensional problem the local and global stiffness matrices comprise 2×2 portions of matrix that describe the interplay between the degrees of freedom of the system. In our example the global system has 10 nodes/vertices and therefore 20 degrees of freedom. This constitutes a 20×20 global stiffness matrix. A schematic global stiffness matrix is given below with each entry representing a 2×2 matrix. The entry in row i and column j is simply $i : j$.

Global Stiffness Matrix	1	2	...	10
1	1:1	1:2	...	1:10
2	2:1	2:2	...	2:10
⋮	⋮	⋮	⋱	⋮
10	10:1	10:2	...	10:10

We represent the local stiffness matrix in the same style below.

Local Stiffness Matrix	9	10	3	2	4
9	9:9	9:10	9:3	9:2	9:4
10	10:9	10:10	10:3	10:2	10:4
3	3:9	3:10	3:3	3:2	3:4
2	2:9	2:10	2:3	2:2	2:4
4	4:9	4:10	4:3	4:2	4:4

The process of assembling the global stiffness matrix involves taking the 2×2 portions of the local stiffness matrix and cumulatively adding them to the correct positions in the global stiffness matrix. The result is a symmetric matrix whose entries sum to zero; these properties can be used as simple checks to ensure assembly is performed correctly.

4.6 Loading term

With the VEM the construction of the loading term is very similar to that for the finite element method, and in the case of tractions is the same as for Q1 elements.

Traction Recalling equation (3.36) we have

$$\boldsymbol{F}_{\bar{\boldsymbol{t}}} = \int_{\partial E} \boldsymbol{N}^T \bar{\boldsymbol{t}} d\Gamma.$$

In our case of a uniformly distributed traction on the right hand edge the only non-zero integrals are those performed on the right hand edge. For our example element we need only concern ourselves with the edge connecting nodes 9 and 10:

$$\begin{aligned}\boldsymbol{F}_{\bar{\boldsymbol{t}}}^{E_1} &= \int_{V_{1(9)}}^{V_{2(10)}} \boldsymbol{N}^T \begin{bmatrix} 0 \\ \frac{P}{16} \end{bmatrix} d\Gamma \\ &= \frac{|e_1|}{2}\frac{P}{16} \begin{bmatrix} 0 \\ 1 \\ 0 \\ 1 \\ 0 \\ 0 \\ 0 \\ 0 \\ 0 \\ 0 \end{bmatrix} = \begin{bmatrix} 0 \\ 24.054 \\ 0 \\ 24.054 \\ 0 \\ 0 \\ 0 \\ 0 \\ 0 \\ 0 \end{bmatrix}.\end{aligned}$$

Body force In our example we neglect body forces. However, if present, one would use equation (3.39) to obtain

$$\boldsymbol{F}_{\boldsymbol{b}}^{E_1} = b_x(\boldsymbol{x}_c)\frac{|E_1|}{5}\begin{bmatrix}1\\0\\1\\0\\1\\0\\1\\0\\1\\0\end{bmatrix} + b_y(\boldsymbol{x}_c)\frac{|E_1|}{5}\begin{bmatrix}0\\1\\0\\1\\0\\1\\0\\1\\0\\1\end{bmatrix}.$$

The resultant loading term for our sample element would then be given by

$$\boldsymbol{F}^{E_1} = \boldsymbol{F}_{\bar{\boldsymbol{t}}}^{E_1} + \boldsymbol{F}_{\boldsymbol{b}}^{E_1}.$$

This local force vector is then assembled into a global load vector in a similar fashion to the the construction of the global stiffness matrix. As the construction of the global force vector is similar to and simpler than the construction of the global stiffness matrix we choose not to illustrate the process.

4.7 Displacement

Once the global stiffness matrix and the global load vector have been created we are ready to calculate the displacement vector. To calculate the displacements we need to impose the boundary conditions. There are several methods to achieve this, but in this example we choose a simple penalty method; this works by choosing some value much larger than those comprising the global stiffness matrix, called a penalty value, and using it to force the boundary conditions to be satisfied. Let us denote by pen the penalty value and by $\bar{\boldsymbol{d}}$ a vector of prescribed displacements/boundary conditions. We choose $pen = 10^{10}$. We then modify the global stiffness matrix such that

$$K_{i,i} = pen,$$

and the load vector such that

$$F_i = pen \times \bar{d}_i.$$

The displacement vector with boundary conditions imposed is then calculated from

$$\boldsymbol{d} = \boldsymbol{K}^{-1}\boldsymbol{F}.$$

For a final comparison we present in Figure 4.3 below the undeformed and deformed meshes, in green and red respectively, of our example problem. Additionally, we present the global displacement vector alongside.

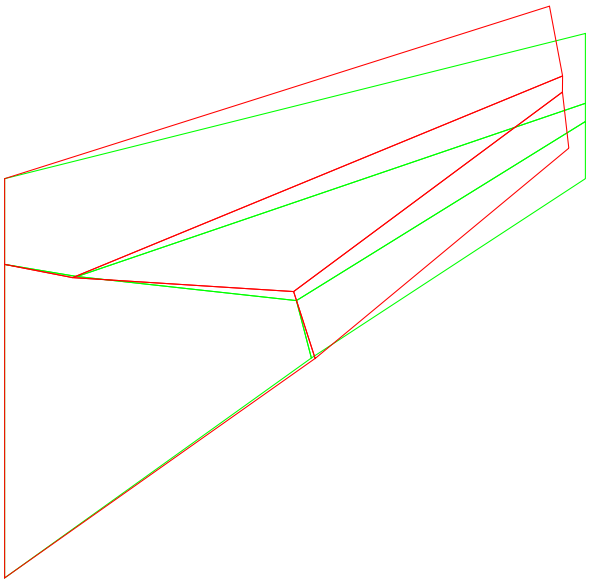

Figure 4.3 Undeformed and deformed meshes

$$\boldsymbol{d} = \begin{bmatrix} 0 \\ 0 \\ 0 \\ 0 \\ 0 \\ 0 \\ -0.361 \\ -0.12 \\ -0.232 \\ 0.994 \\ 0.315 \\ 0.947 \\ -1.37 \\ 3.361 \\ -1.897 \\ 3.246 \\ -1.884 \\ 3.016 \\ -2.968 \\ 3.011 \end{bmatrix}$$

Chapter 5

Numerical results - homogeneous

In this chapter we present results obtained from two common benchmark problems. We compare the numerical results achieved using the VEM with those of the finite element method to evaluate the performance of the VEM. In this section we consider only homogeneous materials.

5.1 Element types

In this chapter and those following we consider a variety of VEM configurations and finite element types. In Table 5.1 below we define the shorthand used to refer to the different elements considered.

Q1	The standard bilinear approximation
Q2	The standard biquadratic approximation
Quad	The VEM formulation with four-noded elements
Hex	The VEM formulation with six-noded elements
Voronoi	The VEM formulation constructed by Voronoi tessellation

Table 5.1 *Element types*

For clarity, Figure 5.1 depicts example meshes constructed for two of the virtual element types.

(a) Hex mesh example **(b)** Voronoi mesh example

Figure 5.1 VEM mesh examples with a mesh density of $d = 7$ elements per side for (a) a Hex mesh, and (b) a Voronoi mesh

We consider first the results from two common benchmark problems, the Cook membrane problem and beam in pure bending, for isotropic materials.

5.2 Cook's membrane problem

The Cook membrane problem consists of an irregularly tapered panel fully fixed along its left edge with a uniformly distributed load along its right edge (Figure 5.2(a)). The applied load is $P = 100N$ and the Young's Modulus is $E_y = 250Pa$. This test problem has no analytical solution. The vertical displacement at point C is recorded. Figure 5.2(b) depicts a sample hexagonal mesh for this problem.

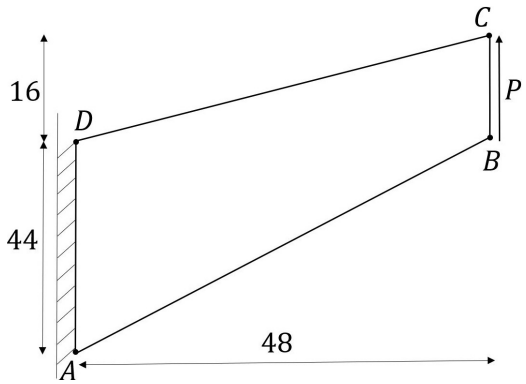

(a) Cook's membrane problem geometry

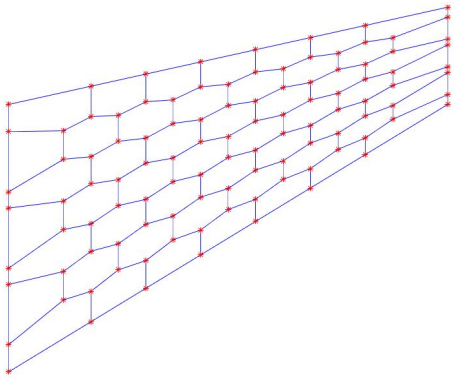

(b) Cook's membrane mesh example

Figure 5.2 Cook's membrane problem: showing (a) the problem geometry, and (b) a sample mesh

Figure 5.3(a) shows a convergence plot of tip displacement vs mesh density (defined by number of elements per side) for a compressible material, with $\nu = 0.3$. The VEM formulations exhibit greater degrees of accuracy than the Q1 approximation but less than the Q2 approximation.

Figure 5.3(b) shows a convergence plot of tip displacement vs mesh density for a nearly incompressible material, with $\nu = 0.49995$. The VEM formulations exhibit degrees of accuracy comparable to that of the Q2 approximation. The VEM formulations show no signs of locking, while the Q1 approximation is seen to lock.

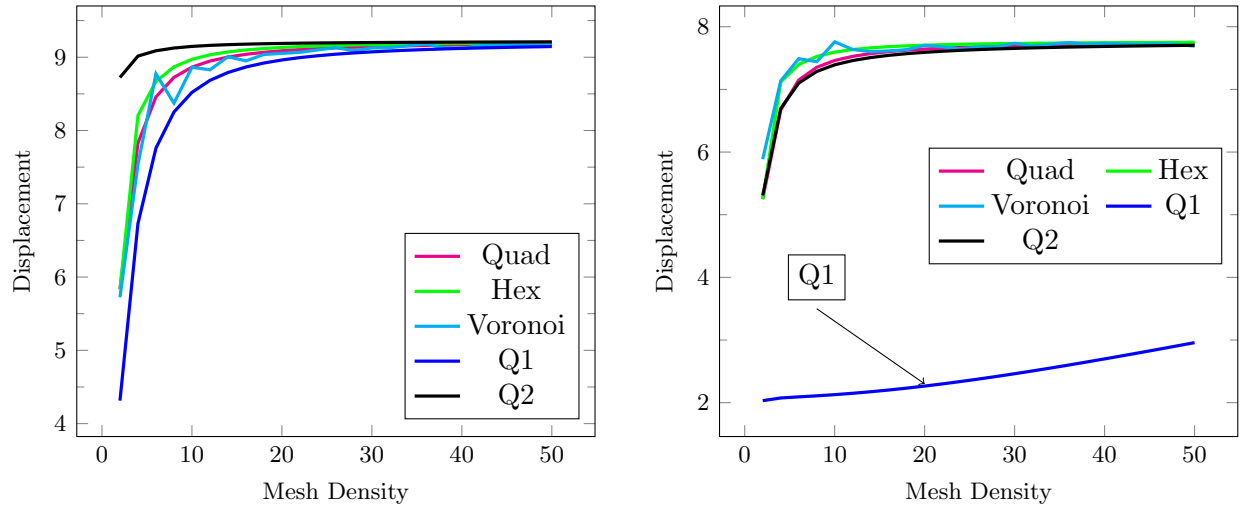

(a) Compressible material - $\nu = 0.3$ **(b)** Nearly incompressible material - $\nu = 0.49995$

Figure 5.3 The Cook problem: convergence tests for compressible (a) and nearly incompressible (b) isotropic materials

5.3 Pure bending problem

This problem consists of a beam subject to a linearly varying load at its right edge with the left edge constrained horizontally as shown in Figure 5.4. The load has maximum and minimum values of $F_{max} = \pm 10N$. The beam has width and height $w = h = 2m$ and Young's Modulus $E_y = 250Pa$. The vertical displacement at point C is recorded.

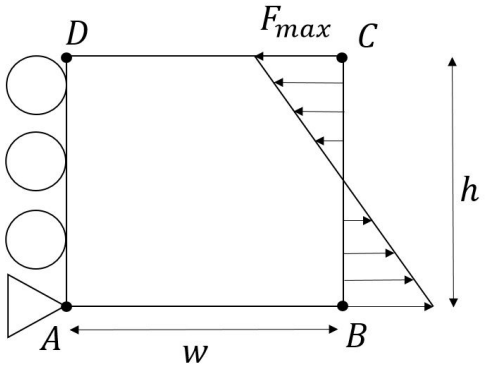

Figure 5.4 Pure bending problem geometry

The displacement at point C is given by (see [49]):

$$u(x,y) = 2F_{max}\frac{1-\nu^2}{E_y h}x\left(\frac{h}{2}-y\right), \tag{5.1a}$$

$$v(x,y) = F_{max}\frac{1-\nu^2}{E_y h}\left[x^2 + \frac{\nu}{1-\nu}y\,(y-h)\right]. \tag{5.1b}$$

Figure 5.5(a) shows a convergence plot of tip displacement vs mesh density for a compressible material, with $\nu = 0.3$. The VEM formulations exhibit greater degrees of accuracy than the Q1 approximation but less than the Q2 approximation.

Figure 5.5(b) shows a convergence plot of tip displacement vs mesh density for a nearly incompressible material, with $\nu = 0.49995$. The VEM formulations exhibit degrees of accuracy comparable to that of the Q2 approximation. The VEM formulations show no signs of locking while the Q1 approximation exhibits well known locking behaviour.

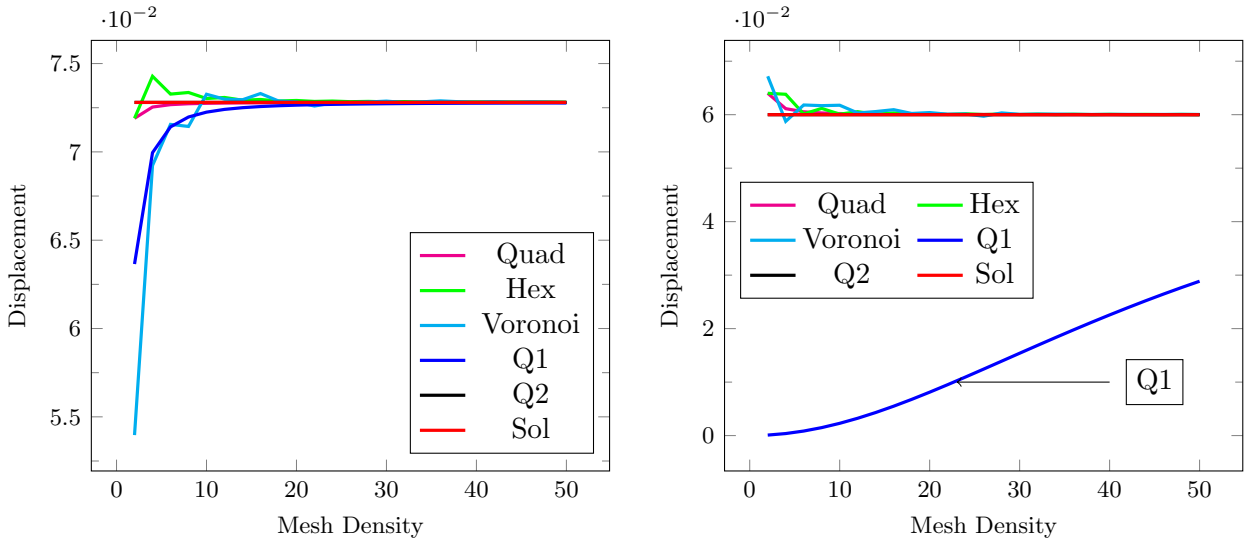

(a) Compressible material - $\nu = 0.3$ **(b)** Nearly incompressible material - $\nu = 0.49995$

Figure 5.5 The pure bending problem: convergence tests for compressible (a) and nearly incompressible (b) isotropic materials

We now present the results from the same benchmark problems but consider homogeneous transversely isotropic materials. We will investigate the performance of the VEM in dealing with nearly incompressible materials while varying the fibre orientation and anisotropy ratio p. We define the fibre orientation $\hat{a}$ as the angle, measured in radians, between the horizontal x-axis and the axis of symmetry of the material, $\boldsymbol{a}$.

5.4 Cook's membrane problem

We present again Cook's membrane problem but now with homogeneous transversely isotropic materials. We set $P = 100N$, $E_T = 250Pa$, $E_L = pE_T$ and consider only the near-incompressible limit with $\nu_T = \nu_L = 0.49995$. As before we record the vertical displacement at point C. Figure 5.6 depicts the problem domain with a sample fibre orientation of $\hat{a} = \frac{\pi}{4}$.

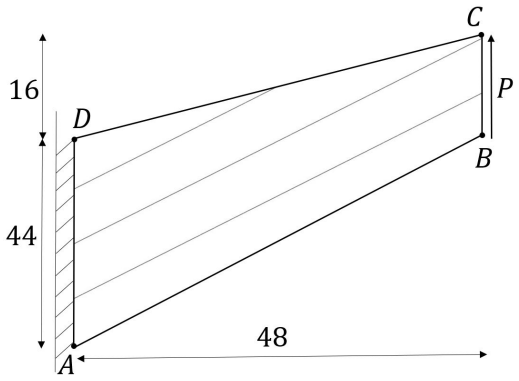

Figure 5.6 Cook's membrane, showing fibres inclined at $\hat{a} = \frac{\pi}{4}$

Figure 5.7 shows a convergence plot of tip displacement vs mesh density for $\hat{a} = \frac{\pi}{4}$ and $p = 5$. The VEM formulations exhibit degrees of accuracy superior to that of the Q1 formulation and comparable to that of the Q2 formulation. The VEM formulation with Voronoi elements converges erratically for coarse meshes due to the unstructured nature of the meshes, but converges much more smoothly as mesh refinement increases.

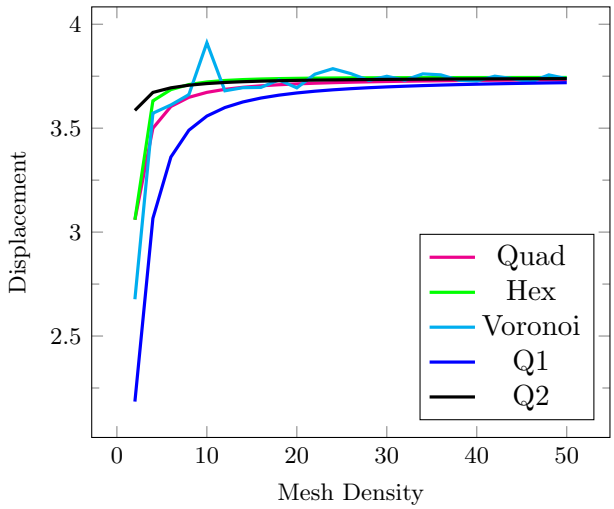

Figure 5.7 The Cook problem: convergence test for fibres angled at $\hat{a} = \frac{\pi}{4}$ with $p = 5$

Figures 5.8(a) and (b) show plots of displacement vs p for fibres oriented at $\hat{a} = \frac{\pi}{4}$ and $\hat{a} = \frac{\pi}{9}$ respectively. A mesh density of $d = 50$ is used for both figures. In both instances the VEM formulations correlate closely with Q1 and Q2 approximations. However, the Q1 approximation exhibits locking as $p \to 1$, corresponding to near incompressible isotropy, while the VEM formulation does not. Consistent with the results in [41], we find that a mild degree of anisotropy overcomes the volumetric locking behaviour of the Q1 approximation.

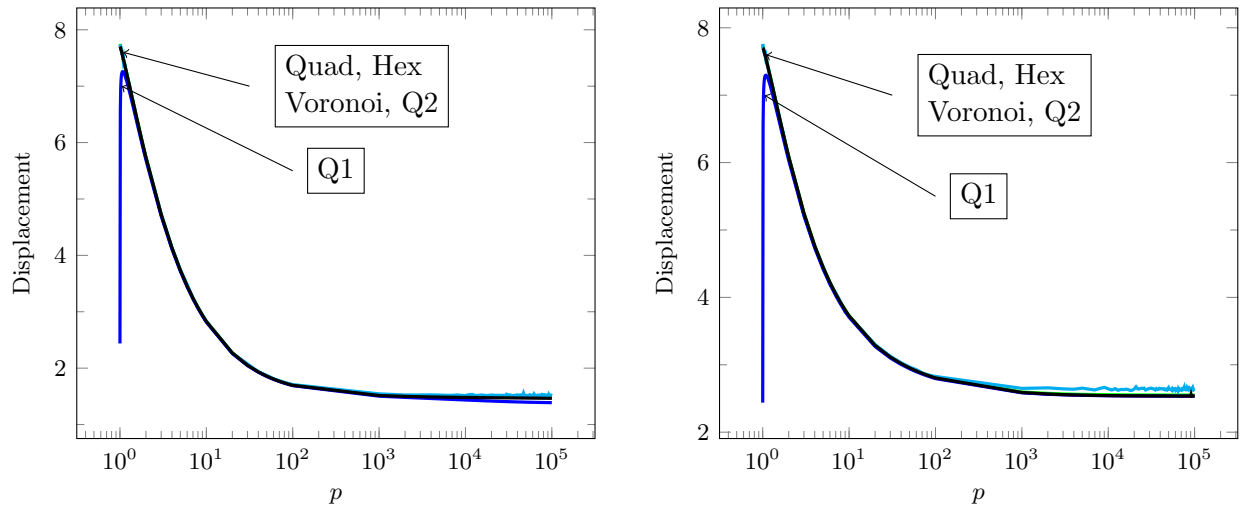

(a) $\hat{a} = \frac{\pi}{4}$ **(b)** $\hat{a} = \frac{\pi}{9}$

Figure 5.8 The Cook problem: tip displacement vs p for fibres angled at (a) $\hat{a} = \frac{\pi}{4}$, and (b) $\hat{a} = \frac{\pi}{9}$

Figure 5.9 shows a plot of displacement vs fire orientation $\hat{a}$ for near-inextensible fibres, $p = 10^5$, with a mesh density of $d = 50$. Again, we note poor performance and locking behaviour of the Q1 approximation for much of the domain, and conversely the robust behaviour of the VEM formulations. The Q2 approximation displays sub-optimal accuracy for fibre angles greater than $\frac{\pi}{2}$ and close to zero. This is somewhat surprising, in that the behaviour of this element in the near-inextensible limit would be expected to mirror its good performance for near-incompressibility. On the other hand, while the element has been shown to be uniformly convergent for incompressible materials, there does not exist a corresponding analysis for near-inextensibility, to the best of the author's knowledge. Such an analysis would shed light on the behaviour seen in Figure 5.9, in one way or another.

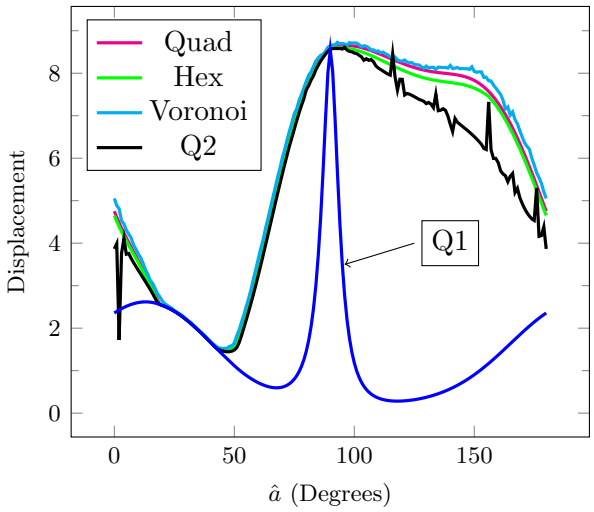

Figure 5.9 The Cook problem: tip displacement vs fire orientation, for $p = 10^5$

5.5 Pure bending problem

We present in this section a slightly different pure bending problem. The beam is now pinned at its left extrema and has dimensions $w = 10m$ and $h = 2m$. The magnitude of the loading is now $F_{max} = \pm 30N$. The material properties are $E_T = 1500Pa$, with $E_L = pE_T$ and $\nu_T = \nu_L = 0.49995$. As before, we record the vertical displacement at point C. Figure 5.10 depicts the problem domain with a sample fibre orientation of $\hat{a} = \frac{\pi}{4}$.

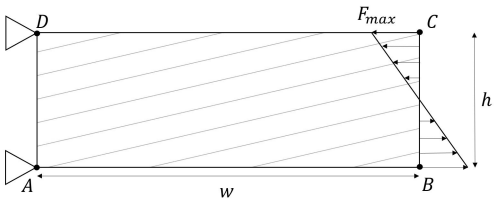

Figure 5.10 Pure bending problem, showing fibres inclined at $\hat{a} = \frac{\pi}{4}$

The analytical solution for this problem is given by (see [42]):

$$u(x,y) = \frac{2F_{max}}{h}\left[\mathbb{S}_{11}xy + \frac{1}{2}\mathbb{S}_{31}\left(y^2 - \frac{h^2}{4}\right)\right], \tag{5.2a}$$

$$v(x,y) = \frac{F_{max}}{h}\left[\mathbb{S}_{21}\left(y^2 - \frac{h}{2}\right) - \mathbb{S}_{11}x^2\right]. \tag{5.2b}$$

The components of the compliance tensor $\mathbb{S}$ are lengthy functions and can be found in Appendix B.

Figure 5.11 shows a convergence plot of tip displacement vs mesh density for $\hat{a} = \frac{\pi}{4}$ and $p = 5$. It is seen that for the various VEM formulations the convergence behaviour is similar to that of the Q2 approximation for sufficiently fine meshes.

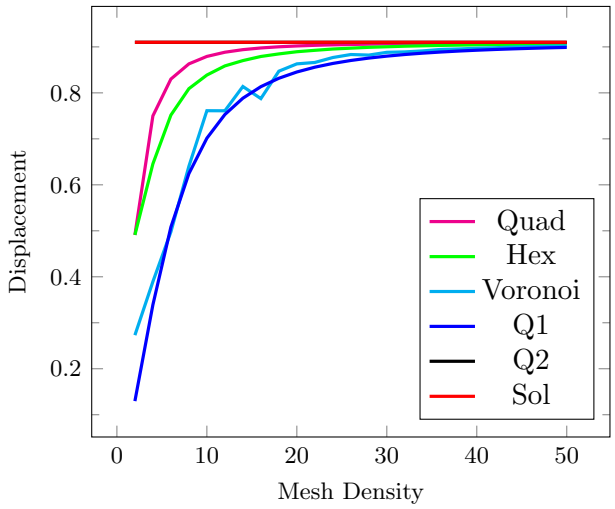

Figure 5.11 The pure bending problem: convergence test for fibre angle $\hat{a} = \frac{\pi}{4}$, with $p = 5$

Figures 5.12(a) and (b) show plots of displacement vs p for fibres oriented at $\hat{a} = \frac{\pi}{4}$ and $\hat{a} = \frac{\pi}{9}$ respectively. A mesh density of $d = 50$ is used for both figures. In both instances the VEM formulation correlates closely with both the Q1 and Q2 approximations as well as the analytical solution. However, the Q1 approximation exhibits locking as $p \to 1$, corresponding to near-incompressible isotropy, as well as for $p \to \infty$ corresponding to near-inextensibility. The Q1 approximation is only accurate for cases of mild anisotropy for $p > 1$ and up to $p \approx 10$ for $\hat{a} = \frac{\pi}{4}$ and $p \approx 100$ for $\hat{a} = \frac{\pi}{9}$.

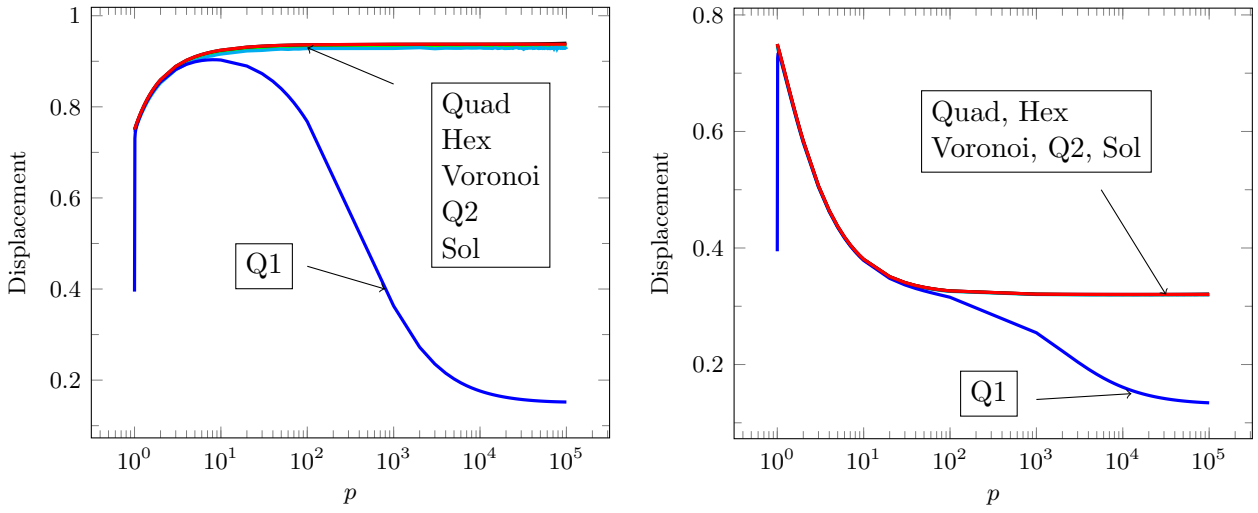

(a) $\hat{a} = \frac{\pi}{4}$ **(b)** $\hat{a} = \frac{\pi}{9}$

Figure 5.12 The pure bending problem: tip displacement vs p for fibres angled at (a) $\hat{a} = \frac{\pi}{4}$, and (b) $\hat{a} = \frac{\pi}{9}$

Figure 5.13 shows a plot of displacement vs fibre orientation $\hat{a}$ for near-inextensible fibres, $p = 10^5$, with a mesh density of $d = 50$. The various VEM formulations agree closely with each other as well as the Q2 approximation and exact solution. The Q1 approximation exhibits locking behaviour and is inaccurate for much of the domain while the Q2 approximation is accurate throughout.

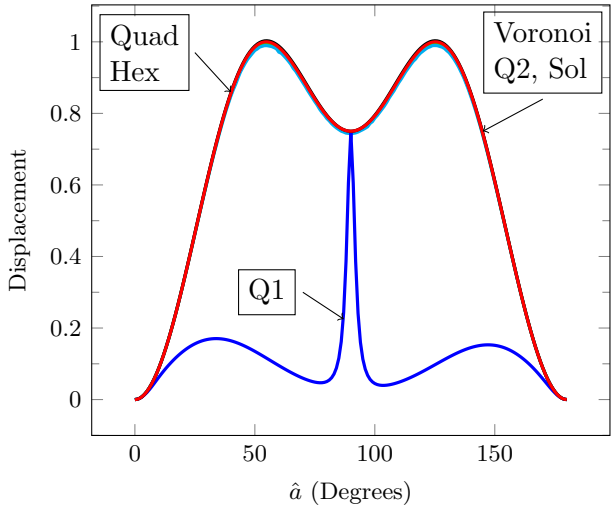

Figure 5.13 The pure bending problem: tip displacement vs fibre orientation, for $p = 10^5$

5.6 Results summary

In Table 5.2 we provide a 'binary-style' summary of the numerical results for homogeneous materials. We measure the performance of the formulations used with a pass/fail criterion. If the formulation is able to accurately or realistically model the behaviour of a test problem a ✓is placed in the appropriate cell. Failure to accurately model a problem, unrealistic behaviour or numerical instability is denoted by a ✗. For compactness of the table we introduce the following shorthand notation; we denote by 'Cook' Cook's membrane problem, by 'Beam' the pure bending problem, by '$\nu \approx 0.5$' the case of near-incompressibility and by 'Conv. Test' a convergence test/analysis.

			Quad	Hex	Voronoi	Q1	Q2
Isotropic Material	Cook & Beam	$\nu = 0.3$	✓	✓	✓	✓	✓
		$\nu \approx 0.5$	✓	✓	✓	✗	✓
Homogeneous Transversely Isotropic Material	Cook	Conv. Test	✓	✓	✓	✓	✓
		Disp vs p - $\hat{a} = \frac{\pi}{4}$	✓	✓	✓	✗	✓
		Disp vs p - $\hat{a} = \frac{\pi}{9}$	✓	✓	✓	✗	✓
		Disp vs $\hat{a}$	✓	✓	✓	✗	✗
	Beam	Conv. Test	✓	✓	✓	✓	✓
		Disp vs p - $\hat{a} = \frac{\pi}{4}$	✓	✓	✓	✗	✓
		Disp vs p - $\hat{a} = \frac{\pi}{4}$	✓	✓	✓	✗	✓
		Disp vs $\hat{a}$	✓	✓	✓	✗	✓

Table 5.2 *Summary of results for homogeneous materials*

In the cases of isotropic materials the VEM formulations and Q2 approximation perform well for both compressible and nearly incompressible materials and show no numerical problems. The standard Q1 approximation locks for nearly incompressible materials.

In the cases of homogeneous transversely isotropic materials the VEM formulations perform well showing no numerical problems. The Q2 approximation did not exhibit numerical instability or locking for Cook's membrane problem in the inextensible limit, but did show sub-optimal accuracy for fibre orientations with $\hat{a} > \frac{\pi}{2}$. Due to this lack of accuracy for part of the domain the Q2 approximation is considered to fail to model the problem. The Q1 approximation performed poorly in most tests only showing accuracy in instances of mild anisotropy.

Chapter 6

Numerical results - non-homogeneous

In this chapter we present the results from common benchmark problems. Here we consider only transversely isotropic materials with fibres of non-constant direction. We will consider directions described by polynomial and sinusoidal functions. We begin this section with an investigation of the convergence behaviour of the VEM for compressible, non-homogeneous, mildly transversely isotropic materials. We then investigate the behaviour as a function of increasing anisotropy, and increasing inhomogeneity.

6.1 Problem types

Throughout this chapter we will use the Cook membrane and pure bending problems as benchmark tests. The problem geometries and loading will be fixed. We will however be dealing with inhomogeneous materials with fibres defined by several different functions. As such we will detail each problem type formally here and in each subsequent test describe only the changes to the problem.

We use families of functions to describe the position of a fibre, denoted by $a(\boldsymbol{x})$; the vector used to determine directional properties is then the unit tangent vector $\boldsymbol{a}(\boldsymbol{x})$. For both problems the transverse Young's Modulus is $E_T = 250Pa$ with an anisotropy ratio of $p = 5$. The material is assumed to be compressible with $\nu = 0.3$.

6.1.1 Cook's membrane problem

We consider Cook's membrane problem as described in Section 5.2 but now with a non-homogeneous transversely isotropic material. In the example problem shown in Figure 6.1 the fibre position is described by a fourth-order polynomial.

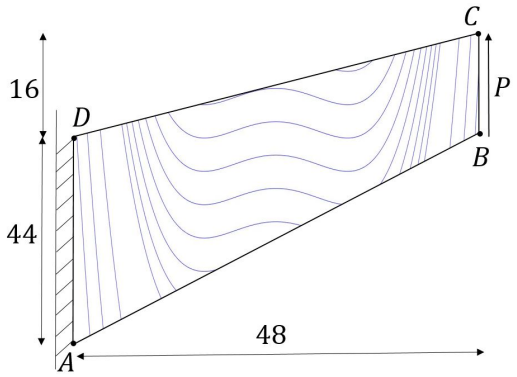

Figure 6.1 The Cook problem, showing fibres of variable orientation

6.1.2 Pure bending problem

We consider a further variation on the pure bending problem. The beam has dimensions and is subjected to loading as described in Section 5.5, with constraints as described in Section 5.3. In the example problem shown in Figure 6.2 the fibre position is described by a sinusoidal function.

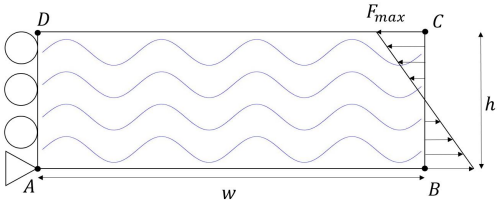

Figure 6.2 The pure bending problem, showing fibres of variable orientation

6.2 Representative fibre orientation

When dealing with non-homogeneous materials we treat them as homogeneous at an element level by determining some representative fibre orientation for each element. Immediately obvious choices for a representative fibre orientation include that at the centroid of an element, as well as the average fibre orientation at the vertices of an element. We will also consider a weighted combination of the fibre orientation at the centroid of an element and the average fibre orientation at the vertices of an element. Figure 6.3 shows a sample mesh for the Cook membrane problem for a non-homogeneous material with fibre position described by a fourth-order polynomial to illustrate the points in an element at which the fibre orientation can be sampled.

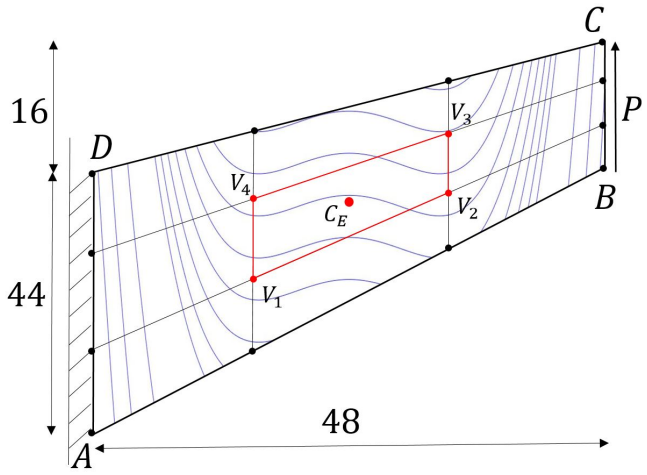

Figure 6.3 The Cook problem, showing points at which fibre orientation can be determined

The following quantities are relevant to the different approaches to calculating average fibre orientations at an element level:

$$\boldsymbol{a}_c = \boldsymbol{a}(\boldsymbol{x}_c) \quad - \quad \text{centroid} \tag{6.1}$$

$$\boldsymbol{a}_{\bar{V}} = \frac{1}{n_V}\sum_{i=1}^{n_V} \boldsymbol{a}(V_i) \quad - \quad \text{mean at vertices} \tag{6.2}$$

$$\boldsymbol{a}_{rep} = w_c\boldsymbol{a}_c + w_{\bar{V}}\boldsymbol{a}_{\bar{V}} \quad - \quad \text{weighted combination} \tag{6.3}$$

$$(w_c + w_{\bar{V}} = 1)$$

We will consider both a constant weighted combination, defined by $w_c = 0.5$, and a varying combination. For the latter case we denote by d_{cr} some user-defined problem-specific critical mesh density. In this work we simply choose $d_{cr} = 10$, and define the varying centroidal weight by

$$w_c = \frac{\frac{\pi}{2} + \arctan(d_{cr} - d)}{2\pi}. \tag{6.4}$$

The weight given to the fibre orientation at the centroid w_c is plotted against mesh density, denoted in this equation by d, in Figure 6.4.

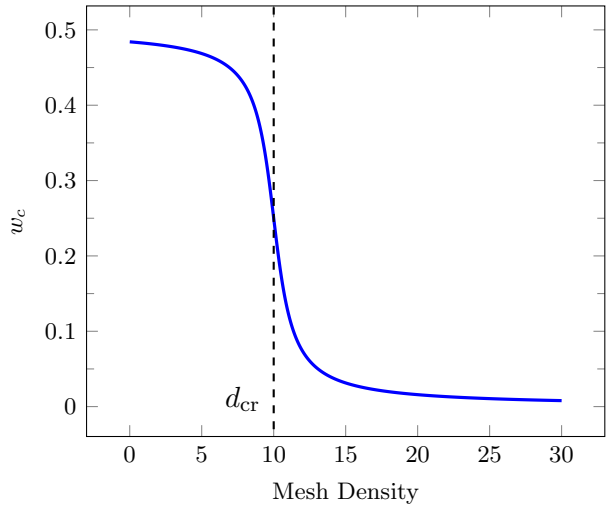

Figure 6.4 Varying weight as a function of mesh density

Figure 6.5 provides insight into the motivation for the formulation of the equation describing the varying weighting. Figures 6.5(a) and (b) show convergence plots for Cook's membrane problem with a fibre position described by $a = 2\sin x$ for fibre positions at the centroid and vertices respectively. Figure 6.5(c) shows a convergence plot for the same problem but considering a varying combination of fibre orientations. We are able to preserve the smoother behaviour of finer meshes when considering the vertices while smoothing out the erratic behaviour seen in coarser meshes when considering either only the centroid or vertices.

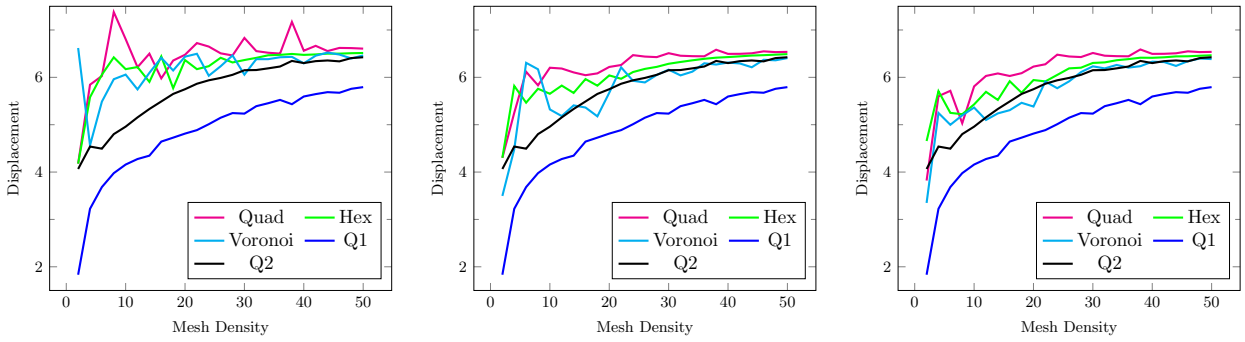

(a) Centroid **(b)** Vertices **(c)** Varying combination

Figure 6.5 Behaviour with respect to mesh density, for various choices of representative material properties

6.3 Polynomial fibre orientations

In this section we present convergence results for the Cook's membrane and pure bending problems for materials with fibre positions described by polynomials of increasing order. As we will use polynomial fibres to test the effects of mild material inhomogeneity, we only consider the results obtained using the centroidal values of the elements and those at the vertices of the elements.

6.3.1 Second-order polynomial fibre

6.3.1.1 Cook's membrane problem

Here we choose an orientation based on the family of curves $a = (x - 24)^2 + c$ where c is a constant (Figure 6.6).

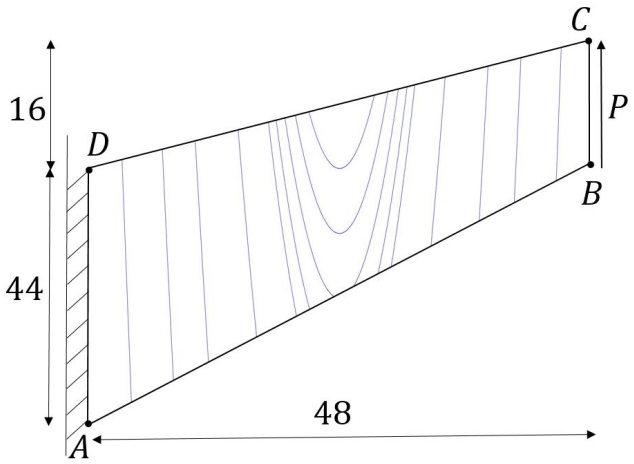

Figure 6.6 The Cook problem, showing fibres described by a second-order polynomial

Figure 6.7(a) shows a plot of vertical tip displacement vs mesh density, using the centroidal value of $\boldsymbol{a}$. The VEM formulations exhibit degrees of accuracy superior to that of the Q1 approximation, and similar to the Q2 approximation, for meshes with a density of $d \geq 4$.

Figure 6.7(b) shows a plot of vertical tip displacement vs mesh density with the representative fibre orientation given by the average over the vertices of an element. All VEM formulations considered exhibit similar convergence behaviour comparable to the Q1 approximation.

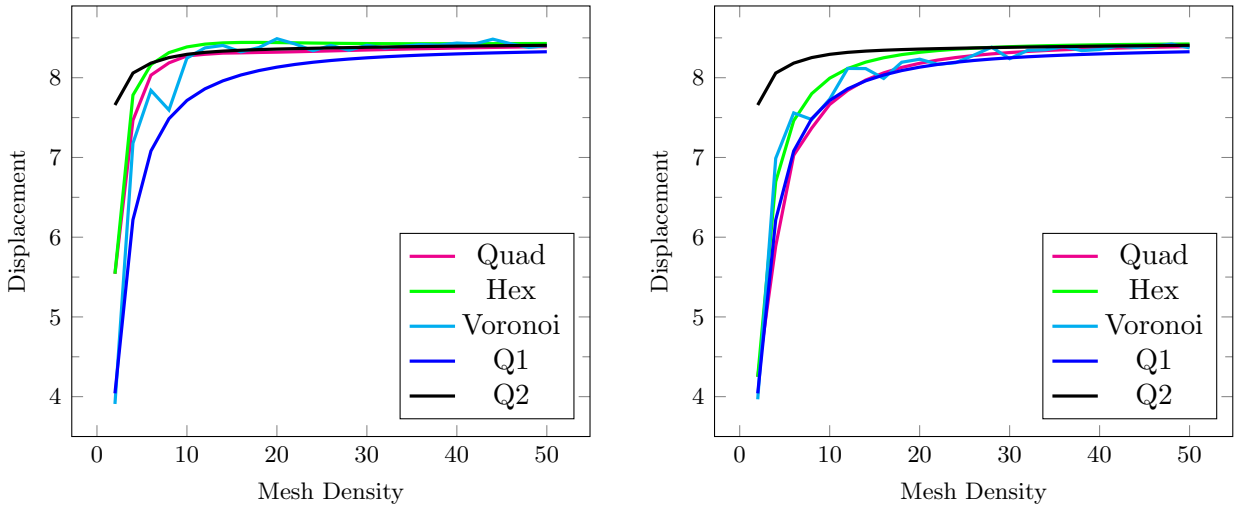

(a) Centroidal value of $\boldsymbol{a}$ **(b)** Average nodal value of $\boldsymbol{a}$

Figure 6.7 The Cook problem: convergence tests for fibres described by a second-order polynomial considering fibre orientations based on; (a) the centroidal value of $\boldsymbol{a}$, and (b) the average nodal value of $\boldsymbol{a}$

6.3.1.2 Pure bending problem

Here we choose an orientation based on the family of curves $a = (x-5)^2 + c$ where c is a constant (Figure 6.8).

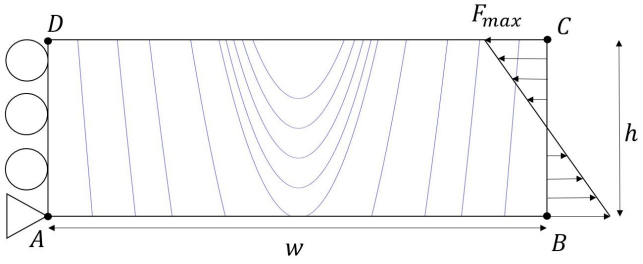

Figure 6.8 The pure bending problem, showing fibres described by a second-order polynomial

Figure 6.9(a) shows a plot of vertical tip displacement vs mesh density with the representative fibre orientation given by the fibre orientation at the centroid of an element. The VEM formulations exhibit degrees of accuracy ranging between that of Q1 and Q2 approximations with Quad elements displaying significantly better accuracy than the other VEM formulations.

Figure 6.9(b) shows a plot of vertical tip displacement vs mesh density with the representative fibre orientation given by the average fibre orientation at the vertices of an element. All formulations exhibit similar convergence behaviour for sufficiently fine meshes. The Voronoi formulation exhibits erratic convergence behaviour for very coarse meshes as a result of the highly unstructured nature of the meshes.

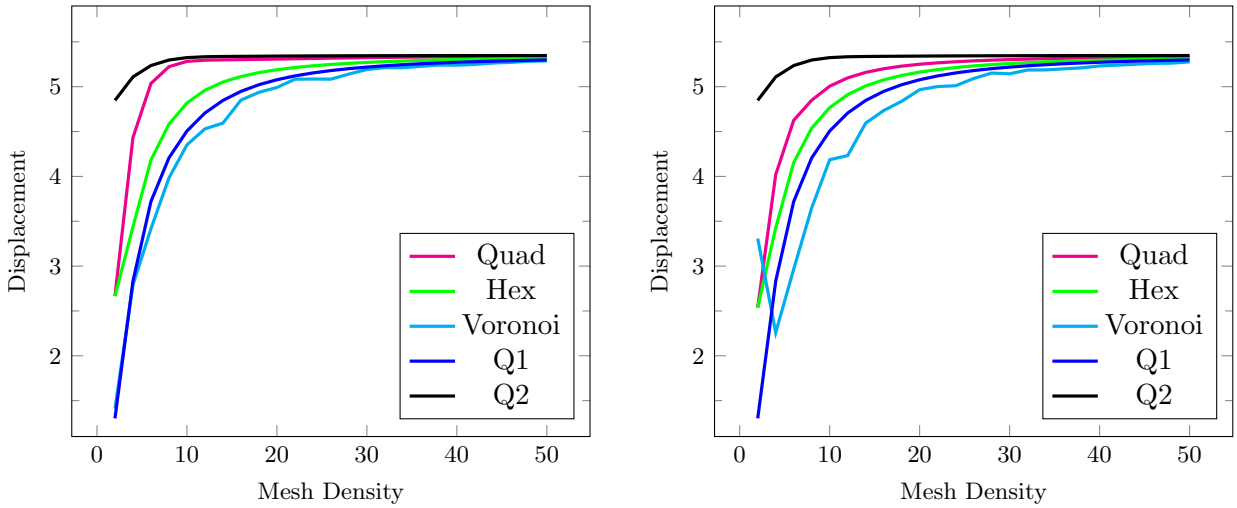

(a) Centroidal value of $\boldsymbol{a}$ **(b)** Average nodal value of $\boldsymbol{a}$

Figure 6.9 The pure bending problem: convergence tests for fibres described by a second-order polynomial considering fibre orientations based on; (a) the centroidal value of $\boldsymbol{a}$, and (b) the average nodal value of $\boldsymbol{a}$

6.3.2 Fourth-order polynomial fibre

6.3.2.1 Cook's membrane problem

Here we choose an orientation based on the family of curves $a = (x-24)^2(x-12)(x-36) + c$ where c is a constant (Figure 6.10).

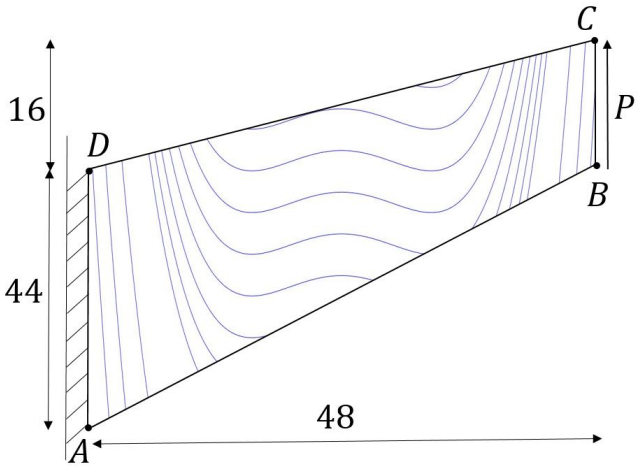

Figure 6.10 The Cook problem, showing fibres described by a fourth-order polynomial

Figure 6.11(a) shows a plot of vertical tip displacement vs mesh density with the representative fibre orientation given by the fibre orientation at the centroid of an element. The VEM formulations exhibit slightly better accuracy than the Q1 approximation but in this instance Q2 approximation is superior.

Figure 6.11(b) shows a plot of vertical tip displacement vs mesh density with the representative fibre orientation given by the average fibre orientation at the vertices of an element. The Hex and Voronoi VEM formulations exhibit convergence behaviour similar to the Q1 approximation. The Quad VEM formulation, however, unexpectedly exhibits convergence behaviour that is poorer than that of the other VEM formulations and the Q1 approximation.

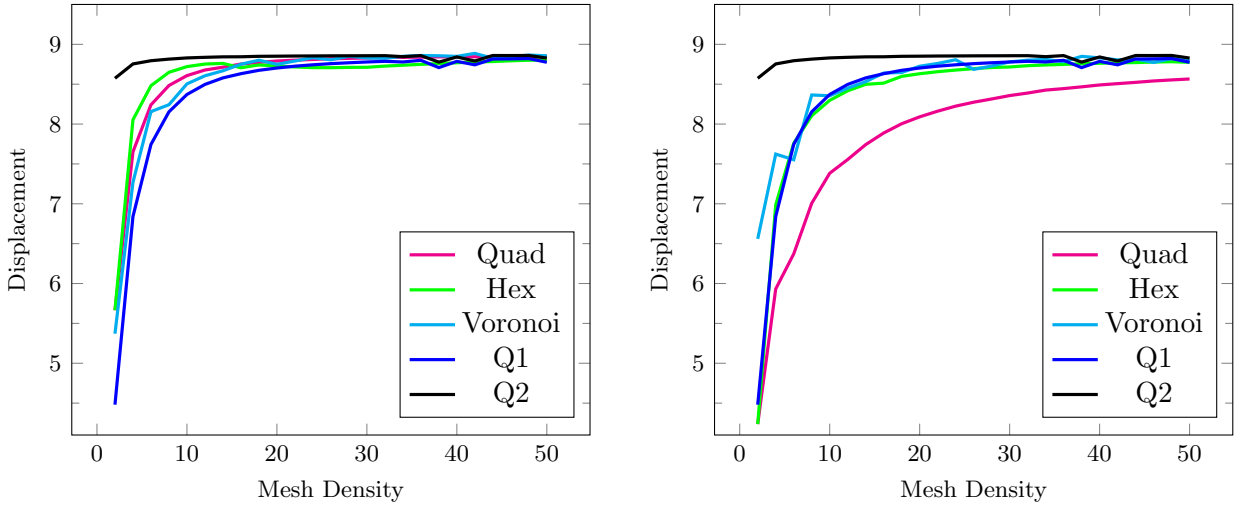

(a) Centroidal value of $\boldsymbol{a}$ **(b)** Average nodal value of $\boldsymbol{a}$

Figure 6.11 The Cook problem: convergence tests for fibres described by a fourth-order polynomial considering fibre orientations based on; (a) the centroidal value of $\boldsymbol{a}$, and (b) the average nodal value of $\boldsymbol{a}$

6.3.2.2 Pure bending problem

Here we choose an orientation based on the family of curves $a = (x-5)^2(x-2.5)(x-7.5) + c$ where c is a constant (Figure 6.12).

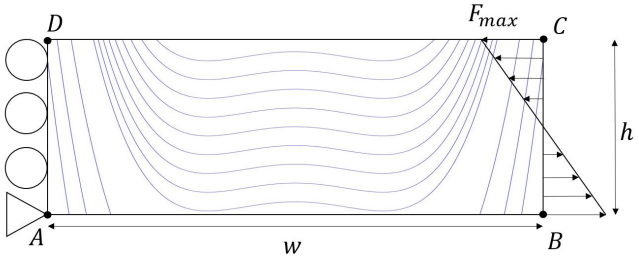

Figure 6.12 The pure bending problem, showing fibres described by a fourth-order polynomial

Figure 6.13(a) shows a plot of vertical tip displacement vs mesh density with the representative fibre orientation given by the fibre orientation at the centroid of an element. We note an initially erratic convergence behaviour of the Q2 approximation that then transitions to a smoother convergence after a mesh density of $d \approx 10$. Conversely we find an initially smooth convergence of the VEM formulations, comparable to that of $Q1$ elements, that starts to behave erratically after a mesh density of $d \approx 10$.

Figure 6.13(b) shows a plot of vertical tip displacement vs mesh density with the representative fibre orientation given by the average fibre orientation at the vertices of an element. In contrast to Figure 6.13(a) there is an initially erratic convergence behaviour of the VEM formulations that then behaves more smoothly after a mesh density of $d \approx 10$. In the smooth region of this plot the convergence behaviour of the VEM is similar to that of the Q1 approximation.

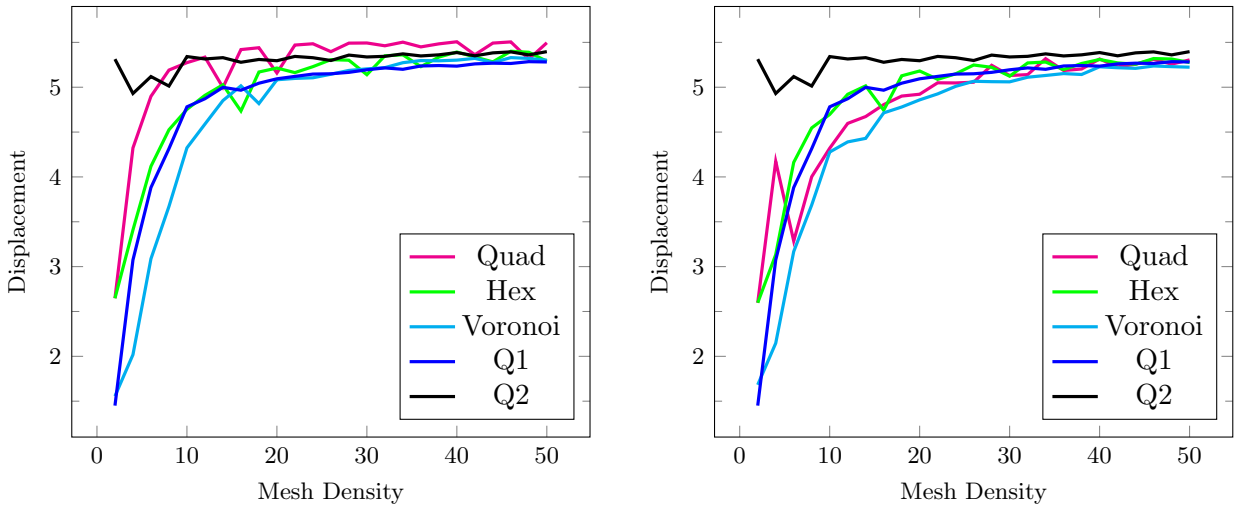

(a) Centroidal value of $\boldsymbol{a}$ **(b)** Average nodal value of $\boldsymbol{a}$

Figure 6.13 The pure bending problem: convergence tests for fibres described by a fourth-order polynomial considering fibre orientations based on; (a) the centroidal value of $\boldsymbol{a}$, and (b) the average nodal value of $\boldsymbol{a}$

6.3.3 Sixth-order polynomial fibre

6.3.3.1 Cook's membrane problem

Here we choose an orientation based on the family of curves $a = (x-24)^2(x-8)(x-16)(x-32)(x-40)+c$ where c is a constant (Figure 6.14).

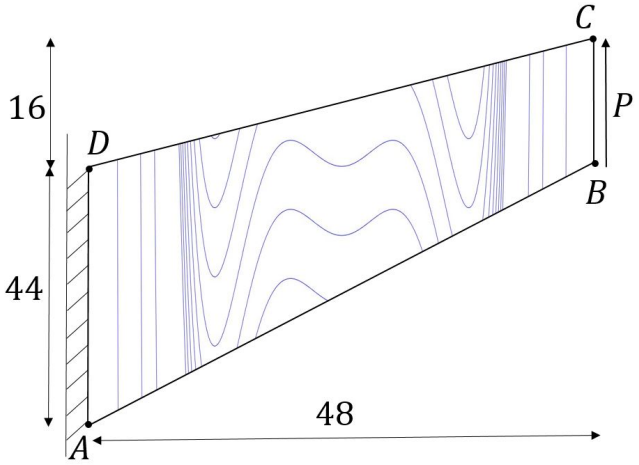

Figure 6.14 The Cook problem, showing fibres described by a sixth-order polynomial

Figure 6.15(a) shows a plot of vertical tip displacement vs mesh density with the representative fibre orientation given by the fibre orientation at the centroid of an element. The VEM formulations exhibit slightly better accuracy than the Q1 approximation but are again not comparable to the Q2 approximation.

Figure 6.15(b) shows a plot of vertical tip displacement vs mesh density with the representative fibre orientation given by the average fibre orientation at the vertices of an element. The Hex and Voronoi VEM formulations exhibit a similar degree of accuracy to the Q1 approximation. The Quad VEM formulation again, unexpectedly, exhibits poorer accuracy than the other VEM formulations and the Q1 approximation.

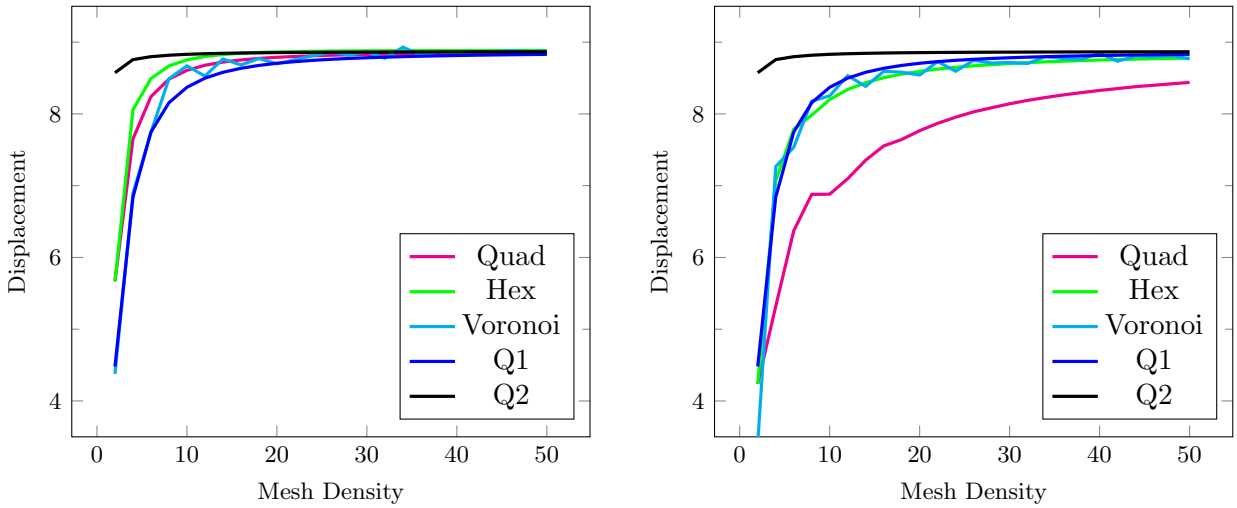

(a) Centroidal value of $\boldsymbol{a}$ **(b)** Average nodal value of $\boldsymbol{a}$

Figure 6.15 The Cook problem: convergence tests for fibres described by a sixth-order polynomial considering fibre orientations based on; (a) the centroidal value of $\boldsymbol{a}$, and (b) the average nodal value of $\boldsymbol{a}$

6.3.3.2 Pure bending problem

Here we choose an orientation based on the family of curves $a = (x-5)^2(x-\frac{5}{3})(x-\frac{10}{3})(x-\frac{20}{3})(x-\frac{25}{3})+c$ where c is a constant (Figure 6.16).

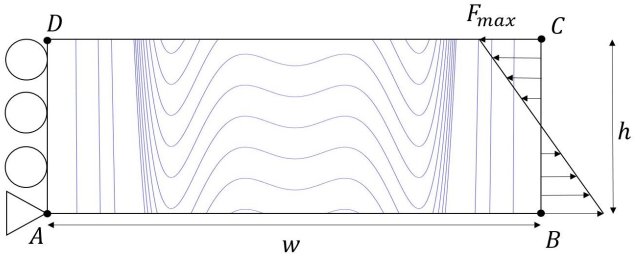

Figure 6.16 The pure bending problem, showing fibres described by a sixth-order polynomial

Figure 6.17(a) shows a plot of vertical tip displacement vs mesh density with the representative fibre orientation given by the fibre orientation at the centroid of an element. The VEM formulations exhibit largely smooth convergence behaviour similar to that of the Q1 approximation. Interestingly, we note much better agreement between all formulations for this nominally more complex distribution than found for the fourth-order case.

Figure 6.17(b) shows a plot of vertical tip displacement vs mesh density with the representative fibre orientation given by the average fibre orientation at the vertices of an element. The VEM Hex formulation exhibits smooth convergence behaviour comparable to that of the Q1 approximation. The VEM Quad and Voronoi formulations show initially erratic behaviour but become smoother as mesh density increases; their accuracy is, however, significantly poorer than that of the VEM Hex formulation and the Q1 approximation.

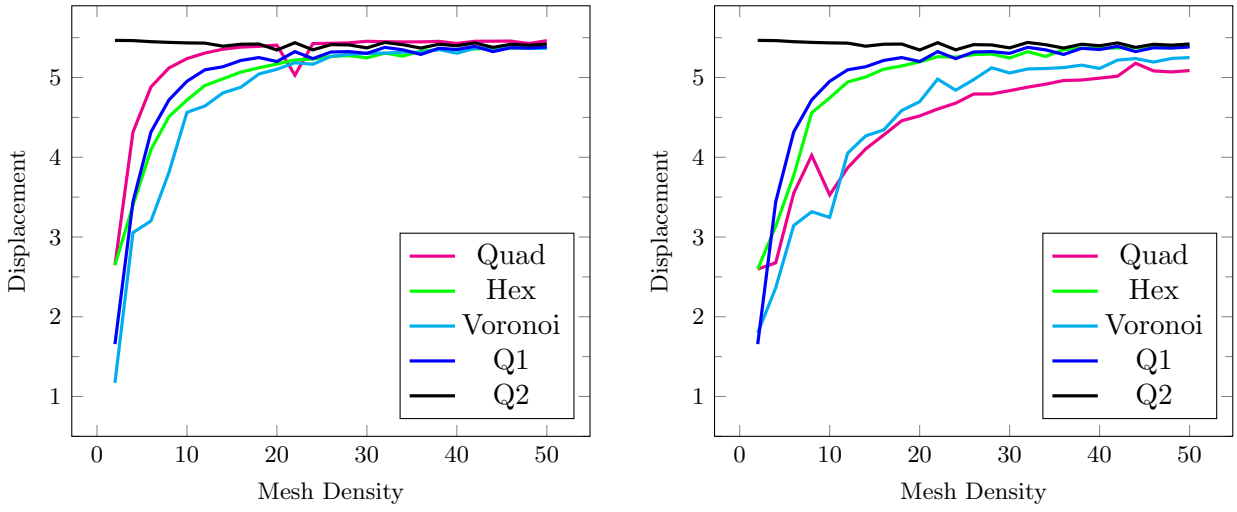

(a) Centroidal value of $\boldsymbol{a}$ **(b)** Average nodal value of $\boldsymbol{a}$

Figure 6.17 The pure bending problem: convergence tests for fibres described by a sixth-order polynomial considering fibre orientations based on; (a) the centroidal value of $\boldsymbol{a}$, and (b) the average nodal value of $\boldsymbol{a}$

6.4 Sinusoidal fibres

In this section we present convergence results of the Cook membrane and the pure bending problems for materials with fibre positions described by sinusoidal functions of increasing amplitude and frequency. As we will use sinusoidal fibres to test the effects of extreme material inhomogeneity, we obtain results for fibre orientations at the centroid of the elements and the vertices of the elements, as well as constant and varying combinations of the fibre orientations at the centroid and vertices.

6.4.1 Variation with $\sin x$

6.4.1.1 Cook's membrane problem

We present the results of a convergence analysis for Cook's membrane problem with a material containing a fibre with orientation described by the family of curves $a = \sin x + c$ where c is a constant, as depicted in Figure 6.18.

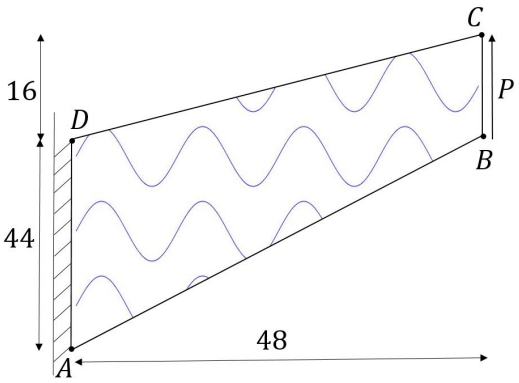

Figure 6.18 The Cook problem, showing fibres described by $a = \sin x + c$

Figure 6.19(a) shows a plot of vertical tip displacement vs mesh density with the representative fibre orientation given by the fibre orientation at the centroid of an element. The convergence behaviour of the VEM formulations is initially erratic, but as mesh density increases they stabilise and closely match the Q2 approximation. In the range of mesh densities presented here the Q1 approximation does not converge.

Figure 6.19(b) shows a plot of vertical tip displacement vs mesh density with the representative fibre orientation given by the average fibre orientation at the vertices of an element. The convergence of the VEM formulations is initially erratic but as mesh density increases they stabilise and yield similar results to the Q2 approximation.

Figure 6.19(c) shows a plot of vertical tip displacement vs mesh density with the representative fibre orientation given by a constant weighted average of the fibre orientation at the centroid and the average fibre orientation at the vertices of an element. Combining the fibre orientations results in less erratic behaviour for coarse meshes. The VEM formulations correlate well with the Q2 approximation as mesh density increases, but the convergence is still not monotonic.

Figure 6.19(d) shows a plot of vertical tip displacement vs mesh density with the representative fibre orientation given by a varying weighted average of the fibre orientation at the centroid and the average fibre orientation at the vertices of an element. The varying combination yields the same improvements for coarse meshes as the constant combination, and also improves the smoothness of convergence as mesh density increases. The VEM formulations show similar accuracy to the Q2 approximation with the Quad element even exhibiting superior accuracy.

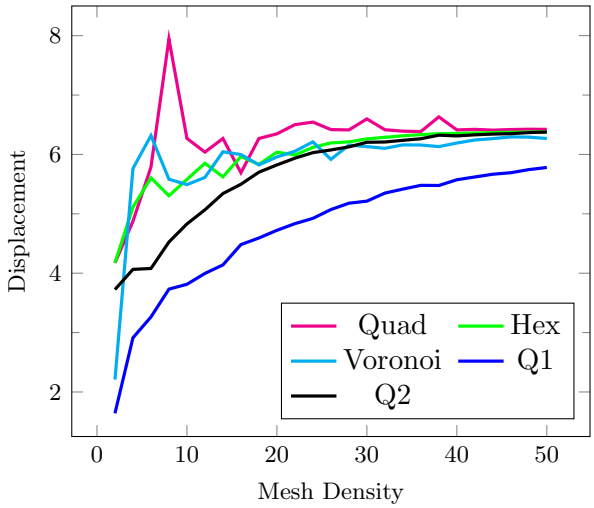

(a) Centroidal value of $\boldsymbol{a}$

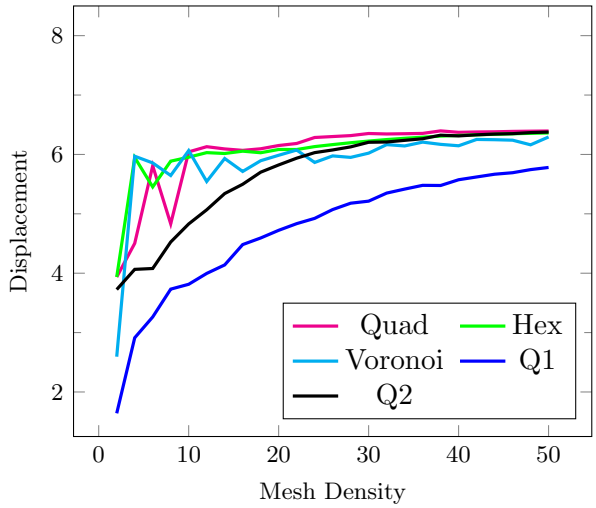

(b) Average nodal value of $\boldsymbol{a}$

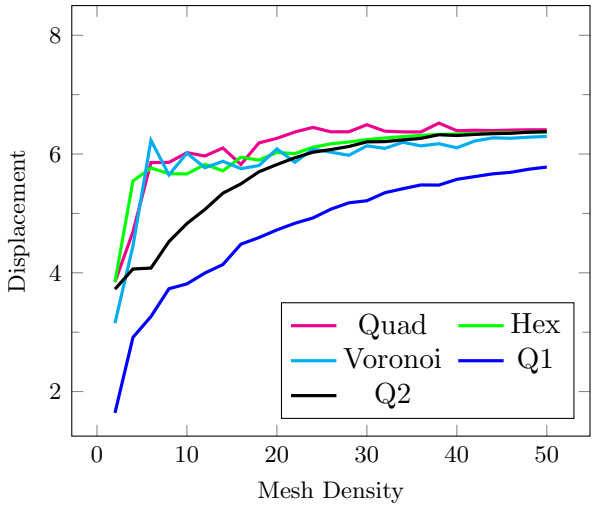

(c) Constant weighted combination - $w = \frac{1}{2}$

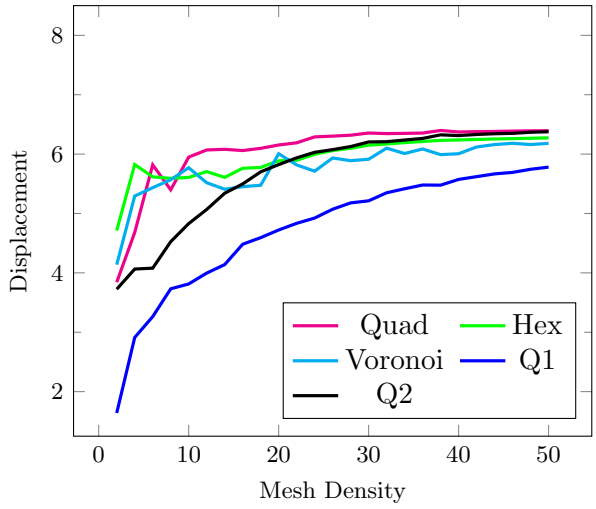

(d) Varying weighted combination

Figure 6.19 The Cook problem: convergence tests for fibres described by $a = \sin x + c$ considering fibre orientations based on; (a) the centroidal value of $\boldsymbol{a}$, (b) the average nodal value of $\boldsymbol{a}$, (c) a constant weighted combination of the centroidal and average nodal values of $\boldsymbol{a}$, and (d) a varying weighted combination of the centroidal and average nodal values of $\boldsymbol{a}$

6.4.1.2 Pure bending problem

We present the results of a convergence analysis for the pure bending problem with a material containing a fibre with orientation described by the family of curves $a = \sin x + c$ where c is a constant, as depicted in Figure 6.20.

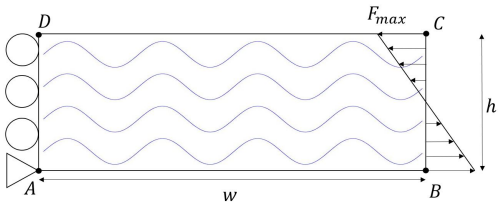

Figure 6.20 The pure bending problem, showing fibres described by $a = \sin x + c$

Figure 6.21(a) shows a plot of vertical tip displacement vs mesh density with the representative fibre orientation given by the fibre orientation at the centroid of an element. The VEM shows some initially erratic behaviour but as mesh density increases it exhibits superior accuracy to the Q1 approximation, with the Quad formulation closely matching the Q2 approximation.

Figure 6.21(b) shows a plot of vertical tip displacement vs mesh density with the representative fibre orientation given by the average fibre orientation at the vertices of an element. The convergence behaviour of the VEM is again initially slightly erratic and shows convergence behaviour similar to the Q1 approximation.

Figure 6.21(c) shows a plot of vertical tip displacement vs mesh density with the representative fibre orientation given by a constant weighted average of the fibre orientation at the centroid and the average fibre orientation at the vertices of an element. The VEM Voronoi formulation is initially very erratic but quickly smooths. Thereafter it shows monotonic behaviour and exhibits very similar accuracy to the Q1 approximation. The other VEM formulations converge smoothly throughout the domain and exhibit accuracy midway between that of the Q1 and Q2 approximations.

Figure 6.21(d) shows a plot of vertical tip displacement vs mesh density with the representative fibre orientation given by a varying weighted average of the orientation at the centroid and the average fibre orientation at the vertices of an element. Making use of the varying weighted average greatly reduces the initially erratic behaviour of the VEM Voronoi formulation in Figure 6.21(c). Again, the other VEM formulations converge smoothly throughout the domain and exhibit accuracy midway between that of the Q1 and Q2 approximations.

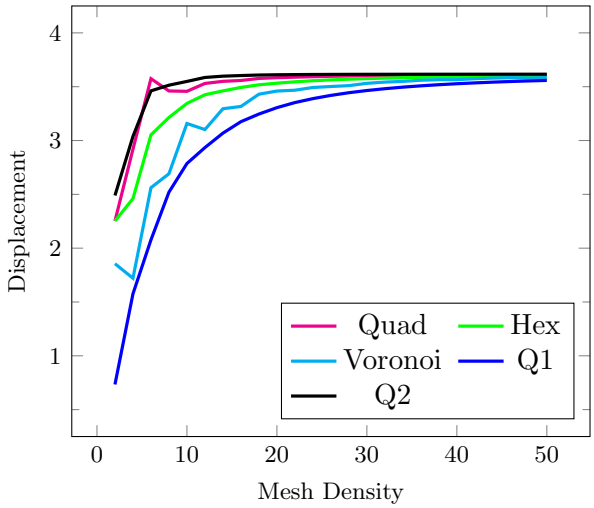

(a) Centroidal value of $\boldsymbol{a}$

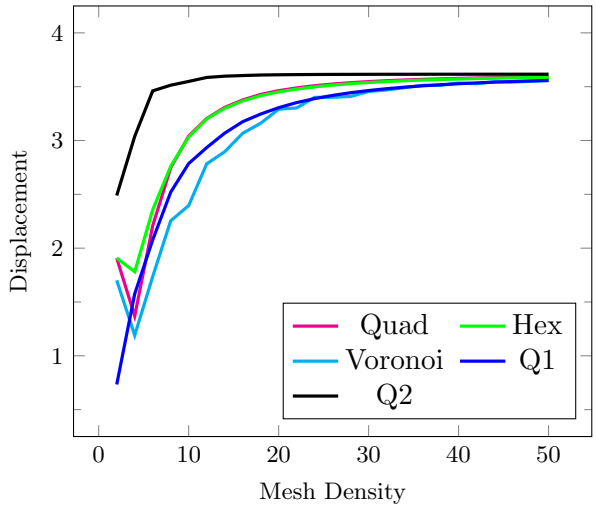

(b) Average nodal value of $\boldsymbol{a}$

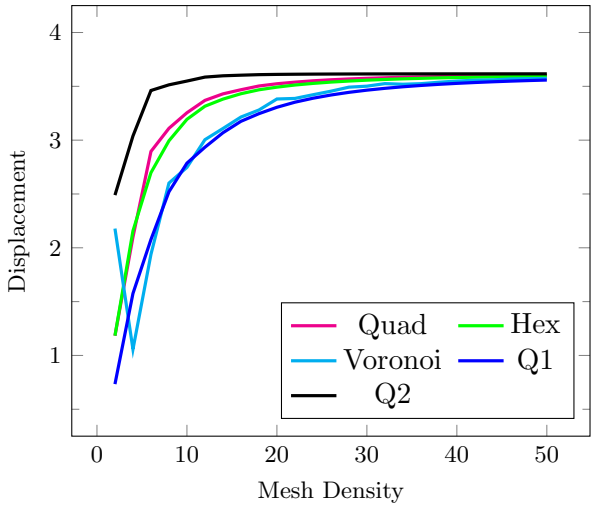

(c) Constant weighted combination - $w = \frac{1}{2}$

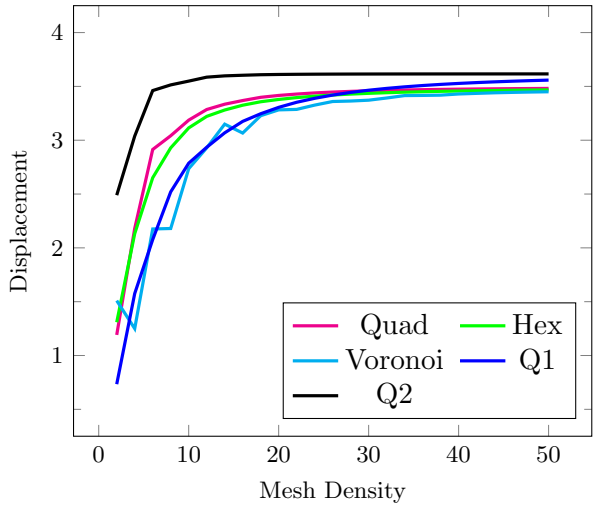

(d) Varying weighted combination

Figure 6.21 The pure bending problem: convergence tests for fibres described by $a = \sin x + c$ considering fibre orientations based on; (a) the centroidal value of $\boldsymbol{a}$, (b) the average nodal value of $\boldsymbol{a}$, (c) a constant weighted combination of the centroidal and average nodal values of $\boldsymbol{a}$, and (d) a varying weighted combination of the centroidal and average nodal values of $\boldsymbol{a}$

6.4.2 Variation with $2\sin x$

6.4.2.1 Cook's membrane problem

We present the results of a convergence analysis for Cook's membrane problem with a material containing a fibre with orientation described by the family of curves $a = 2\sin x + c$ where c is a constant, as depicted in Figure 6.22.

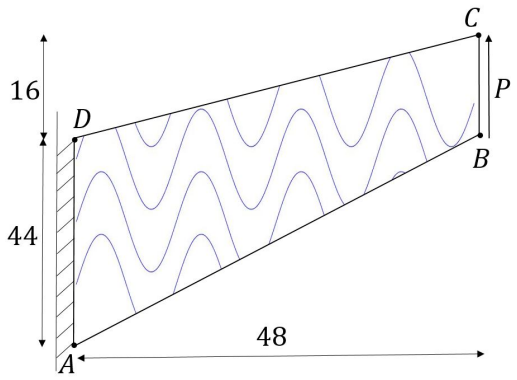

Figure 6.22 The Cook problem, showing fibres described by $a = 2\sin x + c$

Figure 6.23(a) shows a plot of vertical tip displacement vs mesh density with the representative fibre orientation given by the fibre orientation at the centroid of an element. The VEM formulations exhibit erratic convergence behaviour over the whole domain. In the range of mesh densities presented the Q1 approximation does not converge.

Figure 6.23(b) shows a plot of vertical tip displacement vs mesh density with the representative fibre orientation given by the average fibre orientation at the vertices of an element. The VEM formulations converge erratically up to a mesh density of $d \approx 20$ after which they smooth and yield similar results to the Q2 approximation.

Figure 6.23(c) shows a plot of vertical tip displacement vs mesh density with the representative fibre orientation given by a constant weighted average of the fibre orientation at the centroid and the average fibre orientation at the vertices of an element. The constant weighted combination reduces the initially erratic behaviour of the VEM formulations, however, the convergence never shows monotonic behaviour.

Figure 6.23(d) shows a plot of vertical tip displacement vs mesh density with the representative fibre orientation given by a varying weighted average of the fibre orientation at the centroid and the average fibre orientation at the vertices of an element. The varying weighted combination again improves the initially erratic behaviour as well as the overall smoothness of the convergence. For fine meshes the VEM formulations yield similar results to the Q2 approximation.

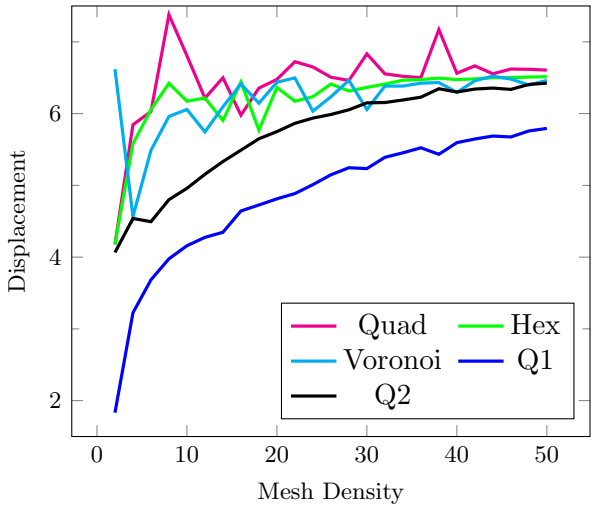

(a) Centroidal value of $\boldsymbol{a}$

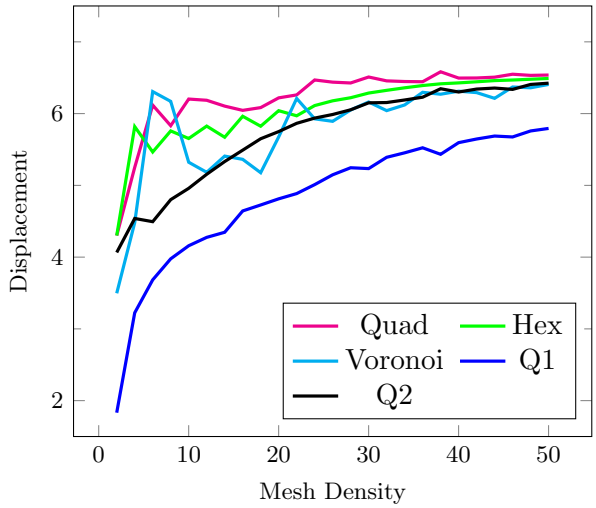

(b) Average nodal value of $\boldsymbol{a}$

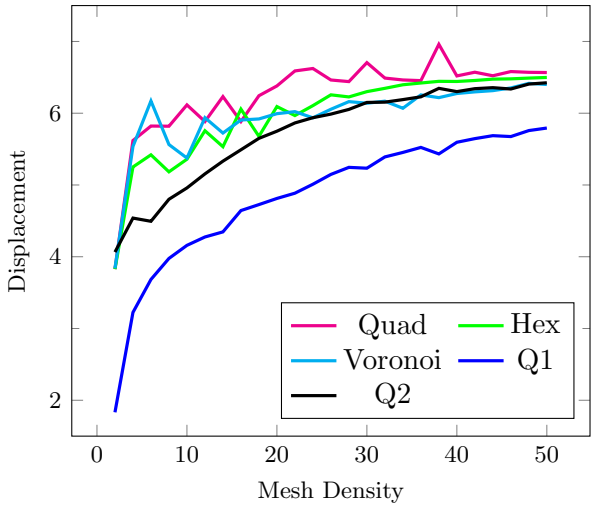

(c) Constant weighted combination - $w = \frac{1}{2}$

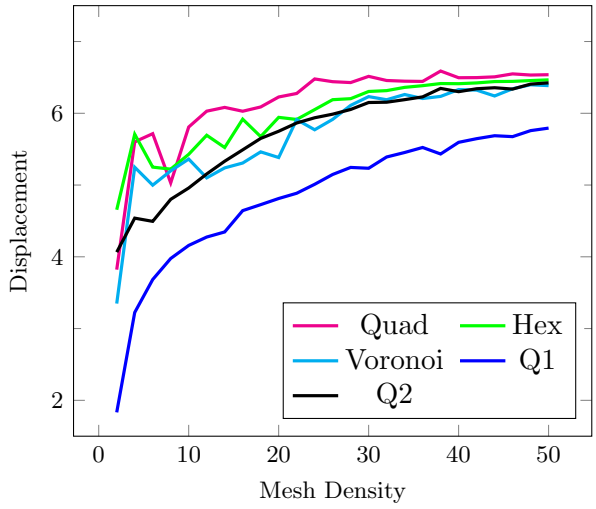

(d) Varying weighted combination

Figure 6.23 The Cook problem: convergence tests for fibres described by $a = 2\sin x + c$ considering fibre orientations based on; (a) the centroidal value of $\boldsymbol{a}$, (b) the average nodal value of $\boldsymbol{a}$, (c) a constant weighted combination of the centroidal and average nodal values of $\boldsymbol{a}$, and (d) a varying weighted combination of the centroidal and average nodal values of $\boldsymbol{a}$

6.4.2.2 Pure bending problem

We present the results of a convergence analysis for the pure bending problem with a material containing a fibre with orientation described by the family of curves $a = 2\sin x + c$ where c is a constant, as depicted in Figure 6.24.

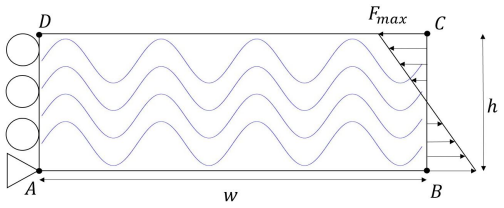

Figure 6.24 The pure bending problem, showing fibres described by $a = 2\sin x + c$

Figure 6.25(a) shows a plot of vertical tip displacement vs mesh density with the representative fibre orientation given by the fibre orientation at the centroid of an element. The convergence of the VEM formulations is initially erratic but behaves more smoothly after a mesh density of $d \approx 15$; after which the VEM formulations show superior accuracy to the Q1 approximation, with the Quad element closely matching the Q2 approximation.

Figure 6.25(b) shows a plot of vertical tip displacement vs mesh density with the representative fibre orientation given by the average fibre orientation at the vertices of an element. The convergence of the VEM formulations is initially erratic. The VEM Quad and Hex formulations exhibit accuracy between that of the Q1 and Q2 approximations throughout the domain.

Figure 6.25(c) shows a plot of vertical tip displacement vs mesh density with the representative fibre orientation given by a constant weighted average of the fibre orientation at the centroid and the average fibre orientation at the vertices of an element. The initially erratic convergence behaviour of the VEM formulations is slightly improved using the constant weighted combination.

Figure 6.25(d) shows a plot of vertical tip displacement vs mesh density with the representative fibre orientation given by a varying weighted average of the fibre orientation at the centroid and the average fibre orientation at the vertices of an element. Using the varying weighted combination further improves the initially erratic behaviour and improves the overall accuracy of the VEM formulations. The VEM Voronoi formulation closely matches the Q1 approximation. The VEM Quad and Hex formulations exhibit accuracy between that of the Q1 and Q2 approximations.

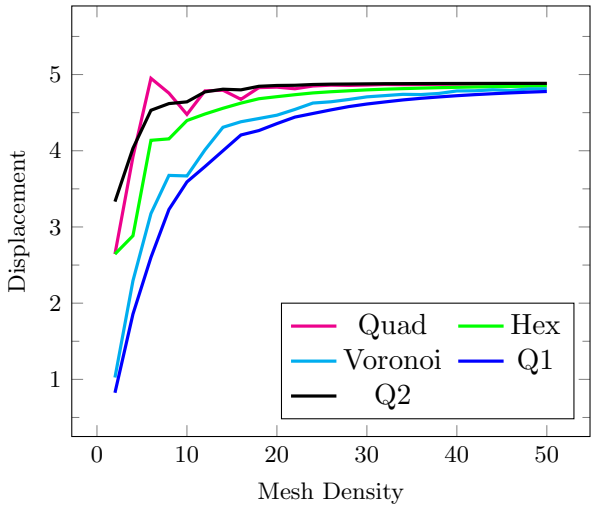

(a) Centroidal value of $\boldsymbol{a}$

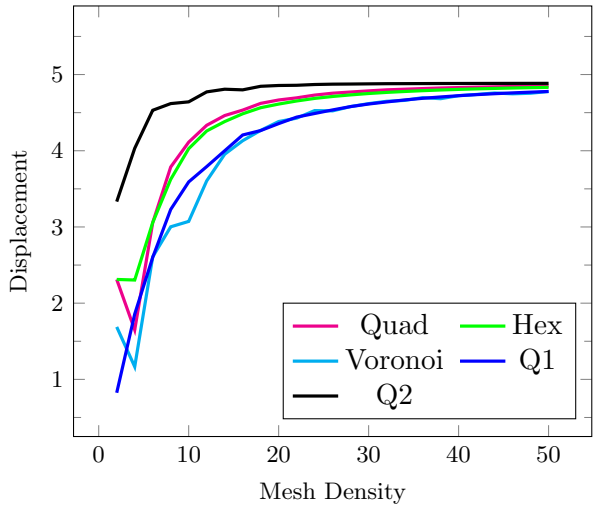

(b) Average nodal value of $\boldsymbol{a}$

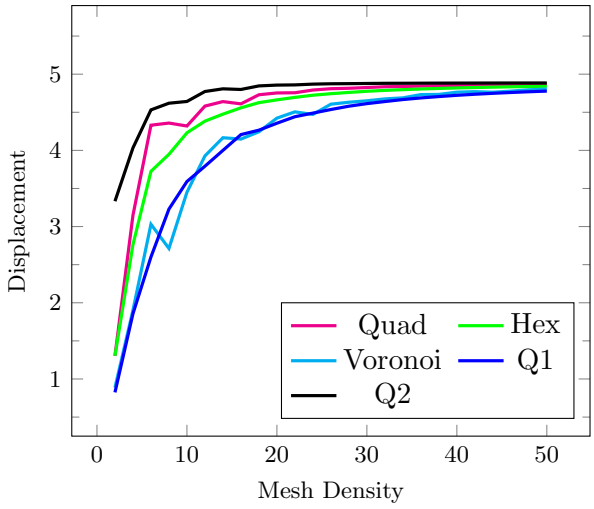

(c) Constant weighted combination - $w = \frac{1}{2}$

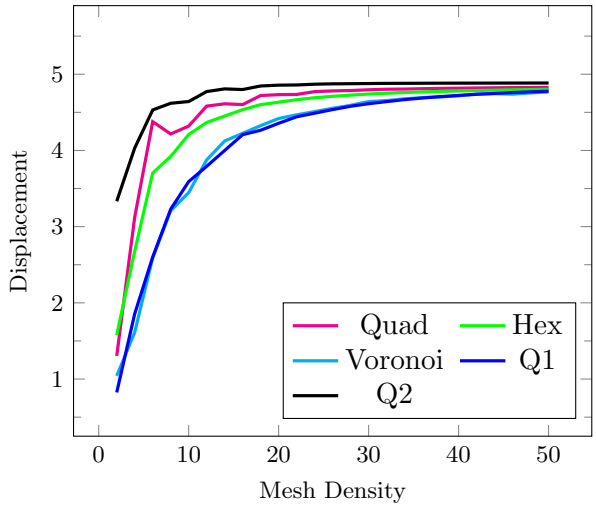

(d) Varying weighted combination

Figure 6.25 The pure bending problem: convergence tests for fibres described by $a = 2\sin x + c$ considering fibre orientations based on; (a) the centroidal value of $\boldsymbol{a}$, (b) the average nodal value of $\boldsymbol{a}$, (c) a constant weighted combination of the centroidal and average nodal values of $\boldsymbol{a}$, and (d) a varying weighted combination of the centroidal and average nodal values of $\boldsymbol{a}$

6.4.3 Variation with $\sin 2x$

6.4.3.1 Cook's membrane problem

We present the results of a convergence analysis for Cook's membrane problem with a material containing a fibre with orientation described by the family of curves $a = \sin 2x + c$ where c is a constant, as depicted in Figure 6.26.

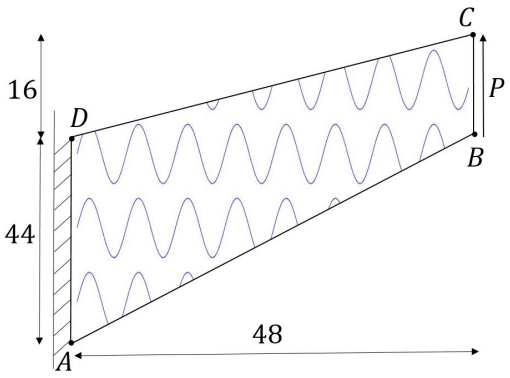

Figure 6.26 The Cook problem, showing fibres described by $a = \sin 2x + c$

Figure 6.27(a) shows a plot of vertical tip displacement vs mesh density with the representative fibre orientation given by the fibre orientation at the centroid of an element. The VEM formulations exhibit extremely erratic convergence behaviour for mesh densities up to $d \approx 25$. In the range of mesh densities presented neither the Q1 nor Q2 approximations converge.

Figure 6.27(b) shows a plot of vertical tip displacement vs mesh density with the representative fibre orientation given by the average fibre orientation at the vertices of an element. The VEM formulations, again, exhibit initially erratic convergence behaviour for meshes up to $d \approx 25$ after which they behave more smoothly than in Figure 6.27(a). The various formulations however do not converge to a similar solution.

Figure 6.27(c) shows a plot of vertical tip displacement vs mesh density with the representative fibre orientation given by a constant weighted average of the fibre orientation at the centroid and the average fibre orientation at the vertices of an element. Use of the constant weighted combination improves the initially erratic behaviour of Figure 6.27(b), the erratic behaviour is now only evident up to a mesh density of $d \approx 10$.

Figure 6.27(d) shows a plot of vertical tip displacement vs mesh density with the representative fibre orientation given by a varying weighted average of the fibre orientation at the centroid and the average fibre orientation at the vertices of an element. Using the varying weighted combination yields erratic convergence behaviour for mesh densities up to $d \approx 20$ after which it is smoothed significantly. For fine meshes the VEM Hex and Voronoi formulations appear to approach a similar solution to the Q2 approximation.

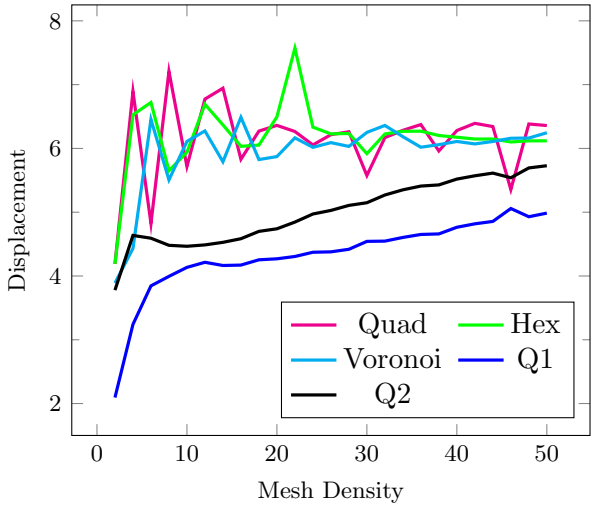

(a) Centroidal value of $\boldsymbol{a}$

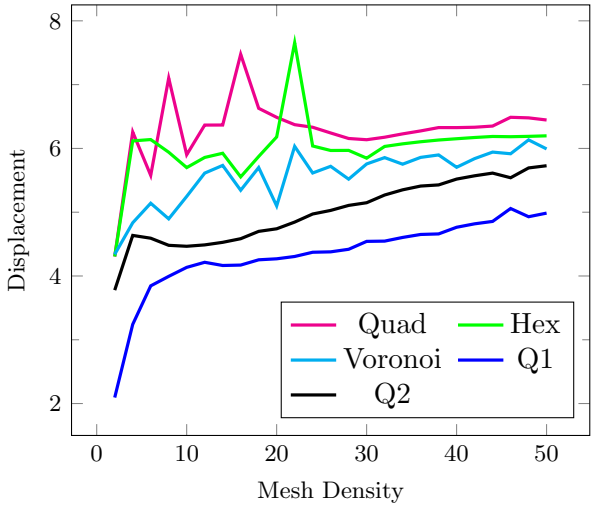

(b) Average nodal value of $\boldsymbol{a}$

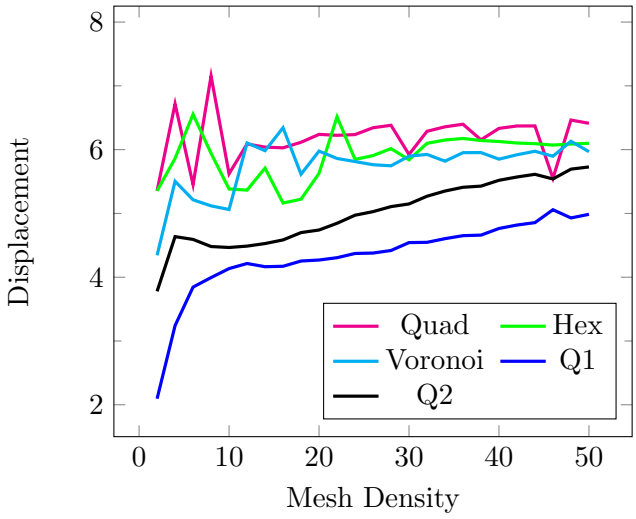

(c) Constant weighted combination - $w = \frac{1}{2}$

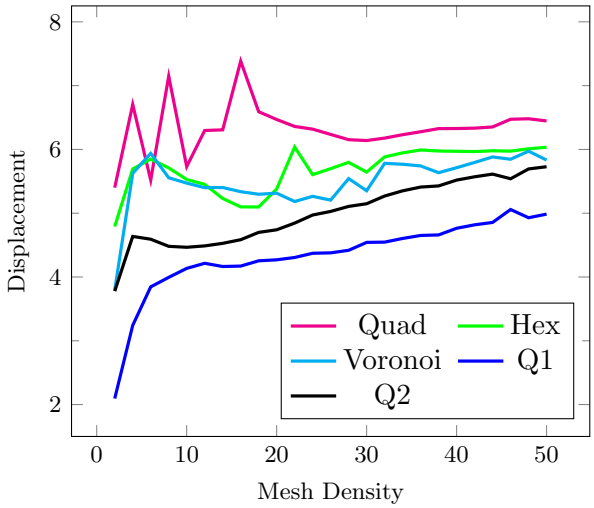

(d) Varying weighted combination

Figure 6.27 The Cook problem: convergence tests for fibres described by $a = \sin 2x + c$ considering fibre orientations based on; (a) the centroidal value of $\boldsymbol{a}$, (b) the average nodal value of $\boldsymbol{a}$, (c) a constant weighted combination of the centroidal and average nodal values of $\boldsymbol{a}$, and (d) a varying weighted combination of the centroidal and average nodal values of $\boldsymbol{a}$

6.4.3.2 Pure bending problem

We present the results of a convergence analysis for the pure bending problem with a material containing a fibre with orientation described by the family of curves $a = \sin 2x + c$ where c is a constant, as depicted in Figure 6.28.

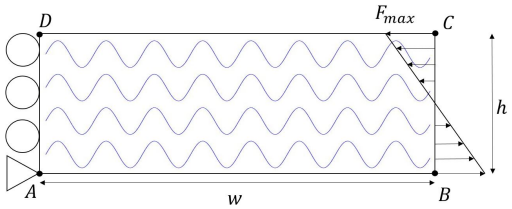

Figure 6.28 The pure bending problem, showing fibres described by $a = \sin 2x + c$

Figure 6.29(a) shows a plot of vertical tip displacement vs mesh density with the representative fibre orientation given by the fibre orientation at the centroid of an element. The VEM formulations exhibit slightly erratic convergence for mesh densities up to $d \approx 20$ after which they behave smoothly and show better accuracy than the Q1 approximation.

Figure 6.29(b) shows a plot of vertical tip displacement vs mesh density with the representative fibre orientation given by the average fibre orientation at the vertices of an element. The VEM formulations converge erratically for mesh densities up to $d \approx 10$ after which they converge smoothly and exhibit accuracy comparable to the Q1 approximation.

Figure 6.29(c) shows a plot of vertical tip displacement vs mesh density with the representative fibre orientation given by a constant weighted average of the fibre orientation at the centroid and the average fibre orientation at the vertices of an element. Use of the constant weighting combination improves the smoothness of convergence over the whole domain. However, the VEM Quad formulation behaves slightly erratically for very coarse meshes.

Figure 6.29(d) shows a plot of vertical tip displacement vs mesh density with the representative fibre orientation given by a varying weighted average of the fibre orientation at the centroid and the average fibre orientation at the vertices of an element. The varying weighted combination produces the smoothest convergence over the domain. This method yielded no notably erratic convergence behaviour whereas the Q2 approximation behaves erratically for very coarse meshes. The VEM Voronoi formulation exhibits similar accuracy to the Q1 approximation with the Quad formulation closely matching the Q2 approximation for meshes with density greater than $d \approx 10$.

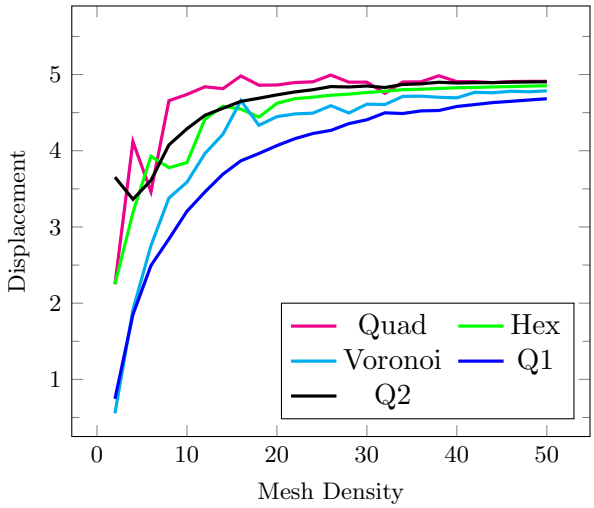

(a) Centroidal value of $\boldsymbol{a}$

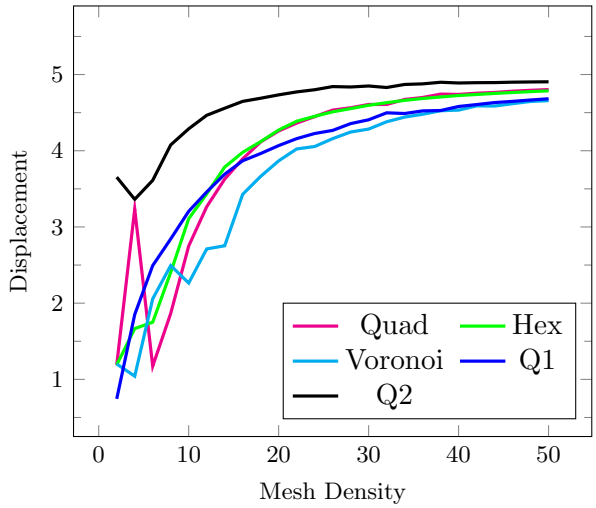

(b) Average nodal value of $\boldsymbol{a}$

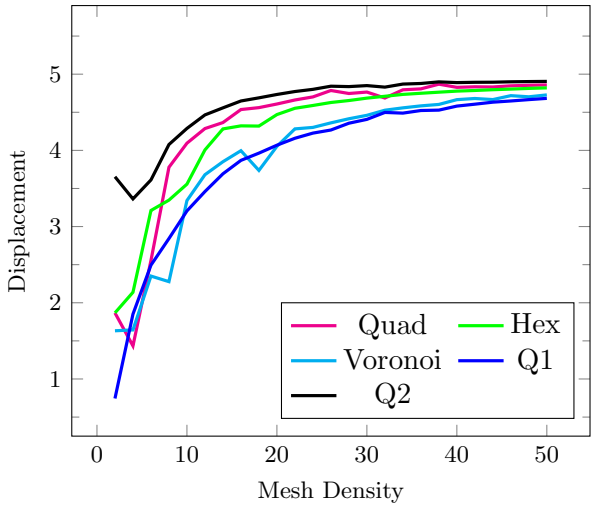

(c) Constant weighted combination - $w = \frac{1}{2}$

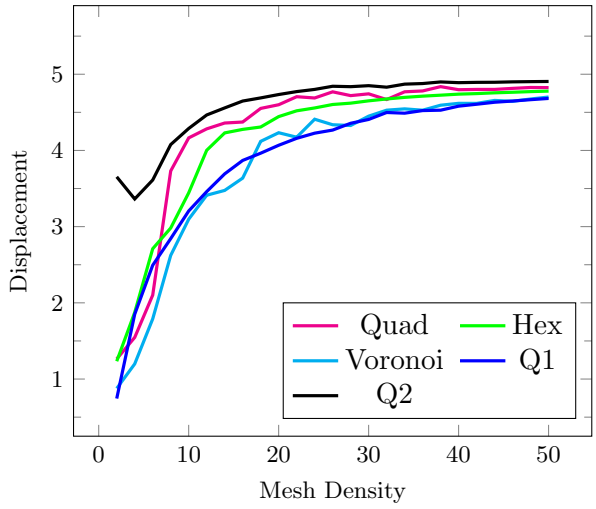

(d) Varying weighted combination

Figure 6.29 The pure bending problem: convergence tests for fibres described by $a = \sin 2x + c$ considering fibre orientations based on; (a) the centroidal value of $\boldsymbol{a}$, (b) the average nodal value of $\boldsymbol{a}$, (c) a constant weighted combination of the centroidal and average nodal values of $\boldsymbol{a}$, and (d) a varying weighted combination of the centroidal and average nodal values of $\boldsymbol{a}$

6.5 Effect of anisotropy

In this section we investigate the effects of the anisotropy ratio p on the robustness and accuracy of the VEM when modelling non-homogeneous transversely isotropic materials. We consider the Cook membrane problem and pure bending problem benchmark tests described in Section 6.1. The problem geometries are unchanged but we now consider both compressible, $\nu = 0.3$, and nearly incompressible, $\nu = 0.49995$, materials. In the subsequent plots we have calculated the averaged fibre direction for each element using the varying weighted combination method with a mesh density of $d = 50$.

6.5.1 Second-order polynomial fibre

6.5.1.1 Cook's membrane problem

We present the results of an anisotropy analysis for Cook's membrane problem with a material containing a fibre with orientation described by the family of curves $a = (x-24)^2+c$ where c is a constant.

Figure 6.30(a) shows a plot of tip displacement vs p for a compressible material over the range $1 \leq p \leq 10^5$. The Q2 approximation shows poor approximability as $p \to \infty$, with the Q1 approximation exhibiting severe locking. The VEM formulations are locking free as before. The VEM Voronoi formulation shows some mild scatter for very large values of p.

Figure 6.30(b) shows a plot of tip displacement vs p for a nearly incompressible material over the range $1 \leq p \leq 10^5$. As with Figure 6.30(a) the Q2 approximation shows poor approximability as $p \to \infty$, with the Q1 approximation exhibiting locking behaviour. The Q1 approximation is locking free for small values of p, for $p > 1$. The VEM formulations are again locking free with the Voronoi formulation showing mild scatter.

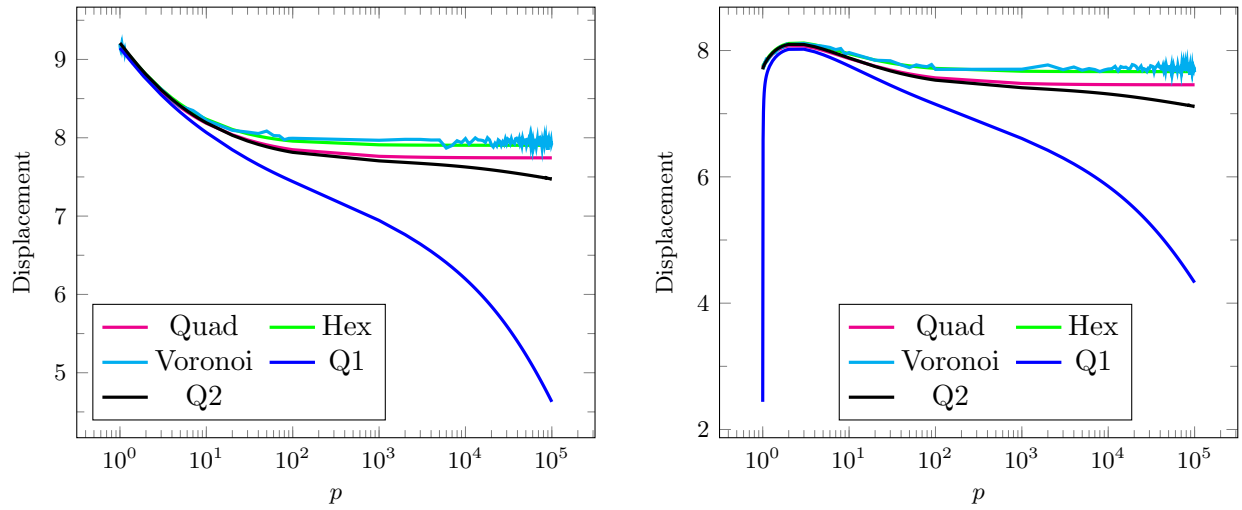

(a) Compressible material - $\nu = 0.3$ **(b)** Nearly incompressible material - $\nu = 0.49995$

Figure 6.30 The Cook problem: tip displacement vs p for fibres described by a second-order polynomial for; (a) compressible material, and (b) nearly incompressible material

6.5.1.2 Pure bending problem

We present the results of an anisotropy analysis for the pure bending problem with a material containing a fibre with orientation described by the family of curves $a = (x-5)^2 + c$ where c is a constant.

Figure 6.31(a) shows a plot of tip displacement vs p for a compressible material over the range $1 \leq p \leq 10^5$. The Q2 approximation and VEM formulations perform well over the domain with the Q1 approximation exhibiting locking as $p \to \infty$.

Figure 6.31(b) shows a plot of tip displacement vs p for a nearly incompressible material over the range $1 \leq p \leq 10^5$. The Q2 approximation and VEM formulations again perform well over the domain with the Q1 approximation exhibiting locking as $p \to \infty$ as well as for $p \to 1$.

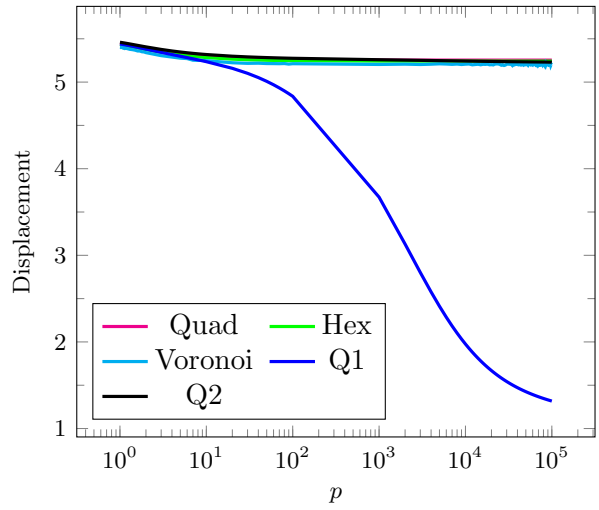

(a) Compressible material - $\nu = 0.3$

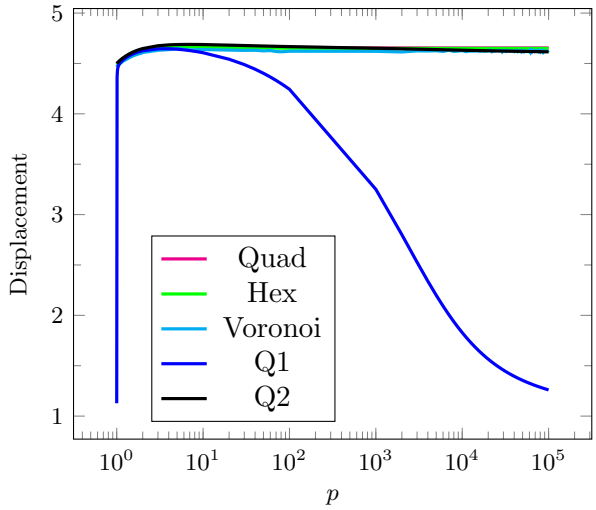

(b) Nearly incompressible material - $\nu = 0.49995$

Figure 6.31 The pure bending problem: tip displacement vs p for fibres described by a second-order polynomial for; (a) compressible material, and (b) nearly incompressible material

6.5.2 Fourth-order polynomial fibre

6.5.2.1 Cook's membrane problem

We present the results of an anisotropy analysis for Cook's membrane problem with a material containing a fibre with orientation described by the family of curves $a = (x-24)^2(x-12)(x-36) + c$ where c is a constant.

Figure 6.32(a) shows a plot of tip displacement vs p for a compressible material over the range $1 \leq p \leq 10^5$. The Q1 and Q2 approximations both exhibit severe locking as $p \to \infty$ while the VEM formulations remain locking free. The VEM Voronoi formulation again shows mild scatter behaviour for large values of p.

Figure 6.32(b) shows a plot of tip displacement vs p for a nearly incompressible material over the range $1 \leq p \leq 10^5$. The Q1 and Q2 approximations again exhibit significant locking as $p \to \infty$, with the Q1 approximation exhibiting its well established locking behaviour as $p \to 1$. The VEM formulations perform well with mild scatter shown by the Voronoi formulation.

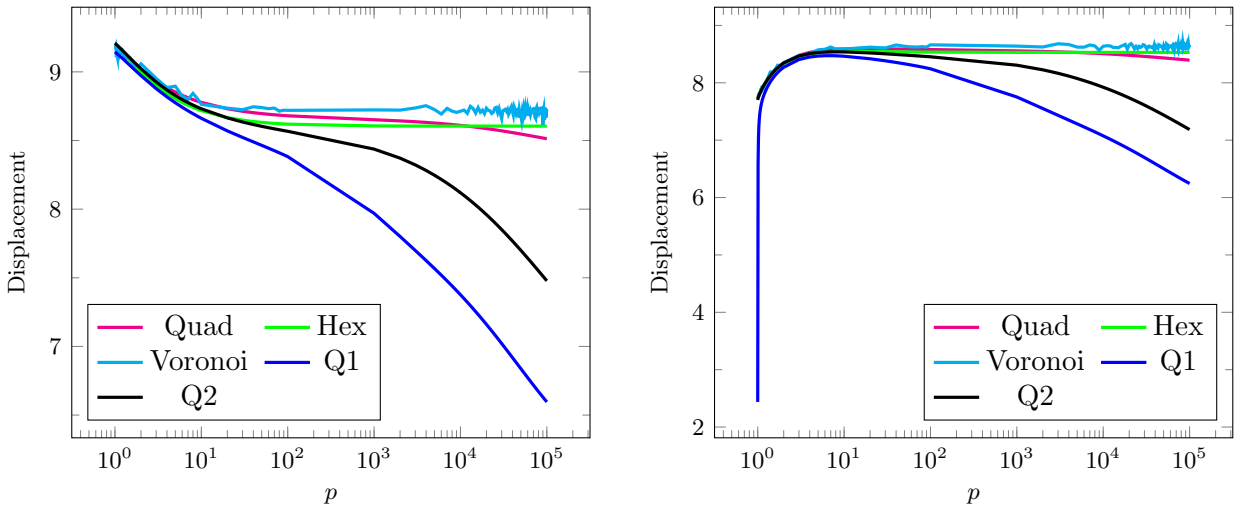

(a) Compressible material - $\nu = 0.3$ **(b)** Nearly incompressible material - $\nu = 0.49995$

Figure 6.32 The Cook problem: tip displacement vs p for fibres described by a fourth-order polynomial for; (a) compressible material, and (b) nearly incompressible material

6.5.2.2 Pure bending problem

We present the results of an anisotropy analysis for the pure bending problem with a material containing a fibre with orientation described by the family of curves $a = (x-5)^2(x-2.5)(x-7.5) + c$ where c is a constant.

Figure 6.33(a) shows a plot of tip displacement vs p for a compressible material over the range $1 \leq p \leq 10^5$. The Q2 approximation shows poor approximability for large values of p, while the Q1 approximation shows locking behaviour as $p \to \infty$. The VEM formulations are locking free and the different formulations yield similar results and trends over the domain with the usual scatter from the Voronoi formulation.

Figure 6.33(b) shows a plot of tip displacement vs p for a nearly incompressible material over the range $1 \leq p \leq 10^5$. The Q2 approximation and VEM formulations perform well over the domain. The Q1 approximation exhibits locking as $p \to \infty$ as well as for $p \to 1$.

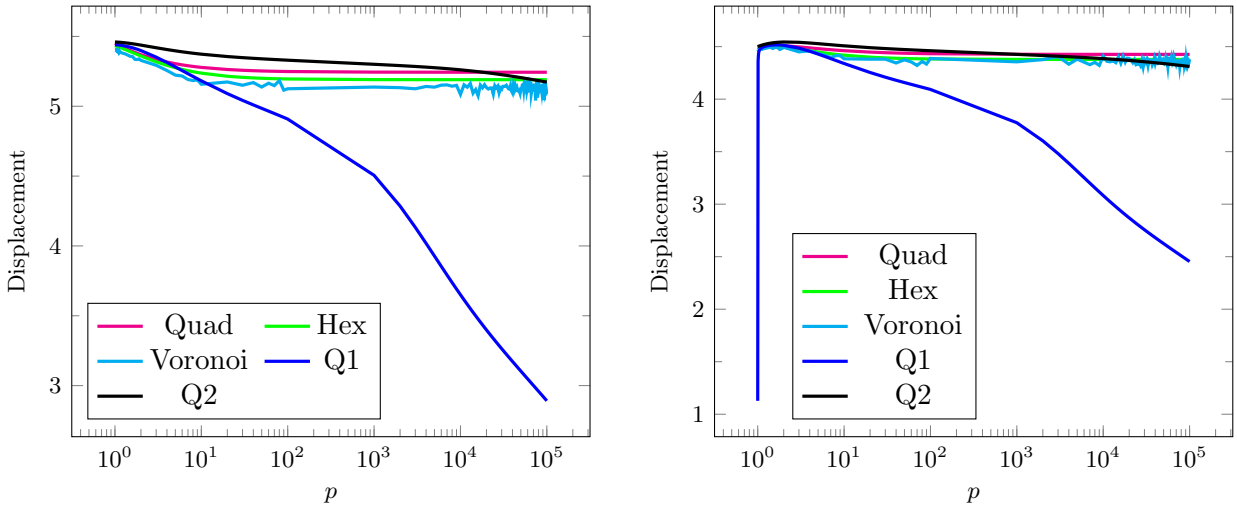

(a) Compressible material - $\nu = 0.3$ **(b)** Nearly incompressible material - $\nu = 0.49995$

Figure 6.33 The pure bending problem: tip displacement vs p for fibres described by a fourth-order polynomial for; (a) compressible material, and (b) nearly incompressible material

6.5.3 Sixth-order polynomial fibre

6.5.3.1 Cook's membrane problem

We present the results of an anisotropy analysis for Cook's membrane problem with a material containing a fibre with orientation described by the family of curves $a = (x-24)^2(x-8)(x-16)(x-32)(x-40) + c$ where c is a constant.

Figure 6.34(a) shows a plot of tip displacement vs p for a compressible material over the range $1 \leq p \leq 10^5$. The Q1 and Q2 approximations as well as the VEM Quad formulation exhibit similar locking free behaviour. The VEM Hex and Voronoi formulations yield a different solution to the other formulations with the Voronoi formulation showing significant scatter. In the absence of an analytical solution or different approximation methods it is difficult to predict which formulations approximate the solution best. There is, however, a difference of only $\approx 1.2\%$ between the formulations.

Figure 6.34(b) shows a plot of tip displacement vs p for a nearly incompressible material over the range $1 \leq p \leq 10^5$. The Q2 approximation and VEM formulations perform well over the domain with very slight scatter from the Voronoi formulation. The Q1 approximation atypically exhibits locking only as $p \to 1$.

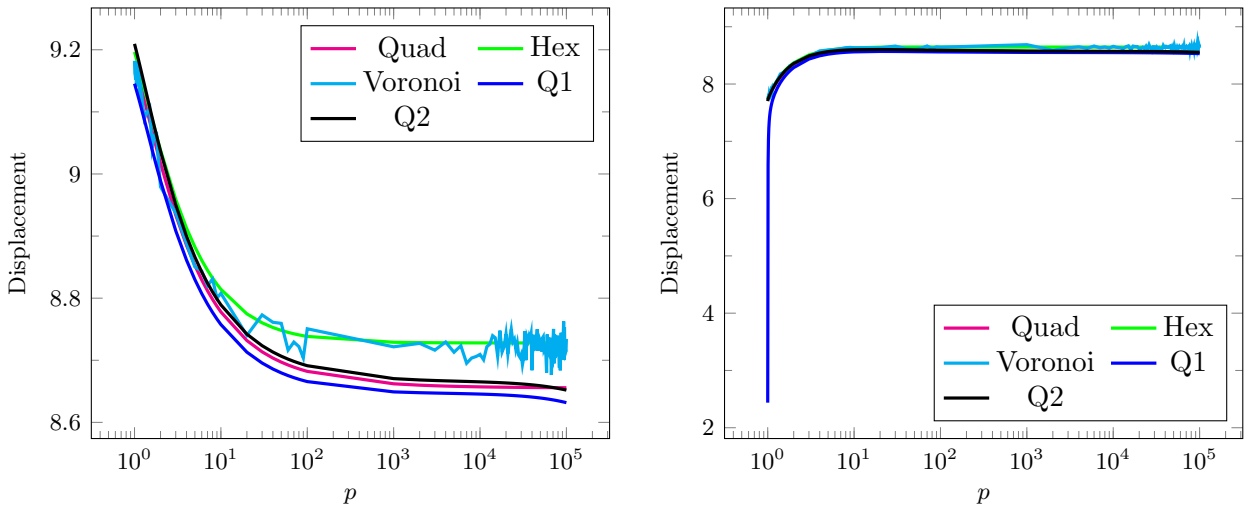

(a) Compressible material - $\nu = 0.3$ **(b)** Nearly incompressible material - $\nu = 0.49995$

Figure 6.34 The Cook problem: tip displacement vs p for fibres described by a sixth-order polynomial for; (a) compressible material, and (b) nearly incompressible material

6.5.3.2 Pure bending problem

We present the results of an anisotropy analysis for the pure bending problem with a material containing a fibre with orientation described by the family of curves $a = (x-5)^2(x-\frac{5}{3})(x-\frac{10}{3})(x-\frac{20}{3})(x-\frac{25}{3})+c$ where c is a constant.

Figure 6.35(a) shows a plot of tip displacement vs p for a compressible material over the range $1 \leq p \leq 10^5$. We note little correlation between the formulations. The Q1 and Q2 approximations both exhibit locking behaviour as $p \to \infty$, and the VEM Voronoi formulation shows significant scatter. The VEM Quad and Hex formulations show no numerical pathologies and both tend to a specific value as $p \to \infty$, the formulations, however, do not tend to the same value. This behaviour is possibly due to regions in which fibres have a very small radius of curvature. The smaller radius of curvature corresponds to more extreme inhomogeneity which is difficult to model accurately.

Figure 6.35(b) shows a plot of tip displacement vs p for a nearly incompressible material over the range $1 \leq p \leq 10^5$. We note largely similar behaviour to that seen in Figure 6.35(a) with the addition of the Q1 approximation locking as $p \to 1$.

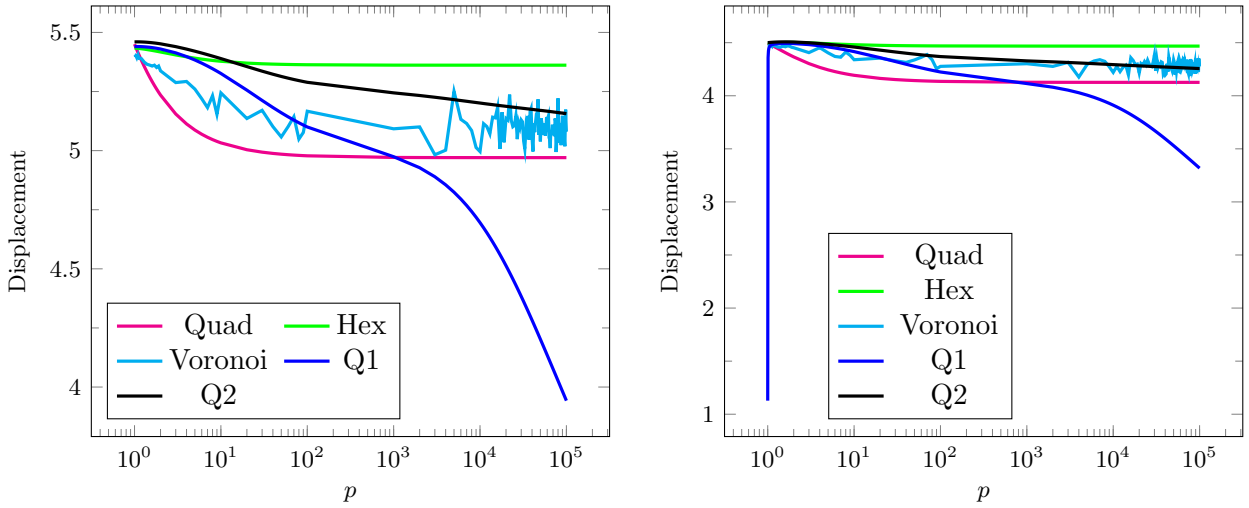

(a) Compressible material - $\nu = 0.3$ **(b)** Nearly incompressible material - $\nu = 0.49995$

Figure 6.35 The pure bending problem: tip displacement vs p for fibres described by a sixth-order polynomial for; (a) compressible material, and (b) nearly incompressible material

6.5.4 Variation with $\sin x$

6.5.4.1 Cook's membrane problem

We present the results of an anisotropy analysis for Cook's membrane problem with a material containing a fibre with orientation described by the family of curves $a = \sin x + c$ where c is a constant.

Figure 6.36(a) shows a plot of tip displacement vs p for a compressible material over the range $1 \leq p \leq 10^5$. The VEM formulations perform well over the domain with mild scatter behaviour from the Voronoi formulation. The Q1 and Q2 formulations both exhibit locking as $p \to \infty$.

Figure 6.36(b) shows a plot of tip displacement vs p for a nearly incompressible material over the range $1 \leq p \leq 10^5$. The VEM formulations again perform well over the domain with mild scatter behaviour from the Voronoi formulation. The Q1 and Q2 formulations both exhibit locking as $p \to \infty$ with the Q1 approximation also locking as $p \to \infty$.

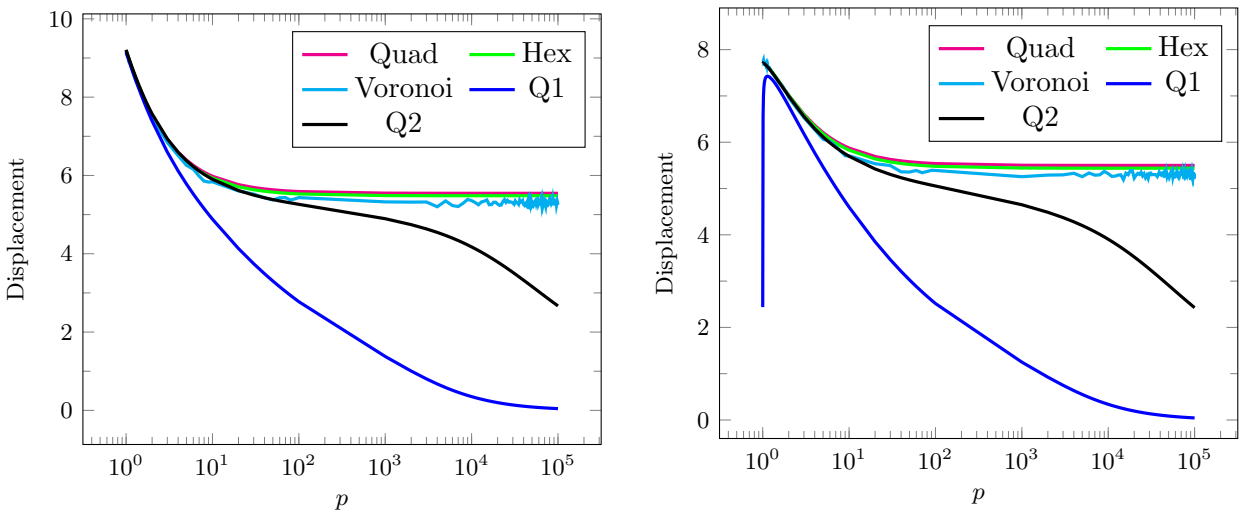

(a) Compressible material - $\nu = 0.3$

(b) Nearly incompressible material - $\nu = 0.49995$

Figure 6.36 The Cook problem: tip displacement vs p for fibres described by $a = \sin x + c$ for; (a) compressible material, and (b) nearly incompressible material

6.5.4.2 Pure bending problem

We present the results of an anisotropy analysis for the pure bending problem with a material containing a fibre with orientation described by the family of curves $a = \sin x + c$ where c is a constant.

Figure 6.37(a) shows a plot of tip displacement vs p for a compressible material over the range $1 \leq p \leq 10^5$. The VEM formulations perform well over the domain. The Q2 formulation exhibits mild locking and the Q1 approximation severe locking as $p \to \infty$.

Figure 6.37(b) shows a plot of tip displacement vs p for a nearly incompressible material over the range $1 \leq p \leq 10^5$. The VEM formulations perform well over the domain. The Q2 formulation exhibits mild locking and the Q1 approximation severe locking as $p \to \infty$. The Q1 approximation also shows its propensity to lock as $p \to 1$.

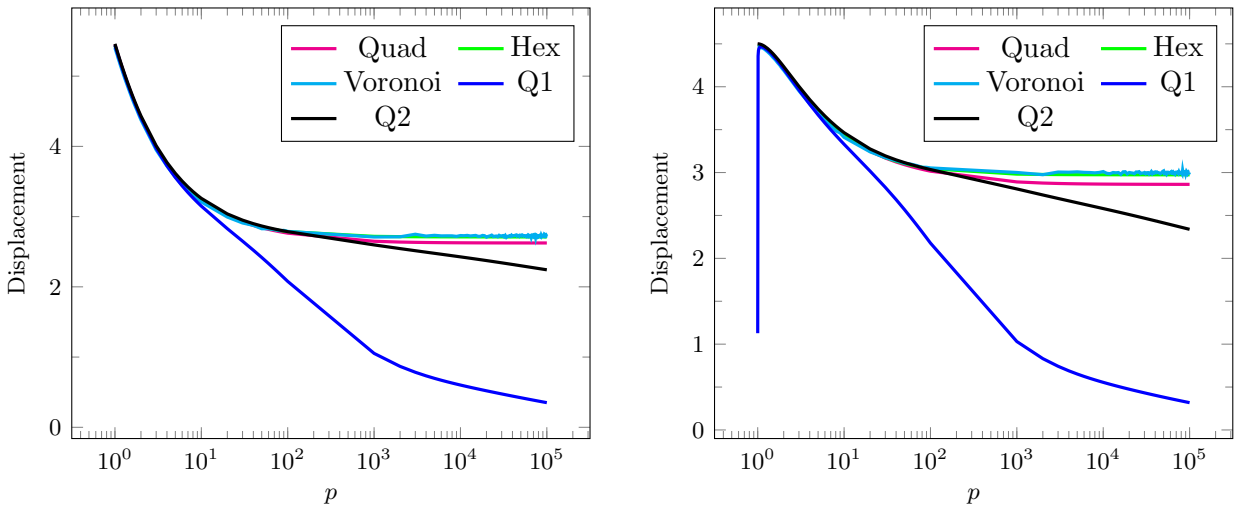

(a) Compressible material - $\nu = 0.3$ **(b)** Nearly incompressible material - $\nu = 0.49995$

Figure 6.37 The pure bending problem: tip displacement vs p for fibres described by $a = \sin x + c$ for; (a) compressible material, and (b) nearly incompressible material

6.5.5 Variation with $2\sin x$

6.5.5.1 Cook's membrane problem

We present the results of an anisotropy analysis for Cook's membrane problem with a material containing a fibre with orientation described by the family of curves $a = 2\sin x + c$ where c is a constant.

Figure 6.38(a) shows a plot of tip displacement vs p for a compressible material over the range $1 \leq p \leq 10^5$. The VEM formulations generally perform well over the domain with the Voronoi formulation showing some mild scatter behaviour. The Q1 and Q2 approximations both lock as $p \to \infty$.

Figure 6.38(b) shows a plot of tip displacement vs p for a nearly incompressible material over the range $1 \leq p \leq 10^5$. The VEM formulations, again, perform well over the domain with the Voronoi formulation showing some mild scatter behaviour. The Q1 and Q2 approximations both lock as $p \to \infty$ with the Q1 approximation also locking as $p \to 1$.

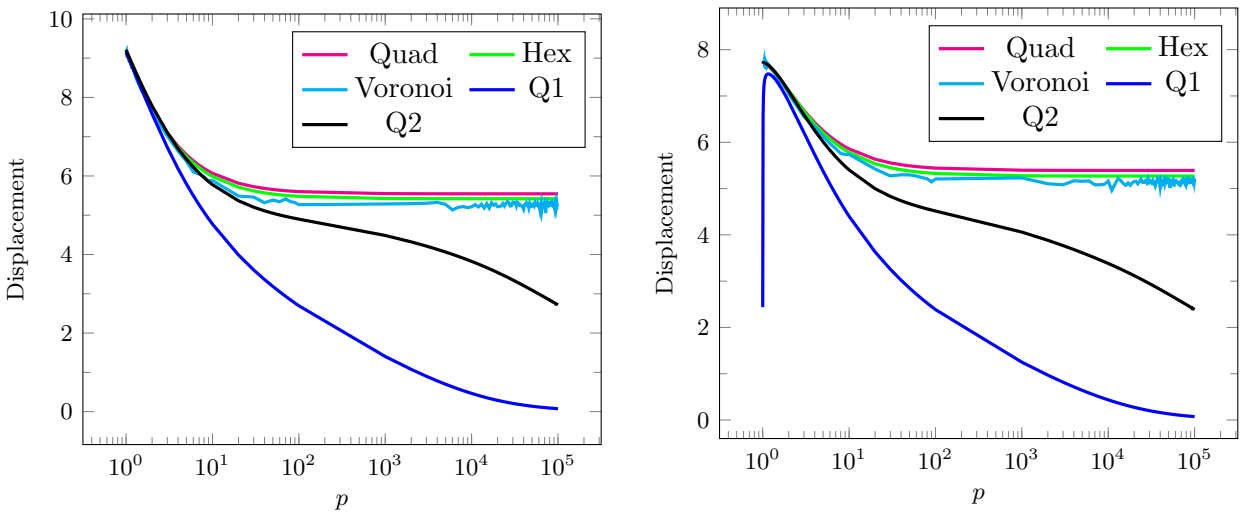

(a) Compressible material - $\nu = 0.3$

(b) Nearly incompressible material - $\nu = 0.49995$

Figure 6.38 The Cook problem: tip displacement vs p for fibres described by $a = 2\sin x + c$ for; (a) compressible material, and (b) nearly incompressible material

6.5.5.2 Pure bending problem

We present the results of an anisotropy analysis for the pure bending problem with a material containing a fibre with orientation described by the family of curves $a = 2\sin x + c$ where c is a constant.

Figure 6.39(a) shows a plot of tip displacement vs p for a compressible material over the range $1 \leq p \leq 10^5$. The Q2 approximation and VEM formulations perform well over the domain with very mild locking of the Q2 approximation as $p \to \infty$. The Q1 approximation exhibits severe locking.

Figure 6.39(b) shows a plot of tip displacement vs p for a nearly incompressible material over the range $1 \leq p \leq 10^5$. The VEM formulations perform well over the domain while the Q2 approximation shows slightly more locking than in Figure 6.39(a). The Q1 approximation locks as $p \to \infty$ and $p \to 1$.

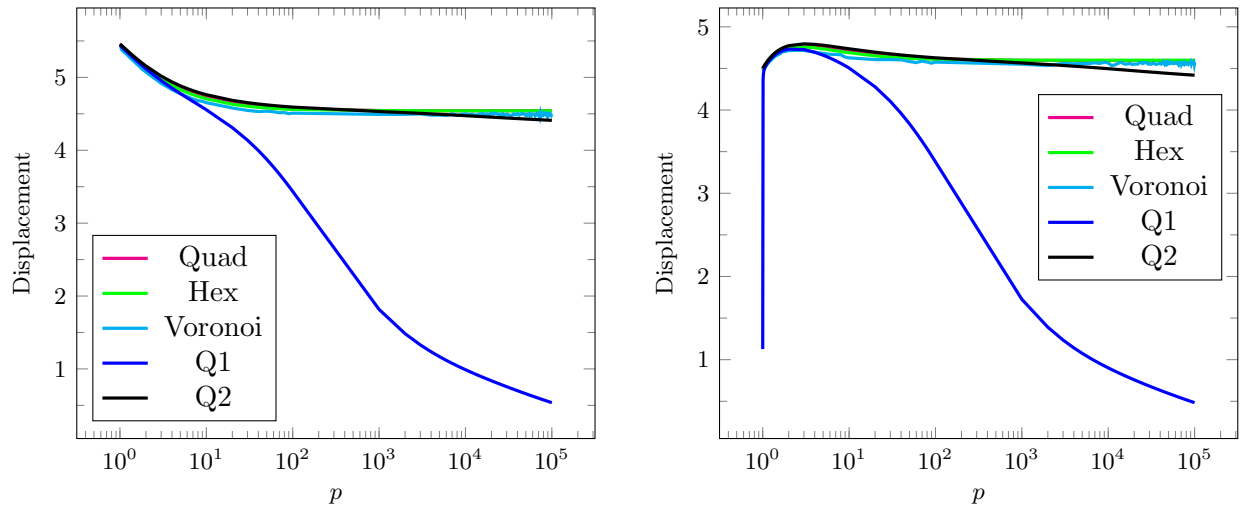

(a) Compressible material - $\nu = 0.3$ **(b)** Nearly incompressible material - $\nu = 0.49995$

Figure 6.39 The pure bending problem: tip displacement vs p for fibres described by $a = 2\sin x + c$ for; (a) compressible material, and (b) nearly incompressible material

6.5.6 Variation with $\sin 2x$

6.5.6.1 Cook's membrane problem

We present the results of an anisotropy analysis for Cook's membrane problem with a material containing a fibre with orientation described by the family of curves $a = \sin 2x + c$ where c is a constant.

Figure 6.40(a) shows a plot of tip displacement vs p for a compressible material over the range $1 \leq p \leq 10^5$. The VEM formulations all exhibit the same locking free trend over the domain, however the solutions from the different formulations do not correlate closely. The Q1 and Q2 approximations both exhibit severe locking as $p \to \infty$.

Figure 6.40(b) shows a plot of tip displacement vs p for a nearly incompressible material over the range $1 \leq p \leq 10^5$. As with Figure 6.40(a) the various VEM formulations show the same locking free trend but again the solutions do not correlate closely. The Q1 and Q2 approximations both exhibit severe locking as $p \to \infty$ with the Q1 approximation also locking as $p \to 1$.

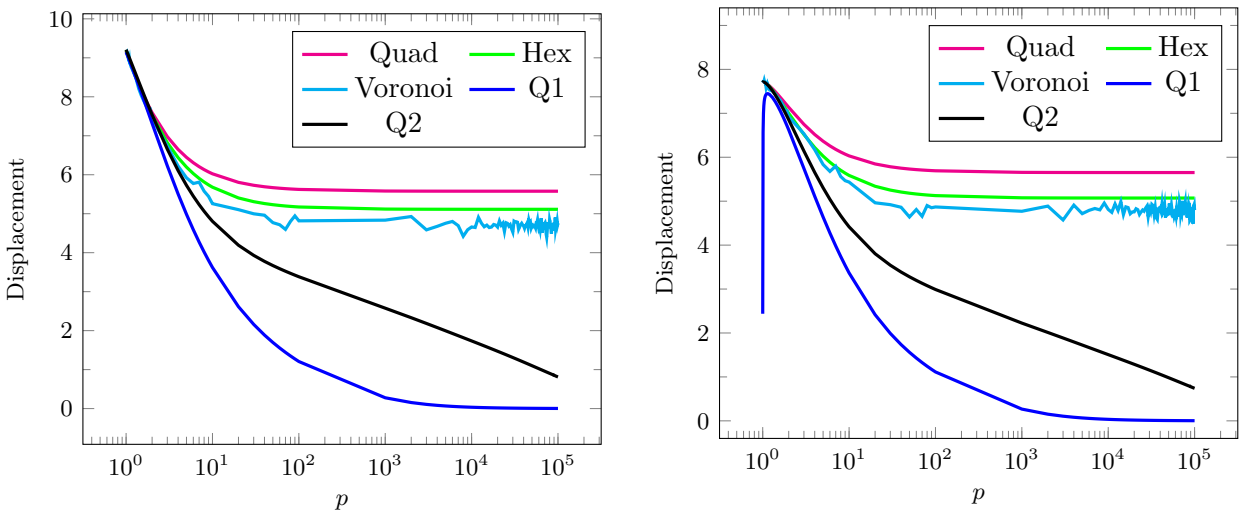

(a) Compressible material - $\nu = 0.3$

(b) Nearly incompressible material - $\nu = 0.49995$

Figure 6.40 The Cook problem: tip displacement vs p for fibres described by $a = \sin 2x + c$ for; (a) compressible material, and (b) nearly incompressible material

6.5.6.2 Pure bending problem

We present the results of an anisotropy analysis for the pure bending problem with a material containing a fibre with orientation described by the family of curves $a = \sin 2x + c$ where c is a constant.

Figure 6.41(a) shows a plot of tip displacement vs p for a compressible material over the range $1 \leq p \leq 10^5$. The VEM formulations perform well and are locking free with the Vornoi formulation showing very mild scatter behaviour. The Q2 approximation exhibits mild locking as $p \to \infty$, with the Q1 approximation locking severely.

Figure 6.41(b) shows a plot of tip displacement vs p for a nearly incompressible material over the range $1 \leq p \leq 10^5$. The VEM formulations, again, perform well and are locking free with the Voronoi formulation showing some mild scatter behaviour. The Q2 approximation exhibits mild locking as $p \to \infty$ with the Q1 approximation locking severely $p \to \infty$.

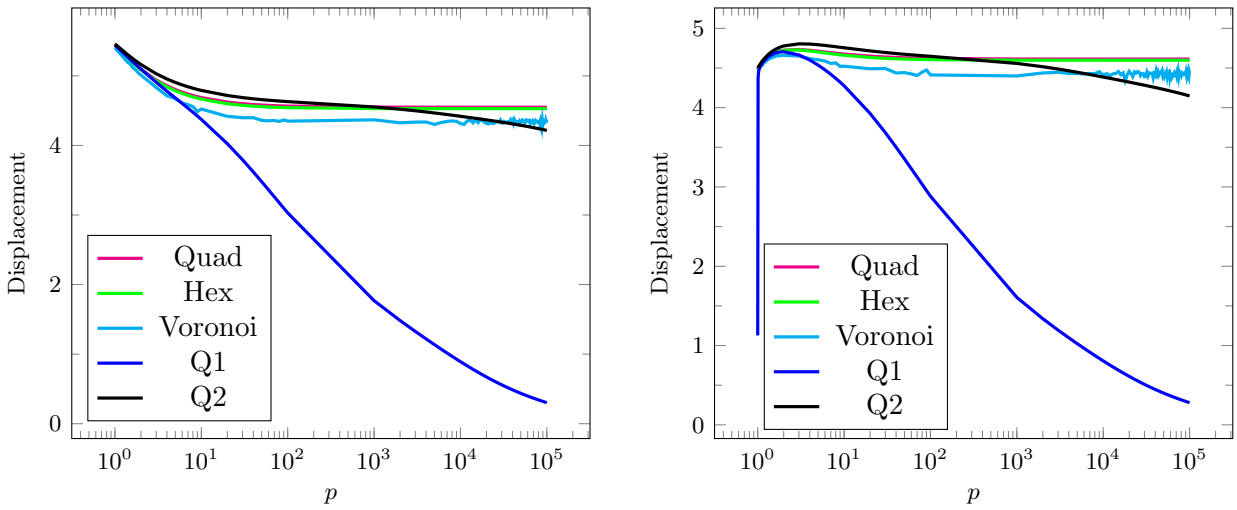

(a) Compressible material - $\nu = 0.3$ **(b)** Nearly incompressible material - $\nu = 0.49995$

Figure 6.41 The pure bending problem: tip displacement vs p for fibres described by $a = \sin 2x + c$ for; (a) compressible material, and (b) nearly incompressible material

6.6 Results summary

In Table 6.1 we provide a summary of the results of the convergence analysis of non-homogeneous transversely isotropic materials in the style described in Section 5.6 with the addition of '-' denoting that no test was performed. We introduce further shorthand to denote the VEM formulations and the methods of fibre calculation used. We will use the form $\mathrm{X_y}$ to describe the formulations. The base X will identify the element geometry, with Q denoting Quad elements, H denoting Hex elements and V denoting Voronoi elements. The subscript y will identify the type of fibre calculation method used; with c denoting the centroid, v the average at the vertices and cw and vw the constant and varying weighted combinations respectively.

From Table 6.1 it is clear that varying the method of fibre calculation can be used to improve the performance of the VEM formulation. Take for example the Quad element, the $\mathrm{Q_c}$ and $\mathrm{Q_v}$ formulations fail in four and seven instances respectively, while the $\mathrm{Q_{cw}}$ and $\mathrm{Q_{vw}}$ formulations fail in only two and one instances respectively. The $\mathrm{H_{vw}}$ and $\mathrm{V_{vw}}$ formulations show even more robust behaviour performing well in all instances and showing no numerical pathologies.

		Q_c	Q_v	Q_{cw}	Q_{vw}	H_c	H_v	H_{cw}	H_{vw}	V_c	V_v	V_{cw}	V_{vw}	Q1	Q2
x^2	Cook	✓	✓	-	-	✓	✓	-	-	✓	✓	-	-	✓	✓
	Beam	✓	✓	-	-	✓	✓	-	-	✓	✓	-	-	✓	✓
x^4	Cook	✓	✗	-	-	✓	✓	-	-	✓	✓	-	-	✓	✓
	Beam	✓	✗	-	-	✓	✓	-	-	✓	✓	-	-	✓	✓
x^6	Cook	✓	✗	-	-	✓	✓	-	-	✓	✓	-	-	✓	✓
	Beam	✓	✗	-	-	✓	✓	-	-	✓	✗	-	-	✓	✓
$\sin x$	Cook	✗	✗	✓	✓	✓	✓	✓	✓	✓	✓	✓	✓	✗	✓
	Beam	✓	✓	✓	✓	✓	✓	✓	✓	✓	✓	✓	✓	✓	✓
$2\sin x$	Cook	✗	✓	✗	✓	✗	✓	✓	✓	✗	✗	✓	✓	✗	✓
	Beam	✓	✓	✓	✓	✓	✓	✓	✓	✓	✓	✓	✓	✓	✓
$\sin 2x$	Cook	✗	✗	✗	✗	✗	✗	✗	✓	✗	✗	✗	✓	✗	✓
	Beam	✗	✗	✓	✓	✗	✓	✓	✓	✓	✓	✓	✓	✓	✓

Table 6.1 *Summary of results of convergence tests for non-homogeneous materials for* $p = 5$ *and* $\nu = 0.3$

In Table 6.2 we provide a summary of the results of the displacement vs p results for non-homogeneous transversely isotropic materials in the style described in Section 5.6.

Table 6.2 shows the VEM formulations to be far more robust than the conforming finite element approximations in dealing with the combined challenges of non-homogeneous materials and near-inextensibility as well as near-incompressibility. The VEM formulations perform well in all instances except for the family of fibres defined by sixth order polynomials, and the Cook membrane problem with fibres defined by $a = \sin 2x + c$. The conforming finite element approximations on the other hand, and in particular the Q1 approximation, perform poorly in almost all instances.

		Quad		Hex		Voronoi		Q1		Q2	
		$\nu = 0.3$	$\nu \approx 0.5$	$\nu = 0.3$	$\nu \approx 0.5$	$\nu = 0.3$	$\nu \approx 0.5$	$\nu = 0.3$	$\nu \approx 0.5$	$\nu = 0.3$	$\nu \approx 0.5$
x^2	Cook	✓	✓	✓	✓	✓	✓	✗	✗	✗	✗
	Beam	✓	✓	✓	✓	✓	✓	✗	✗	✓	✓
x^4	Cook	✓	✓	✓	✓	✓	✓	✗	✗	✗	✗
	Beam	✓	✓	✓	✓	✓	✓	✗	✗	✗	✗
x^6	Cook	✓	✓	✗	✓	✗	✓	✓	✗	✓	✓
	Beam	✗	✗	✗	✗	✗	✗	✗	✗	✗	✗
$\sin x$	Cook	✓	✓	✓	✓	✓	✓	✗	✗	✗	✗
	Beam	✓	✓	✓	✓	✓	✓	✗	✗	✗	✗
$2\sin x$	Cook	✓	✓	✓	✓	✓	✓	✗	✗	✗	✗
	Beam	✓	✓	✓	✓	✓	✓	✗	✗	✓	✓
$\sin 2x$	Cook	✓	✓	✓	✓	✗	✗	✗	✗	✗	✗
	Beam	✓	✓	✓	✓	✓	✓	✗	✗	✗	✗

Table 6.2 *Summary of results of the effect of anisotropy for non-homogeneous materials*

Chapter 7

Discussion and conclusion

In this chapter we conclude the work with a discussion of the numerical results, present a conclusion of the work, and highlight related open problems.

7.1 Homogeneous materials

Isotropic materials The virtual element method was able to model the behaviour of both compressible and nearly incompressible isotropic materials accurately and exhibited no numerical pathologies. In all cases the VEM exhibited superior accuracy to the standard bilinear finite element approximation, and in cases of near-incompressibility the accuracy of the VEM was comparable to that of the biquadratic finite element approximation. In cases of near-incompressibility the bilinear approximation exhibited the well known pathology of locking.

Homogeneous transversely isotropic materials For homogeneous transversely isotropic materials we considered the case of near-incompressibility and focused on the effects of varying the degree of anisotropy and fibre orientation on the formulations. The convergence tests considered a mild degree of anisotropy and showed the VEM to exhibit accuracy superior to the bilinear approximation and accuracy comparable to the biquadratic approximation for sufficiently fine meshes.

Numerical tests of the effects of the degree of anisotropy showed the VEM to be locking free in the cases of both near-incompressibility and near-inextensibility, and show similar accuracy to the biquadratic approximation. The bilinear approximation, however, exhibited locking behaviour in both the near-incompressible and near-inextensible limits, only showing accuracy for mild anisotropy. This behaviour is consistent with that shown in [41].

In the tests of the effects of fibre orientation in the near-inextensible limit the VEM showed robust behaviour and no numerical pathologies with accuracy comparable to that of the biquadratic approximation. The bilinear approximation performed poorly and exhibited locking behaviour. The biquadratic approximation was accurate for fibres of orientation $0 \leq \hat{a} \leq \frac{\pi}{2}$. In the case of the Cook problem for $\hat{a} > \frac{\pi}{2}$ it performed poorly and exhibited atypically erratic behaviour and suboptimal accuracy. This is somewhat surprising, in that the behaviour of this element in the near-inextensible limit would be expected to mirror its good performance for near-incompressibility. On the other hand, while the element has been shown to be uniformly convergent for incompressible materials, there does not exist a corresponding analysis for near-inextensibility, to the best of the author's knowledge.

7.2 Non-homogeneous materials

Convergence analysis The convergence analysis was performed in two parts; first for materials containing fibres with orientation described by polynomials, then for materials containing fibres with orientation described by sinusoidal functions. For both parts only compressible materials with mild anisotropy were considered.

Polynomial fibre descriptions were used to describe materials with mild inhomogeneity, in which increasing polynomial order corresponded to increasing inhomogeneity. For these problems representative fibre orientations were computed from centroidal values as well as the average of nodal values. Both methods of fibre calculation yielded results that for finer meshes corresponded well both the bilinear and biquadratic finite element approximations. We found, however, that using the average of nodal values generally yielded smoother convergence behaviour. This is simply due to the average of nodal values providing a fibre orientation that is more representative of an element. We note that in the case of the VEM Quad formulation the use of average nodal values resulted in significantly slower convergence.

Sinusoidal fibre descriptions were used to describe materials with more severe inhomogeneity, in which increasing amplitude and frequency of the sinusoid corresponded to increasing inhomogeneity. For these problems representative fibre orientations were computed from centroidal values and the average of nodal values, as well as constant and varying combinations of the centroidal and average nodal values. For fibres described by the families of curves $a = \sin x + c$ and $a = 2\sin x + c$ we found similar behaviour as for the polynomial fibres. For finer meshes the various methods yielded results that corresponded well with those of the biquadratic finite element approximation. We again found that the method of average nodal values produced smoother convergence behaviour than that of the centroid, this behaviour was, however, often still quite erratic. The convergence behaviour was found to be smoother when using combinations of the centroidal and average nodal values with the varying combination of the two yielding the smoothest convergence. For fibres described by the curves $a = \sin 2x + c$, for the Cook problem in particular, we found that the degree of inhomogeneity was

too severe for either the virtual or finite element methods to capture the behaviour of the material with neither of the formulations converging. The same improvements in smoothness of convergence behaviour, as with the other sinusoids when using the various methods of representative fibre calculation, were achieved even for this most severe material inhomogeneity. In all instances of the Cook problem for these materials the bilinear finite element approximation was unable to capture the material behaviour and showed non-convergence. For the pure bending problem, however, it generally yielded results comparable to the VEM formulations for fine meshes.

For both the Cook and pure bending problems we found a trend of increasingly non-uniform convergence with decreasing accuracy of the virtual and finite element methods for polynomial and sinusoidal fibres of increasing inhomogeneity. We noted, in particular, the difference between the results of sinusoidal fibre descriptions between the Cook and pure bending problems. The Cook problem generally yielded more erratic convergence than the pure bending problem for the same fibre description. The reason for this is the difference in the size of the domain. The width of the domain for the Cook problem is $48m$ compared to $10m$ for the beam. The larger Cook domain contains ≈ 5 times more sinusoidal periods than the beam. As we used the same level of mesh refinement for both problems, each element for the Cook problem was more inhomogeneous than the equivalent element for the beam problem, resulting in the more erratic convergence behaviour. This behaviour was less evident for the problems with polynomial fibre descriptions as the polynomials were nominally scaled to width of the domain. The degree of inhomogeneity that can be accurately modelled is therefore dependant on the level of mesh refinement.

Effect of anisotropy Varying the degree of anisotropy for a range of inhomogeneous materials for both compressible and nearly incompressible materials provides a good indicator of the numerical robustness of a method. We found, generally, that the virtual element formulation showed no pathologies over the range of anisotropy presented, for both compressible and nearly incompressible materials. However, as noted in the convergence analysis, there is a decrease in accuracy of the formulation with increasing inhomogeneity.

For the range of non-homogeneous fibre descriptions presented, we found a close correlation between the results obtained from the various virtual element formulations, except for the sixth-order fibre description. These results showed similar accuracy to the conforming biquadratic finite element approximation for the range of anisotropy over which it was free from pathological behaviour. The behaviour from sixth-order polynomial fibres was possibly due to regions in which fibres have a radius of curvature much smaller than seen with the other fibre descriptions. The smaller radius of curvature corresponded to more extreme inhomogeneity which is difficult to model accurately.

The conforming finite element formulations exhibited several numerical pathologies. The bilinear approximation was seen to lock for near-incompressible materials as isotropy was approached, $p \to 1$, as well as in the inextensible limit, $p \to \infty$, for both compressible and nearly incompressible materials. The biquadratic approximation showed sub-optimal accuracy, mild locking behaviour, and poor approximability in the inextensible limit, as was noted in the case of homogeneous transversely isotropic materials.

7.3 Concluding remarks

In this work we have formulated and implemented a virtual element for plane homogeneous linear elasticity problems and made provision for non-homogeneous materials. In the latter case various approaches to taking into account the non-constant elasticity tensor have been investigated. A step-by-step implementation of the method has been presented by means of a worked example. The virtual element formulation has been studied numerically through two model problems, and for three different types of meshes. The numerical results have been compared against those obtained using conforming finite element methods with bilinear and biquadratic approximations. Numerical investigations into the behaviour of the virtual element method in modelling isotropic, homogeneous transversely isotropic, and non-homogeneous transversely isotropic materials have been presented.

Isotropic materials For isotropic materials the virtual element formulation was found to be locking free for nearly incompressible materials with no modification to the method, and exhibit superior accuracy to the conforming bilinear finite element approximation. The bilinear approximation exhibited well-known locking behaviour when modelling nearly incompressible isotropic materials.

Homogeneous transversely isotropic materials For homogeneous transversely isotropic materials the virtual element formulation was found to be locking free for the cases of both near-incompressibility and near-inextensibility with no modification to the method. The VEM formulation exhibited similar accuracy to the conforming biquadratic finite element approximation for sufficiently fine meshes. The bilinear approximation exhibited locking behaviour in both the near-incompressible and near-inextensible limits and was only accurate for cases of mild anisotropy. The biquadratic approximation exhibited numerical pathologies and suboptimal accuracy in the case of near-inextesibility for certain fibre orientations.

Non-homogeneous transversely isotropic materials For non-homogeneous transversely isotropic materials the virtual element formulation exhibited no numerical pathologies and similar accuracy to the conforming biquadratic finite element approximation for sufficiently fine meshes. Minor modification of the method was employed to improve the smoothness of the convergence behaviour of the virtual element formulation. The conforming finite element formulations exhibited several numerical pathologies; the bilinear approximation locked in the near-incompressible and near-incompressible limits, and the biquadratic approximation showed suboptimal accuracy and locking behaviour in the inextensible limit.

Recommendations Further investigation could be performed into the methodology employed in approximating the fibre orientation of non-homogeneous materials at an element level. The methods used in this work constitute only a few possibilities and techniques could be developed to obtain smoother convergence behaviour and more accurate results.

Open problems There have been few studies of small-strain transverse isotropy in the context of development of new finite element and related methods. The present study and [41] constitute two new contributions. Further work is in progress on alternative formulations such as the use of Discontinuous Galerkin methods. The extension to problems involving non-linear material behaviour and large deformations is also in progress. It would be of interest to investigate the extension of the work presented here to problems in three dimensions. Of further interest would be an analytical investigation of the conforming biquadratic finite element approximation in the inextensible/near-inextensible limit.

References

[1] W. A. Strauss, Partial Differential Equations: An Introduction, Wiley, 2007.

[2] C. N. Dawson, Q. Du, T. F. Dupont, A finite difference domain decomposition algorithm for numerical solution of the heat equation, Mathematics of Computation 57 (195) (1991) 63–63. doi:10.1090/s0025-5718-1991-1079011-4.

[3] G. D. Smith, Numerical Solution of Partial Differential Equations: Finite Difference Methods, Oxford University Press, 1985.

[4] H. K. Versteeg, W. Malalasekera, An Introduction to Computational Fluid Dynamics: The Finite Volume Method, Pearson Education, 2007.

[5] J. Fish, T. Belytschko, A First Course in Finite Elements, Vol. 1, John Wiley & Sons New York, 2007.

[6] T. Belytschko, W. K. Liu, B. Moran, K. Elkhodary, Nonlinear Finite Elements for Continua and Structures, John Wiley & Sons, 2013.

[7] P. Wriggers, Nonlinear Finite Element Methods, Springer Science & Business Media, 2008.

[8] R. L. Taylor, P. J. Beresford, E. L. Wilson, A non-conforming element for stress analysis, International Journal for Numerical Methods in Engineering 10 (6) (1976) 1211–1219. doi:10.1002/nme.1620100602.

[9] D. Boffi, F. Brezzi, M. Fortin, Mixed Finite Element Methods and Applications, Vol. 44, Springer, 2013.

[10] B. Cockburn, G. E. Karniadakis, C.-W. Shu, The development of discontinuous galerkin methods, in: Lecture Notes in Computational Science and Engineering, Springer Berlin Heidelberg, 2000, pp. 3–50. doi:10.1007/978-3-642-59721-3_1.

[11] T. J. Hughes, The Finite Element Method: Linear Static and Dynamic Finite Element Analysis, Courier Corporation, 2012.

[12] D. S. Malkus, T. J. Hughes, Mixed finite element methods — reduced and selective integration techniques: A unification of concepts, Computer Methods in Applied Mechanics and Engineering 15 (1) (1978) 63–81. doi:10.1016/0045-7825(78)90005-1.

[13] H. Shimodaira, Equivalence between mixed models and displacement models sing reduced integration, International Journal for Numerical Methods in Engineering 21 (1) (1985) 89–104. doi:10.1002/nme.1620210108.

[14] D. N. Arnold, F. Brezzi, B. Cockburn, L. D. Marini, Unified analysis of discontinuous galerkin methods for elliptic problems, SIAM Journal on Numerical Analysis 39 (5) (2002) 1749–1779. doi:10.1137/s0036142901384162.

[15] B. J. Grieshaber, A. T. McBride, B. D. Reddy, Uniformly convergent interior penalty methods using multilinear approximations for problems in elasticity, SIAM Journal on Numerical Analysis 53 (5) (2015) 2255–2278. doi:10.1137/140966253.

[16] P. Hansbo, M. G. Larson, Discontinuous galerkin methods for incompressible and nearly incompressible elasticity by nitsche's method, Computer Methods in Applied Mechanics and Engineering 191 (17-18) (2002) 1895–1908. doi:10.1016/s0045-7825(01)00358-9.

[17] T. P. Wihler, Locking-free DGFEM for elasticity problems in polygons, IMA Journal of Numerical Analysis 24 (1) (2004) 45–75. doi:10.1093/imanum/24.1.45.

[18] L. Beirão da Veiga, F. Brezzi, A. Cangiani, G. Manzini, L. D. Marini, A. Russo, Basic principles of virtual element methods, Mathematical Models and Methods in Applied Sciences 23 (01) (2013) 199–214. doi:10.1142/s0218202512500492.

[19] L. Beirão da Veiga, F. Brezzi, L. D. Marini, A. Russo, The hitchhiker's guide to the virtual element method, Mathematical Models and Methods in Applied Sciences 24 (08) (2014) 1541–1573. doi:10.1142/s021820251440003x.

[20] L. B. da Veiga, C. Lovadina, D. Mora, A virtual element method for elastic and inelastic problems on polytope meshes, Computer Methods in Applied Mechanics and Engineering 295 (2015) 327–346. doi:10.1016/j.cma.2015.07.013.

[21] A. L. Gain, C. Talischi, G. H. Paulino, On the virtual element method for three-dimensional linear elasticity problems on arbitrary polyhedral meshes, Computer Methods in Applied Mechanics and Engineering 282 (2014) 132–160. doi:10.1016/j.cma.2014.05.005.

[22] L. B. da Veiga, F. Brezzi, L. D. Marini, Virtual elements for linear elasticity problems, SIAM Journal on Numerical Analysis 51 (2) (2013) 794–812. doi:10.1137/120874746.

[23] P. Wriggers, B. D. Reddy, W. Rust, B. Hudobivnik, Efficient virtual element formulations for compressible and incompressible finite deformations, Computational Mechanics 60 (2) (2017) 253–268. doi:10.1007/s00466-017-1405-4.

[24] H. Chi, L. B. da Veiga, G. Paulino, Some basic formulations of the virtual element method (VEM) for finite deformations, Computer Methods in Applied Mechanics and Engineering 318 (2017) 148–192. doi:10.1016/j.cma.2016.12.020.

[25] E. Artioli, L. B. da Veiga, C. Lovadina, E. Sacco, Arbitrary order 2D virtual elements for polygonal meshes: part II, inelastic problem, Computational Mechanics 60 (4) (2017) 643–657. doi:10.1007/s00466-017-1429-9.

[26] P. Wriggers, B. Hudobivnik, A low order virtual element formulation for finite elasto-plastic deformations, Computer Methods in Applied Mechanics and Engineering 327 (2017) 459–477. doi:10.1016/j.cma.2017.08.053.

[27] P. Wriggers, W. T. Rust, B. D. Reddy, A virtual element method for contact, Computational Mechanics 58 (6) (2016) 1039–1050. doi:10.1007/s00466-016-1331-x.

[28] P. Wriggers, B. Hudobivnik, J. Korelc, Efficient low order virtual elements for anisotropic materials at finite strains, in: Computational Methods in Applied Sciences, Springer International Publishing, 2017, pp. 417–434. doi:10.1007/978-3-319-60885-3_20.

[29] T. Ting, Recent developments in anisotropic elasticity, International Journal of Solids and Structures 37 (1-2) (2000) 401–409. doi:10.1016/s0020-7683(99)00102-x.

[30] J. Schröder, P. Neff, D. Balzani, A variational approach for materially stable anisotropic hyperelasticity, International Journal of Solids and Structures 42 (15) (2005) 4352–4371. doi:10.1016/j.ijsolstr.2004.11.021.

[31] V. Lubarda, M. Chen, On the elastic moduli and compliances of transversely isotropic and orthotropic materials, Journal of Mechanics of Materials and Structures 3 (1) (2008) 153–171. doi:10.2140/jomms.2008.3.153.

[32] Z. Hashin, B. W. Rosen, The elastic moduli of fiber-reinforced materials, Journal of Applied Mechanics 31 (2) (1964) 223. doi:10.1115/1.3629590.

[33] E. Kuhl, K. Garikipati, E. M. Arruda, K. Grosh, Remodeling of biological tissue: Mechanically induced reorientation of a transversely isotropic chain network, Journal of the Mechanics and Physics of Solids 53 (7) (2005) 1552–1573. doi:10.1016/j.jmps.2005.03.002.

[34] G. Limbert, J. Middleton, A transversely isotropic viscohyperelastic material, International Journal of Solids and Structures 41 (15) (2004) 4237–4260. doi:10.1016/j.ijsolstr.2004.02.057.

[35] H. B. Henninger, S. A. Maas, J. H. Shepherd, S. Joshi, J. A. Weiss, Transversely isotropic distribution of sulfated glycosaminoglycans in human medial collateral ligament: A quantitative analysis, Journal of Structural Biology 165 (3) (2009) 176–183. doi:10.1016/j.jsb.2008.11.013.

[36] V. Tagarielli, V. Deshpande, N. Fleck, C. Chen, A constitutive model for transversely isotropic foams, and its application to the indentation of balsa wood, International Journal of Mechanical Sciences 47 (4-5) (2005) 666–686. doi:10.1016/j.ijmecsci.2004.11.010.

[37] Y. M. Tien, M. C. Kuo, A failure criterion for transversely isotropic rocks, International Journal of Rock Mechanics and Mining Sciences 38 (3) (2001) 399–412. doi:10.1016/s1365-1609(01)00007-7.

[38] Y. Feng, R. J. Okamoto, R. Namani, G. M. Genin, P. V. Bayly, Identification of a transversely isotropic material model for white matter in the brain, in: Volume 2: Biomedical and Biotechnology, ASME, 2012. doi:10.1115/imece2012-88610.

[39] M. Gaff, M. Gašparík, V. Borůvka, E. Haviarová, Stress simulation in layered wood-based materials under mechanical loading, Materials & Design 87 (2015) 1065–1071. doi:10.1016/j.matdes.2015.08.128.

[40] Rock layers diagram of undisturbed description, Online (Oct. 2018).
URL http://scooplocal.co/rock-layers-diagram-of-undisturbed.html

[41] F. Rasolofoson, B. Grieshaber, B. D. Reddy, Finite element approximations for near-incompressible and near-inextensible transversely isotropic bodies, International Journal for Numerical Methods in Engineering, Advanced online publication. doi:10.1002/nme.5972.

[42] F. Auricchio, G. Scalet, P. Wriggers, Fiber-reinforced materials: finite elements for the treatment of the inextensibility constraint, Computational Mechanics 60 (6) (2017) 905–922. doi:10.1007/s00466-017-1437-9.

[43] W. Chen, K. Y. Lee, H. Ding, On free vibration of non-homogeneous transversely isotropic magneto-electro-elastic plates, Journal of Sound and Vibration 279 (1-2) (2005) 237–251. doi:10.1016/j.jsv.2003.10.033.

[44] E. Martínez-Pañeda, R. Gallego, Numerical analysis of quasi-static fracture in functionally graded materials, International Journal of Mechanics and Materials in Design 11 (4) (2014) 405–424. doi:10.1007/s10999-014-9265-y.

[45] R. Radovitzky, 16.20 Techniques of Structural Analysis and Design Spring 2013: Module 3 Constitutive Equations, Online (Feb. 2013).
URL http://web.mit.edu/16.20/homepage/3_Constitutive/Constitutive_files/module_3_with_solutions.pdf

[46] A. P. Schniewind, J. D. Barrett, Wood as a linear orthotropic viscoelastic material, Wood Science and Technology 6 (1) (1972) 43–57. doi:10.1007/bf00351807.

[47] J. E. Marsden, T. J. R. Hughes, Mathematical Foundations of Elasticity (Dover Civil and Mechanical Engineering), Dover Publications, 1994.

[48] E. Artioli, L. B. Da Veiga, C. Lovadina, E. Sacco, Arbitrary order 2D virtual elements for polygonal meshes: Part I, elastic problem, Computational Mechanics 60 (3) (2017) 355–377. doi:10.1007/s00466-017-1404-5.

[49] J. K. Djoko, B. P. Lamichhane, B. D. Reddy, B. I. Wohlmuth, Conditions for equivalence between the hu–washizu and related formulations, and computational behavior in the incompressible limit, Computer Methods in Applied Mechanics and Engineering 195 (33-36) (2006) 4161–4178. doi:10.1016/j.cma.2005.07.018.

Appendices

Appendix A

Sample implementation code

```
%% VEM - LINEAR ELASTICITY
    % Transversely Isotropic Materials
        % Cook's Membrane Problem
            % Sample Problem
%% CLEAR - Clear Workspace, Close Figures, Clear Console
    clear all
    close all
    clc
%% ------------------------ START USER SECTION ------------------------
   %%
%% INPUTS
% DOMAIN - Corners Of Domain Entered Counter-Clockwise
    Corners = [0, 0; 48, 44; 48, 60; 0, 44];
    density = 4;   % Mesh Density - Elements Per Side
% LOAD - Applied Load
    Load = 100;
% MATERIAL PROPERTIES
    E_T = 250;   % Transverse Young's Modulus
    p = 5;  % Ratio of Longitudinal Young's Modulus to Transverse Young's
        Modulus
    v_T = 0.49995;     % Poisson's Ratio
    c = 1.0001;  % Ratio of Longitudinal Poisson's Ratio to Transverse
       Poisson's Ratio
    FibreOrientation = pi/4;     % Fibre Orientation (radians)
%% MESH
    ICA = [9,10,3,2,4;7,8,5,6,0;4,2,1,6,5;9,4,5,8,0];
    Xg = [0,0,0,5.980320000000000,24.117240000000000,25.352904000000000,...
```

```
25              48,48,48,48];
26      Yg = [0,34.5532880000000,44,33.2158761391200,30.5639579784700,...
27              23.2401620000000,44,50.2983520000000,52.3027360000000,60];
28 %% ------------------------------ END USER SECTION ------------------------------
    %%
29 %% MESH-RELATED CALCULATIONS
30      Nodes = length(Xg);
31      n_dof = 2*Nodes;
32      Elements = size(ICA);
33      Elements = Elements(1,1);
34 %% TRANSVERSELY ISOTROPIC MATERIAL PROPERTIES
35      a = [cos(FibreOrientation), sin(FibreOrientation)]; % Axis Of
            Symmetry
36      a1 = a(1);
37      a2 = a(2);
38      E_L = p*E_T;      % Longitudinal Young's Modulus
39      v_L = c*v_T;      % Longitudinal Poisson's Ratio
40      u_T = E_T/(2*(1+v_T));  % Transverse Shear Modulus
41      u_L = u_T;  % Longitudinal Shear Modulus
42      G_L = u_L; % Longitudinal Shear Modulus - Not really neccessary
43      lambda = (E_T*(v_L*v_L*E_T + v_T*E_L))/((1 + v_T)*(E_L*(1 - v_T)-2*
            v_L*v_L*E_T));    % Lambda
44      alpha = (E_T*(E_L*v_L*(1 + v_T) - v_L*v_L*E_T - v_T*E_L))/((1 + v_T)
            *(E_L*(1 - v_T) - 2*v_L*v_L*E_T));  % Alpha
45      beta = (E_L*E_L*(1 - v_T*v_T) - E_T*E_T*v_L*v_L + E_T*E_L*(1 - 2*v_T*
            v_L - 2*v_L))*(1/((1 + v_T)*(E_L*(1 - v_T) - 2*v_L*v_L*E_T))) - 4*
            G_L; % Beta
46      gamma = 2*(u_L-u_T);      % Gamma
47 % Constitutive Tensor - Plane Strain
48      c11 = lambda + 2*u_T + 2*(gamma + alpha)*a1*a1 + beta*a1*a1*a1*a1;
49      c12 = lambda + alpha + beta*a1*a1*a2*a2;
50      c13 = (alpha + gamma)*a1*a2 + beta*a1*a1*a1*a2;
51      c22 = lambda + 2*u_T + 2*(gamma + alpha)*a2*a2 + beta*a2*a2*a2*a2;
52      c23 = (alpha + gamma)*a1*a2 + beta*a1*a2*a2*a2;
53      c33 = u_T + gamma/2 + beta*a1*a1*a2*a2;
54      C = [c11 c12 c13
55           c12 c22 c23
56           c13 c23 c33];
57 %% GLOBAL MATRIX INITIALISATION
```

```
58      % Stiffness Matrix
59          K = zeros(n_dof,n_dof);
60      % Load Vector
61          f = zeros(n_dof,1);
62  %% STIFFNESS MATRIX
63      % LOOP OVER ELEMENTS
64      for i = 1:Elements
65          % Element Information
66              % Vertices
67                  Element_Nodes = ICA(i,:);
68                  Vertices = zeros;
69                  count = 0;
70                  for j = 1:length(Element_Nodes)
71                      node = Element_Nodes(j);
72                      if node ~= 0
73                          count = count + 1;
74                          Vertices(count,1) = Xg(node);
75                          Vertices(count,2) = Yg(node);
76                      end
77                  end
78                  n_v = size(Vertices);   % n_v = Number of Vertices
79                  n_v = n_v(1,1);
80                  n_e = n_v;  % n_e = Number of Edges
81              % Area and Centroid
82                      % As we will need to loop the whole way around the
                            element the
83                      % we modify the 'Vertices' vector to end with its
                            first vertex
84                      Mod_Vertices = zeros(n_v+1,2);
85                      Mod_Vertices(1:end-1,:) = Vertices;
86                      Mod_Vertices(end,:) = Vertices(1,:);
87                  area = 0;
88                  centroid = [0, 0];
89                  for j = 1:n_e
90                      area_component = Mod_Vertices(j,1)*Mod_Vertices(j
                            +1,2) - Mod_Vertices(j+1,1)*Mod_Vertices(j,2);
91                      area = area + area_component;
92                      centroid(1,1) = centroid(1,1) + (Mod_Vertices(j,1) +
                            Mod_Vertices(j+1,1))*area_component;
```

```
93                  centroid(1,2) = centroid(1,2) + (Mod_Vertices(j,2) +
                        Mod_Vertices(j+1,2))*area_component;
94              end
95              area = 0.5*area;
96              centroid = (1/(6*area))*centroid;
97          % Diameter
98              diameter = 0;
99              for m = 1:n_v-1
100                 for n = (m+1):n_v
101                     test_diameter = sqrt((Vertices(m,1)-Vertices(n,1)
                            )^2 + (Vertices(m,2)-Vertices(n,2))^2);
102                     if test_diameter > diameter
103                         diameter = test_diameter;
104                     end
105                 end
106             end
107     % Calculate Consistent Stiffness Matrix
108         % Calculate Nodal Contributions To PI (called B here)
109             B = zeros(3,2*n_v);
110                 % Very Modified Vertices
111                     Mod_Mod_Vertices = zeros(n_v+2,2);
112                     Mod_Mod_Vertices(2:end,:) = Mod_Vertices;
113                     Mod_Mod_Vertices(1,:) = Vertices(end,:);
114                     for j = 1:n_v
115                         current_vertex = Vertices(j,:);
116                         next_vertex = Mod_Vertices(j+1,:);
117                         previous_vertex = Mod_Mod_Vertices(j,:);
118                         Normal_next = [next_vertex(2)-
                                current_vertex(2), current_vertex(1)-
                                next_vertex(1)];
119                         Normal_next = (1/sqrt(Normal_next(1)^2+
                                Normal_next(2)^2))*Normal_next;
120                         Normal_previous = [current_vertex(2)-
                                previous_vertex(2), previous_vertex(1)
                                -current_vertex(1)];
121                         Normal_previous = (1/sqrt(Normal_previous
                                (1)^2+Normal_previous(2)^2))*
                                Normal_previous;
```

```
122                                 Ne_next = [Normal_next(1), 0, Normal_next
                                        (2)
123                                         0, Normal_next(2), Normal_next
                                            (1)];
124                                 Ne_previous = [Normal_previous(1), 0,
                                        Normal_previous(2)
125                                         0, Normal_previous(2),
                                            Normal_previous(1)];
126                                 Edge_next = sqrt((next_vertex(1)-
                                        current_vertex(1))^2+(next_vertex(2)-
                                        current_vertex(2))^2);
127                                 Edge_previous = sqrt((current_vertex(1)-
                                        previous_vertex(1))^2+(current_vertex
                                        (2)-previous_vertex(2))^2);
128                                 B_temp = (Edge_next/2)*(Ne_next)' + (
                                        Edge_previous/2)*(Ne_previous)';
129                                 B(:,2*j-1) = B_temp*[1
130                                                      0];
131                                 B(:,2*j) = B_temp*[0
132                                                    1];
133                             end
134         % Calculate Pi
135             Pi = (1/area).*B;
136     % CONSISTENCY MATRIX
137         Kc = area*Pi'*C*Pi;
138     % Calculate Stabilisation Term
139         D = zeros(2*n_v,6);
140         for j = 1:n_v
141             D(2*j-1,:) = [1, 0, (Vertices(j,1) - centroid(1))/
                    diameter, 0, (Vertices(j,2) - centroid(2))/diameter,
                    0];
142             D(2*j,:) = [0, 1, 0, (Vertices(j,1) - centroid(1))/
                    diameter, 0, (Vertices(j,2) - centroid(2))/diameter];
143         end
144     % STABILISATION MATRIX
145         Ks = u_T*[eye(2*n_v)-D*inv(D'*D)*D'];
146     % Calculate Element Stiffness Matrix
147         Ke = Kc + Ks;
148     % Assemble Global Stiffness Matrix
```

```
149             for j = 1:n_v
150                 for k = 1:n_v
151                     K(2*ICA(i,j)-1:2*ICA(i,j),2*ICA(i,k)-1:2*ICA(i,k)) =
                            K(2*ICA(i,j)-1:2*ICA(i,j),2*ICA(i,k)-1:2*ICA(i,k))
                             + Ke(2*j-1:2*j,2*k-1:2*k);
152                 end
153             end
154     end
155 %% BOUNDARY CONDITIONS
156     tolerance = 10^-10;      % Tolerance on IF statements
157     %% Dirichlet Conditions
158     NDirichletNodes = 0;
159     for i = 1:Nodes
160         if Xg(i) <= 0 + tolerance && Xg(i) >= 0 - tolerance
161             NDirichletNodes = NDirichletNodes + 1;
162         end
163     end
164     Dirichlet = zeros(2*NDirichletNodes, 2);
165     count = 0;
166     for i = 1:Nodes
167         if Xg(i) == 0
168             count = count + 1;
169             Dirichlet(2*count-1,1) = i;
170         end
171     end
172     for i = 1:NDirichletNodes
173         Dirichlet(2*i-1,1) = 2*Dirichlet(2*i-1,1) - 1;
174         Dirichlet(2*i,1) = Dirichlet(2*i-1,1) + 1;
175     end
176     %% Force Vector
177     % If two nodes of an element lie on the line x=48 the element has an
          edge
178     % experiencing a traction
179     Traction = Load/16; %N/m
180     %NForceNodes = density + 1 + AddNodes*density;
181     NForceNodes = 0;
182     for i = 1:Nodes
183         if Xg(i) >= 48 - tolerance && Xg(i) <= 48 + tolerance
184             NForceNodes = NForceNodes + 1;
```

```
185         end
186     end
187     NForceNodes;
188     NForceSides = NForceNodes - 1;
189     ForceSides = zeros(NForceSides,6);
190     SideCount = 0;
191     % Loop Over Elements
192         for i = 1:Elements
193             % Vertices
194             Element_Nodes = ICA(i,:);
195             Vertices = zeros;
196             count = 0;
197             for j = 1:length(Element_Nodes)
198                 node = Element_Nodes(j);
199                 if node ~= 0
200                     count = count + 1;
201                     Vertices(count,1) = node;
202                     Vertices(count,2) = Xg(node);
203                     Vertices(count,3) = Yg(node);
204                 end
205             end
206             n_v = size(Vertices);    % n_v = Number of Vertices
207             n_v = n_v(1,1);
208             Mod_Vertices = zeros(n_v+1,3);
209             Mod_Vertices(1:end-1,:) = Vertices;
210             Mod_Vertices(end,:) = Vertices(1,:);
211             for j = 1:n_v
212                 X1 = Mod_Vertices(j,2);
213                 X2 = Mod_Vertices(j+1,2);
214                 if X1 <= 48 + tolerance && X1 >= 48 - tolerance
215                     if X2 <= 48 + tolerance && X2 >= 48 - tolerance
216                         Y1 = Mod_Vertices(j,3);
217                         Y2 = Mod_Vertices(j+1,3);
218                         N1 = Mod_Vertices(j,1);
219                         N2 = Mod_Vertices(j+1,1);
220                         SideCount = SideCount + 1;
221                         ForceSides(SideCount,1) = SideCount;
222                         ForceSides(SideCount,2) = N1;
223                         ForceSides(SideCount,3) = N2;
```

```
224                             ForceSides(SideCount,4) = Y1;
225                             ForceSides(SideCount,5) = Y2;
226                             ForceSides(SideCount,6) = abs(Y2-Y1);
227                         end
228                     end
229                 end
230             end
231         % Create Force Vector
232         for i = 1:NForceSides
233             f(2*ForceSides(i,2)) = 0.5*ForceSides(i,6)*Traction;
234         end
235         for i = 1:NForceSides
236             f(2*ForceSides(i,3)) = f(2*ForceSides(i,3)) + 0.5*ForceSides(i,6)
                *Traction;
237         end
238 %% Solve - Penalty Method
239         B = 10^10;  % Penalty
240         Kp = K;
241         for i = 1:2*NDirichletNodes
242             Kp(Dirichlet(i,1),Dirichlet(i,1)) = B;
243             f(Dirichlet(i,1)) = B*Dirichlet(i,2);
244         end
245         d = sparse(Kp)\f;   % Sparse Used To Improve Speed
246         %% Find the tip (Point C)
247         for i = 1:Nodes
248             if Xg(i) == 48 && Yg(i) == 60
249                 tip = i;
250             end
251         end
252         % Display Vertical Displacement
253         disp('The tip is Node: ')
254         disp(tip)
255         disp('Tip Displacement = ')
256         disp(d(2*i));
```

Appendix B

Compliance relations

For a transversely isotropic material under the assumption of plane strain with fibre orientation $\boldsymbol{a} = [a_1,\, a_2]^T$ the compliance relation is given by [41]

$$\begin{bmatrix} \varepsilon_{11} \\ \varepsilon_{22} \\ 2\varepsilon_{12} \end{bmatrix} = \begin{bmatrix} \mathbb{S}_{11} & \mathbb{S}_{12} & \mathbb{S}_{13} \\ \mathbb{S}_{12} & \mathbb{S}_{22} & \mathbb{S}_{23} \\ \mathbb{S}_{13} & \mathbb{S}_{23} & \mathbb{S}_{33} \end{bmatrix} \begin{bmatrix} \sigma_{11} \\ \sigma_{22} \\ \sigma_{12} \end{bmatrix}, \tag{B.1}$$

where

$$\begin{aligned}
\mathbb{S}_{11} &= \frac{1}{det\mathbb{C}}\Big[\big(\lambda + 2\mu_t + 2(\gamma+\alpha)a_2^2 + \beta a_2^4\big)\big(\mu_t + \frac{\gamma}{2} + \beta a_1^2 a_2^2\big) - \big((\alpha+\gamma)a_1a_2 + \beta a_1 a_2^3\big)^2\Big], \\
\mathbb{S}_{12} &= \frac{1}{det\mathbb{C}}\Big[\big((\alpha+\gamma)a_1a_2 + \beta a_1^3 a_2\big)\big((\alpha+\gamma)a_1a_2 + \beta a_1 a_2^3\big) - \big(\lambda + \alpha + \beta a_1^2 a_2^2\big)\big(\mu_t + \frac{\gamma}{2} + \beta a_1^2 a_2^2\big)\Big], \\
\mathbb{S}_{13} &= \frac{1}{det\mathbb{C}}\Big[\big(\lambda + \alpha + \beta a_1^2 a_2^2\big)\big((\alpha+\gamma)a_1a_2 + \beta a_1 a_2^3\big) - \big((\alpha+\gamma)a_1a_2 + \beta a_1^3 a_2\big)\big(\lambda + 2\mu_t + 2(\gamma+\alpha)a_2^2 + \beta a_2^4\big)\Big], \\
\mathbb{S}_{22} &= \frac{1}{det\mathbb{C}}\Big[\big(\lambda + 2\mu_t + 2(\gamma+\alpha)a_1^2 + \beta a_1^4\big)\big(\mu_t + \frac{\gamma}{2} + \beta a_1^2 a_2^2\big) - \big((\alpha+\gamma)a_1a_2 + \beta a_1^3 a_2\big)^2\Big], \\
\mathbb{S}_{23} &= \frac{1}{det\mathbb{C}}\Big[\big(\lambda + \alpha + \beta a_1^2 a_2^2\big)\big((\alpha+\gamma)a_1a_2 + \beta a_1^3 a_2\big) - \big(\lambda + 2\mu_t + 2(\gamma+\alpha)a_1^2 + \beta a_1^4\big)\big((\alpha+\gamma)a_1a_2 + \beta a_1 a_2^3\big)\Big], \\
\mathbb{S}_{33} &= \frac{1}{det\mathbb{C}}\Big[\big(\lambda + 2\mu_t + 2(\gamma+\alpha)a_1^2 + \beta a_1^4\big)\big(\lambda + 2\mu_t + 2(\gamma+\alpha)a_2^2 + \beta a_2^4\big) - \big(\lambda + \alpha + \beta a_1^2 a_2^2\big)^2\Big]
\end{aligned}$$

and

$$\begin{aligned}
\frac{1}{det\mathbb{C}} =& \big(\lambda + 2\mu_t + 2(\gamma+\alpha)a_1^2 + \beta a_1^4\big)\Big[\big(\lambda + 2\mu_t + 2(\gamma+\alpha)a_2^2 + \beta a_2^4\big)\big(\mu_t + \frac{\gamma}{2} + \beta a_1^2 a_2^2\big) \\
&\qquad - \big((\alpha+\gamma)a_1a_2 + \beta a_1 a_2^3\big)^2\Big] \\
&- \big(\lambda + \alpha + \beta a_1^2 a_2^2\big)\Big[\big(\lambda + \alpha + \beta a_1^2 a_2^2\big)\big(\mu_t + \frac{\gamma}{2} + \beta a_1^2 a_2^2\big) \\
&\qquad - \big((\alpha+\gamma)a_1a_2 + \beta a_1^3 a_2\big)\big((\alpha+\gamma)a_1a_2 + \beta a_1 a_2^3\big)\Big] \\
&+ \big((\alpha+\gamma)a_1a_2 + \beta a_1^3 a_2\big)\Big[\big(\lambda + \alpha + \beta a_1^2 a_2^2\big)\big((\alpha+\gamma)a_1a_2 + \beta a_1 a_2^3\big) \\
&\qquad - \big((\alpha+\gamma)a_1a_2 + \beta a_1^3 a_2\big)\big(\lambda + 2\mu_t + 2(\gamma+\alpha)a_2^2 + \beta a_2^4\big)\Big].
\end{aligned}$$